CHEMICAL REVIEWS

Subscriber access provided by V. Vernadsky | National Library of Ukraine

Fabrication Approaches for Generating Complex Micro- and Nanopatterns on Polymeric Surfaces

Arnzazu del Campo, and Eduard Arzt

Chem. Rev., **2008**, 108 (3), 911-945 • DOI: 10.1021/cr050018y

Downloaded from http://pubs.acs.org on December 24, 2008

More About This Article

Additional resources and features associated with this article are available within the HTML version:

- Supporting Information
- Links to the 3 articles that cite this article, as of the time of this article download
- Access to high resolution figures
- Links to articles and content related to this article
- Copyright permission to reproduce figures and/or text from this article

View the Full Text HTML

ACS Publications
High quality. High impact.

Chemical Reviews is published by the American Chemical Society. 1155 Sixteenth Street N.W., Washington, DC 20036

Fabrication Approaches for Generating Complex Micro- and Nanopatterns on Polymeric Surfaces

Aránzazu del Campo[†,*] and Eduard Arzt[†]

Max-Planck-Institut für Metallforschung, Heisenbergstraβe 3, 70569 Stuttgart, Germany

Received June 19, 2006

Contents

1. Introduction 911
2. Advanced Photolithography 912
2.1. High Aspect Ratio Patterns 912
2.1.1. Photoresist Materials 912
2.1.2. Particularities of HAR Processing 914
2.1.3. Examples and Actual Limits 916
2.2. Hierarchical Patterns by Layer-by-Layer Exposure 916
2.3. Tilted Patterns by Inclined/Rotated Lithography 916
2.4. 3D Patterns by Modulated Exposure 917
2.5. Periodic 3D Patterns by Holographic Lithography 918
3. Laser Scanning 918
3.1. Stereolithography by Scanning Resist Multilayers 919
3.2. Two-Photon Lithography (TPL) 919
4. Serial Writing with Charged Particles 920
4.1. Electron Beam Lithography 920
4.2. Ion Beam Lithography 920
4.3. Scanning Probe Resist Lithography 921
5. Micro- and Nanomachining 921
5.1. Focused Ion Beam 921
5.2. Scanning Probe Nanomachining 921
6. Direct Writing and Material Deposition 921
7. Moulding 922
7.1. Mould Fabrication 922
7.2. Demoulding: Mould Treatment 924
7.3. Embossing Thermoplastic Materials: Nanoimprint Lithography (NIL) 924
7.3.1. HAR Structures Produced by NIL 925
7.3.2. Secondary Structures by NIL 925
7.3.3. 3D Patterns with NIL 926
7.4. Moulding UV-Sensitive Materials: UV NIL 926
7.5. Soft Lithography 927
7.6. Solvent-Assisted Moulding 928
8. Transfer Printing 929
8.1. 3D Patterns by Multistep Transfer Printing 930
9. Filling Mesoporous Matrices 930
9.1. With Polymer Precursors 931
9.2. With Polymeric Melts 931
10. Surface Instabilities 932
10.1. Electric Field-Induced Instabilities 932
10.2. Temperature-Induced Instabilities 935
11. Patterning Through Self-Assembly of Block Copolymers 935
11.1. BC Morphology in Thin Film Geometry 935
11.2. Hierarchical Patterns 936
12. Comparison of Patterning Methods 938
13. Applications 939
13.1. Biosensors with Increased Sensitivity, Miniaturization, and Throughput 939
13.2. Drug Delivery 939
13.3. Force Sensors 939
13.4. Tissue Engineering and Implant Fabrication 939
13.5. Biofouling 940
13.6. Biomimetic Surfaces 940
13.7. Photonic Structures 940
14. Conclusions 940
15. References 940

1. Introduction

Recent innovations in the area of micro- and nanofabrication have created a unique opportunity for patterning surfaces with features with lateral dimensions spanning over the nano- to millimeter range. The microelectronics industry and need for smaller and faster computing systems have pushed this development during the last two decades, mainly focused on obtaining patterns with the smallest possible lateral dimensions via optical lithography in its multiple variants.[1] In parallel, new application fields for miniaturized devices have emerged, analytical chips or "lab-on-a-chip" devices for application in biochemistry being the most notable example. The interest in light and low-cost devices has caused the development of alternative patterning technologies more suited for plastics manufacturing.[2−4]

Increased effort has been paid in the last 10 years to establishing fabrication technologies which allow production of structured surfaces with greater geometrical complexity at reduced operation time and cost. These include patterns made of polymer materials possessing elongated features in the vertical dimension (aspect ratio > 3), exhibiting several hierarchy levels, or in intricate tilted, suspended, or curved three-dimensional (3D) arrangements. Such surface structures find applications in emerging fields like biosensors with increased sensitivity and throughput due to higher effective surface area; fibrillar surfaces with controlled adhesion as better scaffolds for tissue engineering, nonbiofouling coatings for undersea pipelines, high adherence wheels, and haptic devices; or high-luminosity lighting panels and photonic structures for the visible spectrum.

* To whom correspondence should be addressed. Phone: +49 (0)711 6893416. Fax: +49 (0)711 6893412. E-mail: delcampo@mf.mpg.de.
† Current address: Leibniz Institut für Neve Materialien, Campus D2 2, 66123 Saarbrücken, Germany.

10.1021/cr050018y CCC: $71.00 © 2008 American Chemical Society
Published on Web 02/26/2008

Aránzazu del Campo was born in 1972 in Coomonte (Spain) and studied chemistry at the Universidad Complutense and Polymer Science and Engineering at the Instituto de Ciencia y Tecnología de Polímeros (Madrid, Spain). She received her Ph.D. degree in 2000 working in the field of liquid crystalline polymers. She then joined the Max-Planck-Institut für Polymerforschung in Mainz (Germany) as Marie Curie Fellow and started to work in the field of surface chemistry and nanotechnology. In 2003 she moved to the Universitá degli Studi di Urbino (Italy), and since 2004 she has been leading the group "Complex, Multifunctional Surfaces" at the Max-Planck-Institute in Stuttgart (Germany). Her group is mainly engaged in developing novel synthetic approaches for manufacturing hierarchical, chemically, and topographically patterned surfaces. These are based on challenging organic chemistry concepts and conceived to understand adhesion phenomena at different levels.

Eduard Arzt was born in 1956 in Linz, Austria, and studied physics and mathematics at the University of Vienna. He completed his Ph.D. degree there in 1980 with a metallurgical project carried out at the University of Leoben. Following a period as a research associate at Cambridge University, U.K., he joined the Max Planck Institute for Metals Research as a group leader in 1982. After a tenure as Visiting Professor at Stanford University, he was appointed in 1990 to Professor of Physical Metallurgy/Metal Physics at the University of Stuttgart and jointly Director at the Max Planck Institute for Metals Research. He is the recipient of several national and international awards, among them the Acta Metallurgica Outstanding Paper Award (1990), the highest German science award Gottfried Wilhelm Leibniz Prize (1996), and inclusion among the highly cited materials scientists by ISI (2003). He has been Visiting Professor at the Massachusetts Institute of Technology, Cambridge, MA (1996), and delivered distinguished lectures there and at the University of Minnesota (2005). He is a corresponding member of the Austrian Academy of Sciences and a member of the German Academy Leopoldina, an editor of *Progress in Materials Science*, and a member of several international science and technology advisory boards. He has authored and coauthored about 300 research papers, including about 180 in refereed journals, and 4 patents. His highly interdisciplinary research interests range from metallic micro- and nanostructures, thin film mechanics, and reliability in submicron dimensions to micromechanics of biological systems and new bioinspired materials and surfaces.

In this review we present available processing methods suitable for the fabrication of such complex micro- and nanostructured surfaces made out of polymeric materials. The steps and polymeric materials involved and the achieved structures will be described. With this work, we intend to complement recent reviews on surface patterning,[2−4] mainly concentrated on less complicated surface designs and applications in microelectronics, and provide the reader with a critical understanding of this topic at an early stage of its development.

2. Advanced Photolithography

Lithography is the technique used to transfer a pattern onto a substrate by means of an etching process. Resist lithography makes use of an irradiation source and a photosensitive polymer material to perform the pattern transfer (Figure 1a). This process starts with the coating of a planar substrate (typically a silicon wafer) with the photoresist in liquid form. After the coating process, the substrate is "soft baked" in order to remove the solvents from the resist and improve resist−substrate adhesion. In a subsequent step, selected parts of the photoresist film are exposed to a light source (typically a UV lamp, electron beam, or X-rays). Light initiates a series of photochemical processes in the resist which alter the physical and chemical properties of the exposed areas such that they can be differentiated in a subsequent image development step. Most commonly, the solubility of the film is modified, either increasing the solubility of exposed areas (yielding a positive image after development) or decreasing the solubility to yield a negative-tone image. After development, substrates patterned with negative-tone photoresists can be baked a second time ("hard bake") at higher temperatures to further activate cross-linking processes and improve the mechanical stability of the pattern; however, this process may cause thermal flow of the patterned features and consequently distortion of their initial geometry.

During the last three decades, most efforts and developments in lithography have been directed at shrinking the lateral dimensions of the imaged features.[1,5−10] The application of different resolution enhancement approaches (illumination sources with shorter irradiation wavelength, projection and immersion optics, phase-shifting masks, etc.) and development of advanced photoresist materials (e.g., chemically amplified resists[11]) have permitted a reduction of lithographic structures down to sub-100 nm dimensions. Current trends have been predicted to improve shrinking to at least 45 nm in the year 2010.[5] Only recently have lithographic approaches been extended to the fabrication of more complex patterns including high aspect ratio (HAR), tilted, suspended, or curved geometries. Initially, such structures were fabricated in layer-by-layer processes where multiple coating/irradiation steps are concatenated or iterated, each of them defining structures at different levels. To overcome the complexity of the layer-by-layer approach and minimize the number of process paths required to obtain the final structure, new fabrication methodologies are trending toward lithography techniques with intrinsic 3D structuring capability. Some of the available approaches will be discussed in this section.

2.1. High Aspect Ratio Patterns

2.1.1. Photoresist Materials

Resist materials must satisfy stringent requirements as the lateral feature size shrinks and the aspect ratio increases.[11]

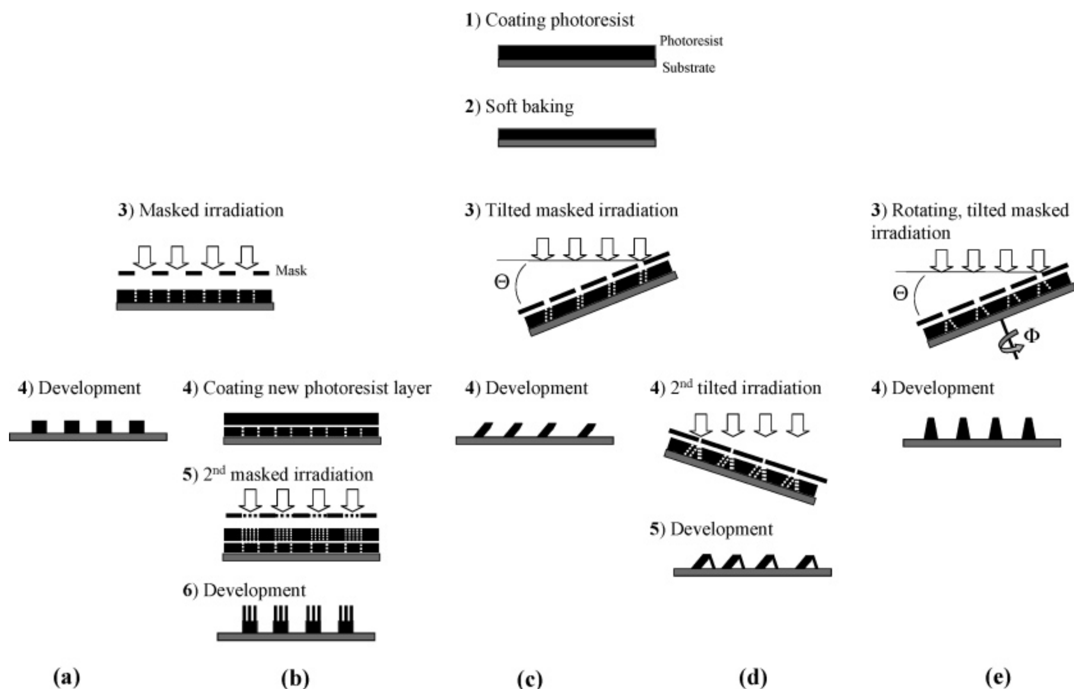

Figure 1. Photolithographic structuring methods using masked irradiation and a negative photoresist material: (a) HAR patterning by single exposure, (b) hierarchical patterning by layer-by-layer coating and exposure, (c) tilted patterning by single inclined exposure, (d) interconnected patterns by double inclined exposure, (e) tapered patterns by rotating tilted exposure.

A suitable viscosity is of particular importance in order to balance opposite requirements involved in different processing steps. Low viscosity facilitates spin coating of uniform, defect- and stress-free films, and, later on, removal of unsolidified resin during development; however, high viscosity is required for reducing lateral flow and obtaining stable resist films, especially when the thickness increases. The resist must also possess high reaction efficiency upon light irradiation at the selected irradiation wavelength to achieve high contrast, high resolution, and high sensitivity. A high Young's modulus after processing is important to guarantee mechanical stability of the lithographic structures. In the case of negative photoresists, low shrinkage during polymerization is necessary for dimensional accuracy and to avoid film stress.

There are a number of commercially available photoresists suitable for HAR applications. Diaplate and Ordyl P-50100 are acrylate-based negative photoresists. A positive variant is the Novolak resin SPR 220-7. These systems are commercialized in solution form for spin-coating applications. Alternatively, thick photoresists are available in dry film format, like Riston,[12] Ordyl BF 410,[13] Etertec 5600,[14] DF 4615,[15] and DFR-15.[16] Some advantages and disadvantages of each system have been recently described.[17]

Undoubtedly, the favorite photoresist for HAR lithography is the SU-8 system.[18] SU-8 is a negative-tone, chemically amplified resist. Its main components are Bisphenol A Novolak epoxy oligomer (EPON SU-8 resin, Shell Chemical) and up to 10 wt % triarylsulfonium hexafluoroantimonate salt (CYRACURE UVI, Union Carbide) photoacid generator with peaks of UV light absorption at 310 and 230 nm, allowing protolysis in the wavelength range of conventional broadband mask aligners.[19] Upon irradiation, the photoacid generator decomposes to form hexafluoroantimonic acid, which protonates the epoxides on the oligomer. These protonated oxonium ions are available to react with neutral epoxides in a series of cross-linking reactions after application of heat and regenerate the acid catalyst, amplifying the sensitivity of the resist.[19] Each monomer molecule contains eight reactive epoxy sites; thus, a high degree of cross-linking can be obtained. This results in high mechanical and thermal stability of the lithographic structures after processing. In fact, fully cross-linked SU-8 has a glass-transition temperature around ~200 °C, degradation temperature of ~380 °C, and a Young's modulus $E \approx 4-5$ GPa (Table 1).

Table 1. Physical Properties of EPON SU-8 Photoresist[19]

property	value
Young's modulus, E (postbake at 95 °C)	4.02 GPa
Young's modulus, E (hardbake at 200 °C)	4.95 ± 0.42 GPa
biaxial modulus of elasticity, $E/(1-n)$	5.18 ± 0.89 GPa
film stress (postbake at 95 °C)	16−19 MPa
maximum stress (hardbake at 200 °C)	34 MPa
griction coefficient (postbake at 95 °C)	0.19
glass temperature, T_g (unexposed)	~50 °C
glass temperature, T_g (fully cross-linked)	>200 °C
degradation temperature (fully cross-linked)	~380 °C
thermal expansion coefficient (postbake at 95 °C)	52 ± 5.1 ppm/K
polymer shrinkage upon cross-linking	7.5%

SU-8 is available in a wide range of formulations to cover a wide film thickness range. Resist thicknesses from 2 to 300 μm in a single coating process or to 3 mm by multicoating processes can be achieved.[20] Its chemical stability enables it to be used as a moulding material for HAR electroplated structures (as alternative material for LIGA technology, see section 7.1) and as structural material for microfluidics. It can be also used as a mask for prolonged reactive ion etching of an underlying Si wafer, leading to features with increased aspect ratio and vertical sidewalls.

Poly(methyl methacrylate) (PMMA) is a positive resist which undergoes chain scission under high-energy exposure. X-ray irradiation typically reduces its molecular weight by 3 orders of magnitude. X-ray patterning of PMMA yields high-quality HAR structures with high resolution, high precision, and low surface roughness. PMMA, however, has

low sensitivity, and therefore, patterning requires extremely long exposure times. In fact, PMMA has been replaced by SU-8 (with a 70-fold higher X-ray sensitivity) in many applications. Poly(methyl 2-chloroacrylate) can also be used and shows higher sensitivity than PMMA.

Over the past decade, silicate-based inorganic−organic hybrid polymers (e.g., ORMOCER) have also attracted interest as lithographic materials because of the physical and chemical properties resulting from their hybrid nature.[21,22] These are mixtures of alkoxysilanes containing organic polymerizable units (typically methacryl, styryl, or epoxy groups), catalysts, and photoinitiators. During sol−gel processing, the inorganic network is formed first (via hydrolysis and polycondensation of the alkoxysilane precursors) and the organic cross-linking occurs via UV-activated reactions in the final curing step. The resulting hybrid networks are amorphous and typically optically transparent. Their refractive index can be tuned by the polymer composition. These systems can display high mechanical stability, which is an important requirement for building HAR patterns.

Hydrogen silsesquioxane (HSQ) is another silicate-based high-resolution negative-tone resist used in electron-beam and X-ray lithography. HSQ is a highly ordered oligomer with a cage-like structure in which a one and one-half (sesqui) stoichiometry of oxygen is bound to a silicon hydride (Si−H) group. Irradiation converts Si−H bonds to silanol (Si−OH) groups. Silanol groups rapidly condense into siloxane bonds (Si−O−Si), whereby the initial cage structure is transformed into a 3D network insoluble in aqueous base developers such as tetramethylammonium hydroxide. Significant drawbacks of HSQ are its low contrast and poor storage stability.[23]

2.1.2. Particularities of HAR Processing

Processing elongated structures involves dealing with resist layers with thickness much higher the lateral dimensions of the pattern features. This creates difficulties in accurate pattern generation associated with resist surface roughness, inhomogeneous illumination dose across the resist film, long development times, or mechanical instability of HAR features during processing. Different strategies have been reported that help in partially overcoming these issues.

2.1.2.1. Planarization Effects. Photoresist materials are specially engineered to render planar surfaces after spin coating. However, planarization becomes more difficult as the viscosity of the resist solution (and therefore the thickness of the spin-coated film) increases. As an example, typical flatness errors for the SU-8 system range from 10 to 100 μm for a resist thickness around 1 mm. Other factors such as unintentional tilt during baking, dirt particles, curvature of the substrate or mask, etc., also contribute to reduced surface flatness.[24,25]

If irradiation is performed through a mask in contact with the resist surface, the flatness errors hinder conformal contact at the interface. The resulting air gaps cause diffraction effects (Fresnel diffraction), which result in pattern edges being irradiated with a higher dose and finally pattern enlargement at the border (T-profile). The diffraction error increases with increasing resist thickness and gap distance. For example, exposure of a 156 μm thick SU-8 film to irradiation through a 25 μm striped pattern and a 100 μm gap resulted in a 45% pattern width error.[25] This can be corrected by filling the gap between mask and photoresist with a refractive index (n) match material. Glycerol (n = 1.470−1.475) filling of the 100 μm gap provided a SU-8 (n = 1.668 at λ = 365 nm, n = 1.650 at λ = 405 nm) stripe pattern with nearly vertical sidewalls (Figure 2).[25] A Cargille refractive index matching liquid provided patterns with 6 μm feature size and 1150 μm height (aspect ratio > 190) and vertical sidewalls.[24]

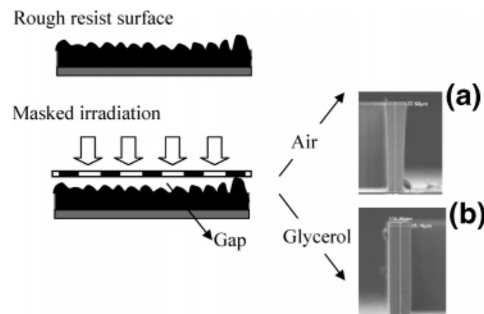

Figure 2. SU-8 walls obtained after exposure with a 100 μm air gap between resist and mask. In (a) the gap was open, whereas in (b) the gap was filled with glycerol as refractive index matching liquid. (Reprinted from ref 25 with kind permission of Springer Science and Business Media.)

2.1.2.2. Resist UV Absorption. Photosensitive organic materials typically absorb light in the UV range. As a consequence, there is a gradual light intensity drop across the film thickness as the UV beam penetrates the resist layer from the top to the bottom. This results in the top part of the resist being irradiated with higher dosage than the bottom part. In negative photoresists, like SU-8, this is one of the major reasons why inexperienced operators often produce microstructures with T-profiles instead of vertical profiles.[24] It is also one of the reasons why X-ray lithography is preferred for high-quality vertical sidewall in HAR patterning. X-rays are not absorbed by organic materials and can deeply penetrate thick films without losing intensity.

2.1.2.3. Long Development Times. Pattern development involves diffusion of developer molecules into the non-cross-linked regions of the resist film and diffusion of solvated polymer chains out of those regions and into the developer solution. The time required for development is determined by the resist thickness, the exposure dose, the soft-baking time and temperature, the temperature and agitation during development, and the geometry of the pattern. HAR features such as narrow and deep holes or tubes or horizontally orientated long channels are extremely difficult to develop. This process, if possible at all, may take many hours and cause dramatic damage of fine features as a consequence of swelling of cross-linked regions or debonding of the resist layer from the wafer.

Development can be accelerated by moderately increasing the temperature of the developing solution,[26] reducing the exposure time and consequently the cross-linking degree,[27] or agitation. Stirring of the developer solution enhances diffusion, which increases the development rate. Downward orientation of the wafer during stirring has been demonstrated to improve development of HAR structures as it allows gravitational forces to aid in removal of the resist.[28,29] In fact, PMMA pillars with diameter 15 μm and aspect ratio 6.25 have been successfully obtained after downward development. Equal development times after using an upward-development method yielded a pattern with a residual layer of resist material on the wafer.

Stirring during development is not always beneficial. Strong stirring may cause HAR structures to deflect in the

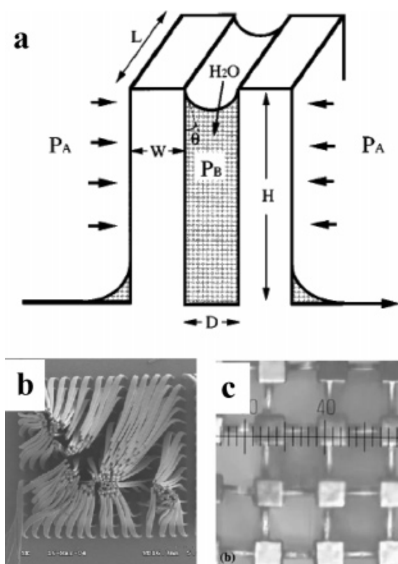

Figure 3. Pattern collapse due to capillary forces during drying. The acting forces are represented in a. (Reused with permission from ref 33. Copyright 1995 American Institute of Physics.) (b) Collapsed HAR micropillars (height 1 mm, diameter 30 μm) after lithographic processing using wet development. (Reprinted with permission from ref 414. Copyright 2005 IOP.) (c) HAR pillars reinforced with bridges for avoiding collapse. (Reprinted from ref 56 with kind permission of Springer Science and Business Media.)

pressure gradient, and this may lead to pattern deformation, debonding, adhesion between nearby structures, and finally pattern loss. Sonic development in its two categories, ultrasonic and megasonic, can be applied to solve this problem. Ultrasonic development uses frequencies in the kilohertz range to agitate the developer. This increases the pressure at the resist surface and accelerates diffusion and development. However, ultrasonic waves also cause vibrations in the pattern structure which may result in cracking and debonding over time. For this reason, ultrasonic baths are not always beneficial in HAR processing.

Megasonic agitation, which uses frequencies well above the vibrational modes of the resist structures (typically 1−10 MHz), has been proved to be more effective. SU-8 structures ranging from 20 μm to 1.5 mm in height and with aspect ratios up to 50 by optical and well over 100 by X-ray lithography have been reported.[30,31] Conventional development restricted the feature's aspect ratio to 30. Parameters such as damping capacity, agitation power density, and orientation of the sonic wave relative to the features and substrate may also influence the process but have not yet been considered.

2.1.2.4. Collapse of Structures During Rinsing. Collapse of pattern structures may occur as a consequence of the low mechanical stability of the resist material and adhesive failure between resist and wafer. During lithographic processing of HAR structures, collapse is usually associated with the drying step, during which solvent evaporation generates capillary forces that cause bending and sticking of neighboring features (Figure 3).[6,32−34]

Several strategies have been explored experimentally to reduce pattern collapse. Various studies have focused on improving the mechanical properties of resist by adding reinforcing fillers to the polymer forming a nanocomposite[35] or by increasing cross-linking density.[36,37] However, composite materials exhibit higher viscosities, and this is a disadvantage during the spin-coating process. Increased cross-linking results in higher volume shrinkage and increases film stress. Consequently, dimensional stability of the pattern is decreased, and in the worst case, film cracking may occur.

Capillary forces increase with increasing surface tension of the rinsing liquid and decreasing contact angle between liquid and resist (i.e., increased wetting of the resist by the liquid).[38] Substitution of the rinse water by water/alcohol mixtures with lower surface tension (72 mN m^{-1} for water and 21.8 mN m^{-1} for isopropanol) has been proposed as an alternative to avoid collapse during drying;[39] however, this method has been rejected by other authors because of the stronger wetting of organic resists by isopropanol.[38] Other low-surface-tension solvents such as perfluorohexane (10 mN m^{-1}) have also been suggested.[40,41] These solvents, however, lack miscibility with common developers and rinse solutions, often water based. Furthermore, the finite value of their surface tension is still not sufficient to prevent pattern collapse in nanolithography, even though it is so small.

Supercritical (SC) drying provides an interesting alternative.[41,42] Under SC conditions, liquid and gas phases do not coexist above the critical point. This means that the liquid can be continuously converted into gas without forming a liquid−gas interface. As a consequence, the surface tension of the rinsing solution is zero and pattern collapse caused by capillary forces is prevented. Carbon dioxide is the leading candidate for SC drying in lithography.[43−46] CO_2 critical pressure and temperature are 73.8 bar and 31.1 °C, respectively, and its surface tension is only 1.5 mN/m at 25 °C and reaches zero at the critical point. From an environmental, health, and safety viewpoint, CO_2 is nontoxic, nonflammable, relatively inert, and easy to recycle, resulting in potentially large savings in overall cost and reduced waste streams.

SC−CO_2 drying involves replacement of the rinsing water by CO_2. However, CO_2 is a poor solvent for nonvolatile polar or ionic species and, consequently, not miscible with water. Therefore, rinsing with other solvents is necessary prior to drying with SC−CO_2. One strategy involves washing with alcohols to replace rinsing water, provided that the resist does not dissolve in alcohol, as is the case in some polyvinylphenol- and novolac-based resists.[47] Alternatively, water can be replaced with surfactant-stabilized microdomains in hexane, followed by liquid and SC−CO_2 exchange.[47−49] Even though collapse may be avoided by this method, excessive use of solvents and long drying periods are serious disadvantages. Addition of surfactants with one or more fluorocarbon tails to the rinsing water, which have low polarizability densities, has shown good results and reduces the number of steps.[47] In fact, 150 nm patterns with aspect ratios up to 4 have been reported using this method.[50] However, the high cost and potential toxicity of fluorosurfactants limit their application.

The best way to reduce pattern collapse using SC−CO_2 while avoiding the above-mentioned limitations involves performing direct CO_2 resist development. This requires designing new CO_2-philic photoresist materials. Conventional hydrophilic or lipophilic polymers are relatively insoluble in CO_2, but fluoropolymers and silicon-containing polymers fall into the CO_2-philic category and have been exploited for this purpose.[46,51,52] Copolymers of *tert*-butyl methacrylate with 3-methaacryloxypropyl-pentamethyldisoloxane or pentafluoropropyl methacrylate have been demonstrated to be interesting negative-tone photoresists for 193 nm lithography[51,53−55]

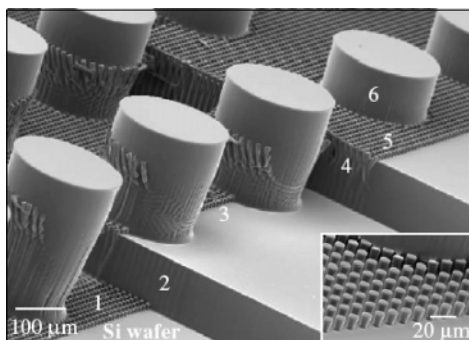

Figure 4. Example of hierarchical pattern by layer-by-layer coating and exposure. Each layer is numbered in the order that it was coated. (Reprinted with permission from ref 66. Copyright 2006 IOP.)

SC−CO_2 processing would be especially advantageous in HAR structures as it rapidly wets all surfaces and penetrates in narrow geometries. In addition, the solvation capability of CO_2 can be easily tuned by changing its density through slight variations of temperature and pressure conditions. As an important limitation, SC−CO_2 processing requires pressure chambers and is therefore more complicated than processing in water.

Another way of avoiding pattern collapse consists of reinforcement of the HAR structures using ''bridges'' that prevent them from lateral bending.[56] Figure 3c shows an example.

2.1.3. Examples and Actual Limits

Optimized UV lithography conditions have yielded line patterns with aspect ratios up to 20 from SU-8 films with thickness ranging from 200 to 700 μm.[57] Isolated SU-8 structures with up to 1.5 mm height and an aspect ratio of 15 have also been reported.[58−60] Carefully optimized post-baking conditions have improved the aspect ratio of isolated structures with 1150 μm height up to 40.[61]

X-rays are also applied in HAR lithography, although the difficult access to synchrotron radiation strongly restricts the use of this lithography to the broad public. Structures with lateral dimensions down to 400 nm and aspect ratio up to 9 have been obtained using hard X-rays ($\lambda \approx 0.4$ nm).[62−64] The aspect ratio of the structures is limited by the low mechanical stability of the PMMA resist. SU-8 pillars with a diameter of 8 μm and an aspect ratio of 60 have also been reported. The aspect ratio was increased up to 100 by optimizing the development and rinsing conditions.[65]

2.2. Hierarchical Patterns by Layer-by-Layer Exposure

Lithographic fabrication by superposition of coating and irradiation steps enables fabrication of lithographic structures with several organization levels using traditional 2D setups and alignment markers on the mask for guiding superposition (Figure 1b). Depending on the final geometry of the pattern, resist development needs to be performed after each irradiation step or can be left to the end and performed in a single step. In the case of HAR structures, single development is specially recommended because of the risk of pattern collapse during drying and the difficulty of achieving planar resist layers over underlying HAR topographies. Using this method, SU-8 hierarchical patterns comprised of features with lateral dimensions ranging from 5 μm to 2 mm and heights from 10 to 500 μm have been reported (Figure 4). In order to reduce film stress and avoid SU-8 cracking during the multicoating processing, SU-8 resists of different viscosities were sequentially processed and simultaneously developed.[66]

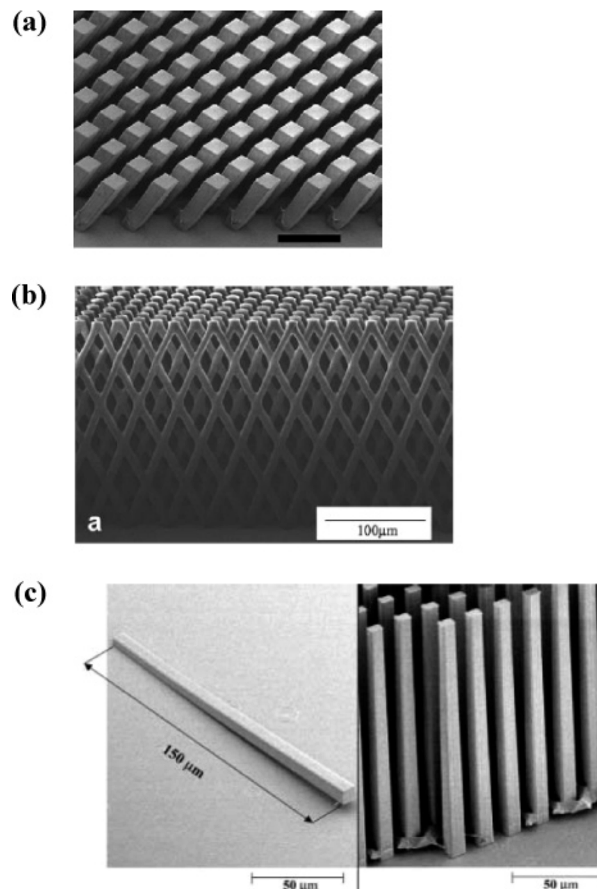

Figure 5. Tilted patterns obtained by inclined lithography. (a) Tilted SU-8 pillars obtained by tilted UV single exposure. Scale bar corresponds to 100 μm. (Reprinted from ref 67, Copyright 2004, with permission from Elsevier.) (b) SU-8 pillars with 10 μm diameter and aspect ratio 20 obtained by double-backside UV exposure of the resist. (Reprinted from ref 69 with kind permission of Springer Science and Business Media.) (c) Asymmetric PMMA pillars with an aspect ratio of 10 obtained by combining X-ray vertical and tilted exposure. The lateral dimensions along the pillar increase from the top (10 μm) to the bottom in one of the lateral walls. (Reprinted from ref 71 with kind permission of Springer Science and Business Media.)

2.3. Tilted Patterns by Inclined/Rotated Lithography

In conventional lithography, the mask and resist film are perpendicularly aligned with respect to the irradiation source. The light is shadowed by the mask, resulting in vertical, binary-contrast, lithographic profiles. By tilting the mask and resist film with respect to the beam using a tilting stage, inclined structures can be produced (Figure 1c).[67] By these means, oblique cylinders, embedded channels, bridges, V-grooves, and truncated cones with aspect ratios >4 have been fabricated using 100 μm thick SU-8 layers and a conventional UV mask aligner (Figure 5a).[67] Using a similar approach, arrays of tilted pillars with a 550 nm diameter and an aspect ratio of 45 were obtained using X-ray irradiation and PMMA resist.[68]

Multiple inclined UV exposures along different axes can be exploited to generate more complex 3D structures (Figures 1d and 5b).[67,69,70] Tilted exposure can be also combined with

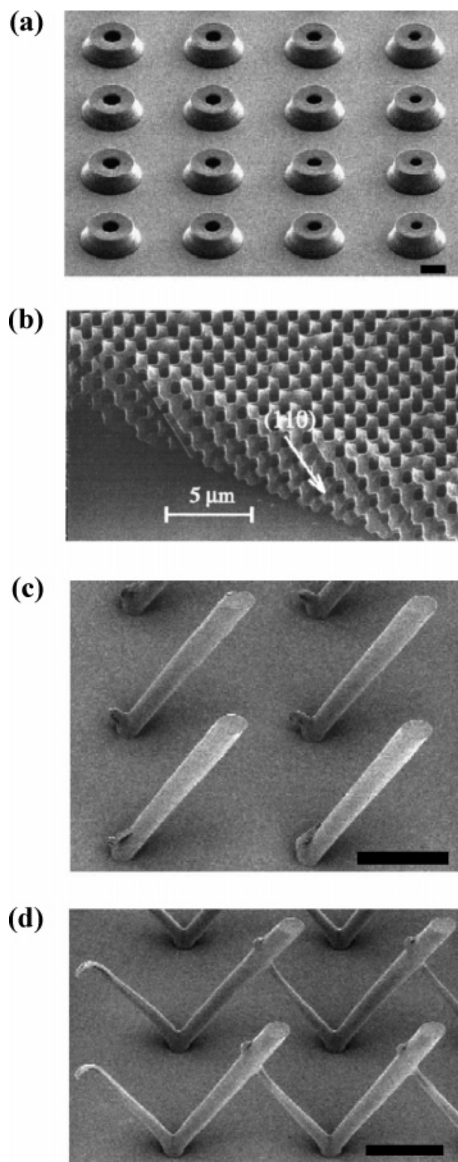

Figure 6. (a) Tapered structures obtained by tilted and rotated UV exposure (scale bar 50 μm). (Reprinted from ref 67, Copyright 2004, with permission from Elsevier.) (b) Structures generated after three consecutive tilted and rotating X-ray exposures. It is comprised of six lattice periods of 1.3 μm and holes with 0.65 μm diameter. (Reused with permission from ref 75. Copyright 2000 AVS The Science & Technology Society.) (c, d) SU-8 structures fabricated by tilted UV on (c) nonreflective (silicon) and (d) reflective (aluminum-coated silicon) substrates (scale bar 100 μm). (Reprinted from ref 67, Copyright 2004, with permission from Elsevier.)

vertical exposure to create asymmetric pillars with vertical and inclined sidewalls (Figure 5c).[71]

If the photomask and photoresist-coated substrate are tilted and simultaneously rotated during irradiation (Figure 1e), tapered structures with nonvertical sidewalls can also be generated (Figure 6a).[67,72] Such tapered structures are interesting if the structured surface is needed as a master for a subsequent replication step because they provide a draft angle and facilitate demoulding (see LIGA technology in section 7.1).[73] Combination of multiple X-ray exposures, tilting, and rotation has generated PMMA patterns with tilted and crossed features like those shown in Figure 6b.[74−76]

During irradiation, the incident light which penetrates the resist film is always reflected at the photoresist−substrate interface. Typically the energy of the reflected UV is too low to initiate cross-linking of the resist, and therefore, this effect is usually not considered; however, if the energy of the reflected UV is increased (by raising exposure times or using reflective substrates), cross-linking may be initiated along the path of the reflected beam.[67] Figure 6c shows the structures obtained after single tilted exposure using a silicon wafer, where no influence of the reflected UV is noticeable. Figure 6d shows microstructures fabricated on reflective Al-coated silicon wafer under the same irradiation conditions for comparison.

Figure 7. Suspended 10 μm thick grid structures on the top of 100 μm height SU-8 pillars made by gray scale lithography. (Reprinted from ref 78, Copyright 2003, with permission from Elsevier.)

2.4. 3D Patterns by Modulated Exposure

A number of novel approaches to generate multilevel structures from single resist layers have been demonstrated which avoid time-consuming multiexposure strategies. These are based on special masks and projection optics which allow modulated exposure doses of the resist film. This results in multiple depths of exposed photoresist across the surface and, consequently, different heights of the photoresist structure remaining after development.

"Gray scale" lithography makes use of special photomasks which modulate the light intensity according to their gray levels. Two types of gray scale masks can be used: halftone chrome masks and high-energy beam-sensitive (HEBS) glass masks. Halftone masks are essentially binary chrome masks with gray levels simulated by different densities of opaque pixels on a transparent background. HEBS glass masks are fabricated by exposing this glass to controlled doses of a high-energy electron beam, causing the reduction of silver ions in the glass. Areas of the mask with high concentrations of reduced silver ions correspond to high levels of gray shading. This method has been used to produce suspended 10 μm thick grid structures on the top of 15−100 μm height SU-8 pillars (Figure 7).[77,78]

An alternative modulated exposure strategy uses proximity lithography to induce diffraction patterns from a conventional chrome-on-glass mask by leaving a controlled air gap between the resist film and the mask.[79] Diffraction creates a modulated intensity pattern across the surface of the photoresist-covered substrate. The intensity pattern depends fundamentally on the mask (feature size, geometry, and spacing) and the gap between the mask and the resist layer. Other ways of generating ranges of exposure levels include microlens arrays[80] or conformable phase-shift edge masks.[81,82] The latter are masks with a topographical relief that modulates the phase of the transmitted exposure light.[83−87] The geometry of the intensity pattern depends on the design

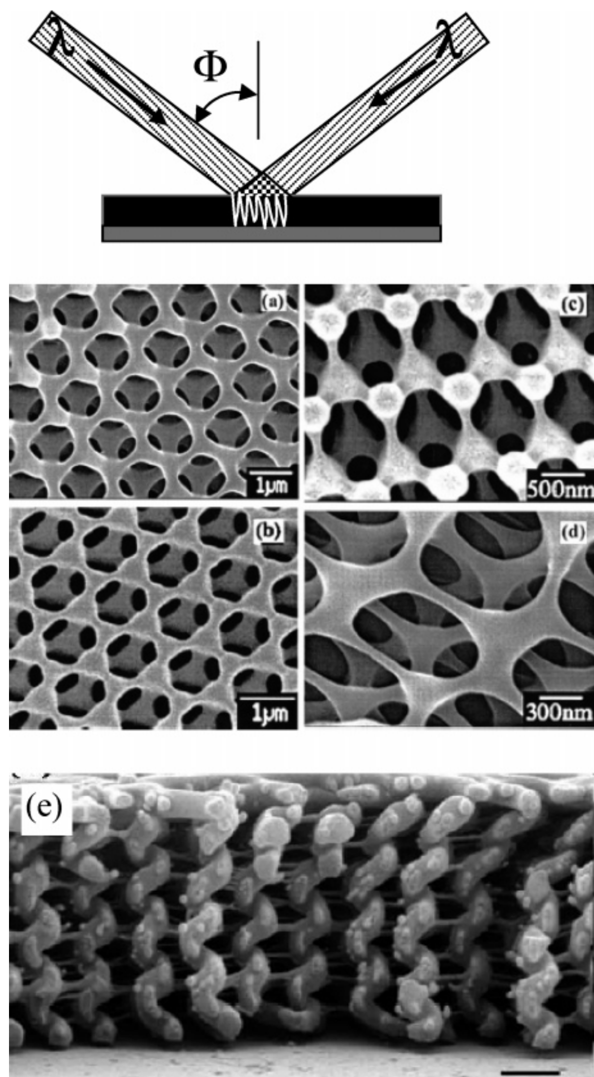

Figure 8. Scheme of the simplest optical arrangement for interference lithography. SEM images of structures with fcc symmetry fabricated with four-beam holographic lithography using decreasing exposure dosage: (a) 160, (b) 130, (c) 100, and (d) 60 mJ cm^{-2}. (Reprinted with permission from ref 95. Copyright 2003 American Institute of Physics.) (e) Chiral 3D structures (spirals) produced by holographic lithography. Scale bar is 1 μm. (Reprinted with permission from ref 100. Copyright 2005 Optical Society of America.)

(depth and layout of the relief structures and refraction index) of the mask and wavelength, coherence, and polarization of the exposure light.

2.5. Periodic 3D Patterns by Holographic Lithography

Holographic lithography (or interference lithography, IL) is based on the interference of coherent laser beams to form a periodic, sinusoidal intensity pattern in space (Figure 8). By exposing a photosensitive material to this illumination pattern, periodic structures of various symmetries can be obtained after development. The period of the pattern is determined by the wavelength of light and the angle of intersection of the beams according to the equation

$$P = \frac{\lambda}{2}\sin \Phi$$

where λ is the wavelength and Φ is the angle of incidence of the beams from the normal. According to this equation, the spatial resolution that can be achieved far exceeds that of conventional projection lithography using the same irradiation wavelength (typically $\lambda/4$). The depth of field is determined by the beam diameter, intensity profile, and angle of intersection and is typically so large that for most purposes it may be considered infinite. Different symmetry patterns can be generated by controlling the number, amplitude, phase, wave vector, and polarization of the interfering beams.

IL has now been successfully applied for two decades to manufacturing of periodic structures for a wide variety of uses. Surface gratings were produced by interference of three beams or overlaying two sequential exposures at 90°.[88,89] Using additional beams in a single exposure or overlaying multiple exposures, 3D periodic structures have also been fabricated.[90−92] Theoretical works have predicted the appropriate laser beam configurations to achieve different periodic 3D structures (e.g., bcc, fcc, gyroid, or diamond symmetries).[93,94] Among them, only a few have been manufactured up to now. Four-beam IL has proven to give fcc[95,96] (Figure 8), simple cubic, bcc,[97] and diamond-like[98,99] patterns. The interference pattern of six equally spaced circumpolar linear polarized side beams and a circular polarized central beam has been used to fabricate spiral microstructures (Figure 8e).[100] The pitch and separation of the spirals was varied by changing the angle between the side beams and the central beam. Ten-beam IL has produced 3D periodic quasicrystals.[101]

IL has been preferentially applied in the field of photonic crystals (see section 13.7). This application requires resist materials with a refractive index > 2 to open omnidirectional band gaps. Therefore, structures formed from organic resists (e.g., SU-8 with $n = 1.6$) are not appropriate for this application. Instead, they have been used as templates for inorganic structures with a larger index contrast, whereas the SU-8 pattern is infiltrated with silica precursors and burned away. The remaining silica negative is then filled with silicon, and the silica is selectively etched away. Alternatively, hybrid sol−gel materials like ORMOSIL have been proposed as more suitable photoresists for these applications.[102]

IL offers numerous advantages over the previously discussed 3D lithographic strategies. It is both maskless and lenseless, minimizing cost and eliminating the optical aberrations associated with complex lens systems. IL can be scaled up to pattern fields as large as 1 m.[2] However, IL is limited to the fabrication of periodic structures and combinations thereof.[103]

3. Laser Scanning

The difficulty, cost, and delay associated with designing and making the masks strongly limits the flexibility of masked lithography, especially when a limited number of wafers are to be fabricated. Maskless techniques like laser prototyping constitute a suitable alternative. Laser prototyping makes use of UV, nanosecond pulsed, excimer, and Nd:YAG lasers for scanning the resist surface. Picosecond and femtosecond lasers have more recently raised interest by enabling 3D structuring with higher precision in a single step using two-photon polymerizable systems. These techniques can be applied to pattern larger areas than possible with photolithography. Since they also rely on photoactivation and development of resist layers, the same issues concerning

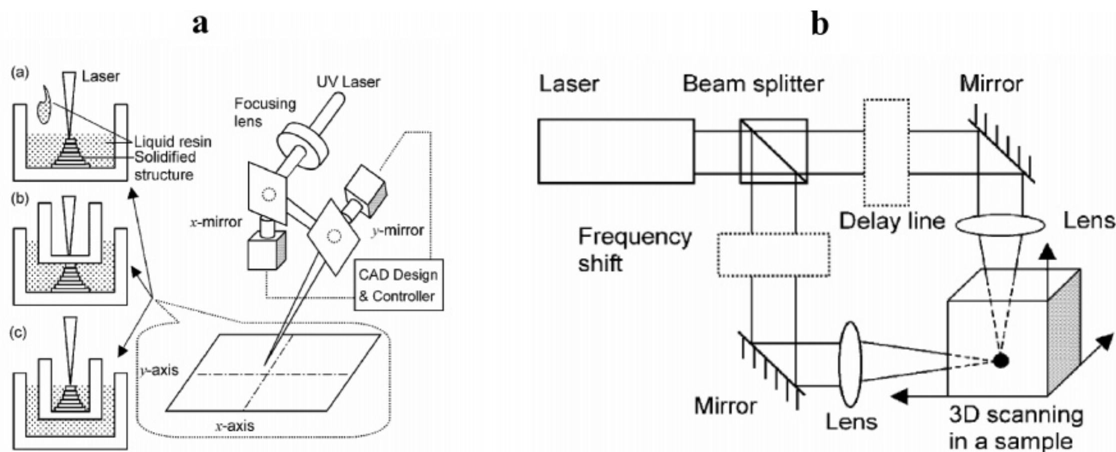

Figure 9. (a) Schematic of a laser rapid prototyping system for stereolithography. Writing is accomplished by mirror angle scanning. The height of the resist layer (and therefore the vertical resolution) can be controlled by film casting, surface regulation, or open surface method. (b) Schematic of a two-photon lithography system based on a cross-beam two-photon two-color scanning laser microscope. Pulses from two beams split from an identical laser output overlap in both time and temporal domains, so that a TPA process can be launched by simultaneously absorbing two photons. (Reprinted from ref 105 with kind permission of Springer Science and Business Media.)

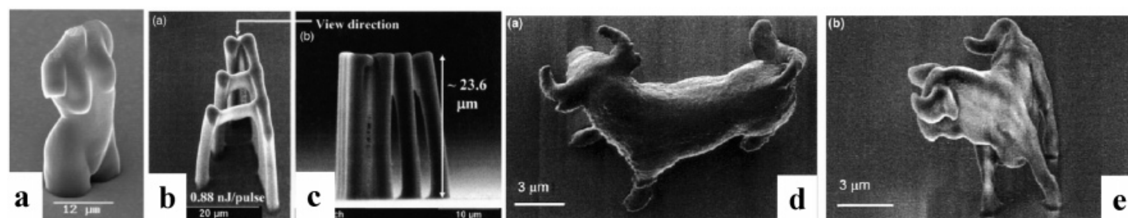

Figure 10. (a) 3D structures obtained by TPL from ORMOCER. (Reprinted with permission from ref 21. Copyright 2003 Wiley-VCH.) (b, c) Structures obtained by TPL from SU-8. (Reprinted with permission from ref 19. Copyright 2005 American Institute of Physics.) (d, e) Images of a microbull structure produced by (d) raster scanning and (e) vector scanning TPL. (Reprinted from ref 129, Copyright 2004, with permission from Elsevier.)

coating, development, and rinsing specified for photolithography in section 2 also apply to laser prototyping.

3.1. Stereolithography by Scanning Resist Multilayers

Stereolithography historically refers to the technology of creating 3D objects from computer-aided design patterns by adding and exposing photoresist layers to scanning UV lasers (Figure 9a). When the process is repeated sequentially after adding new resin layers on top of the cured one, 3D structures can be created with micrometer precision.[104]

3.2. Two-Photon Lithography (TPL)

Under sufficient light intensity, conventional electronic transitions caused by the absorption of a single photon of energy $h\nu_1$ may be produced by the simultaneous absorption of two photons, each photon providing one-half the energy of the transition ($h\nu_{1/2}$). This is the principle behind two-photon lithography (TPL), by which 3D structures can be fabricated using two-photon polymerizable systems and scanning pulsed femtosecond lasers.[105] Local activation of resist polymerization occurs by simultaneous absorption of two photons with wavelengths ranging in the near-infrared spectral region.

The probability of a molecule absorbing two photons simultaneously (defined by the two-photon absorption cross section, δ_{TPA}) is proportional to the square of the intensity of the input beam. This implicates that the two-photon absorption (TPA) process is intrinsically weak under normal light intensities relative to one-photon absorption and that TPL requires the use of very powerful light sources (lasers). A typical experimental configuration used in TPL is represented in Figure 9b. Two beams are split from a single laser source and overlap in time and temporal domains at defined locations of the resist film which define the final pattern.[105]

Although selection rules for single-photon and two-photon excitation are different, most resins that polymerize under UV exposure can undergo similar reactions by TPA, provided that the irradiation intensity is high enough. As examples, TPL fabricated pillars, planes, and cage microstructures from SU-8[19,106,107] and Ormocer[108] films and 3D nanostructures with lateral sizes as small as 120 nm[109] have been reported (Figure 10). However, typical initiators used in UV photoresists possess small δ_{TPA} and therefore yield a very low photoefficiency in TPL. This fact pushes the development of novel TPA dyes[110−113] and radical and acid generators[114−118] with larger δ_{TPA}. These will permit the use of less powerful, inexpensive lasers, making TPL a more reliable and economically feasible patterning method.

The key to the design of molecules with high sensitivity to TPA (δ_{TPA} >50 Göppert−Mayer (GM), where GM = 10^{-50} cm^4 s photon^{-1}) is a fundamental understanding of how δ_{TPA} depends on the molecular structure.[105] In general, molecules with large δ_{TPA} possess extended conjugation, polarizability, and high extinction coefficients for $\pi-\pi^*$ transitions. Systems such as phenylethenyl, fluorenyl, or polyenyl constructs have been demonstrated to be good candidates.[112,119,120] These molecules contain electron-donating and/or electron-withdrawing moieties separated by a

conjugated π-electron system. Increasing the conjugation length and the donor and acceptor strengths has been shown to enhance δ_{TPA}. Therefore, conjugated polymers[121,122] and multibranched structures[123] have become the target of TPA interest. In fact, the largest δ_{TPA} has been reported for a ladder-type polymer with low flexibility, high planarity, and good effective conjugation.[121,122,124]

Since the probability of TPA is proportional to the square of the intensity, TPA falls off as the fourth power of the distance from the focus. This implies that TPA is negligible at very short distances above and below the focal plane. As a consequence, processes based on TPA present much higher lateral resolution than those based on single-photon absorption. However, one should note that because of this nonlinearity, the voxel size depends more sensitively on laser intensity variation for TPA than in single-photon absorption, thus requiring better intensity control to maintain reproducibility.

Compared with other fabrication schemes, TPL offers the following advantages. (i) It has an intrinsic ability to produce 3D structures. (ii) It has large penetration depth, since common polymers have negligible absorption in the NIR region. This is especially important in HAR patterning, where intensity loss across the film thickness is a major issue in processes based on single-photon excitation (section 2.1.2.2). (iii) It offers high flexibility in the pattern design as no mask, mould, or stamp is required. (iv) Processing does not involve vacuum conditions, and the equipment is easy to operate and maintain.

TPL also has some limitations. The use of relatively long wavelengths worsens the spatial resolution of this technique due to the optical diffraction limit. However, this can be circumvented if the photopolymerization process has a threshold response to light excitation. This means that polymerization can only be initiated at the regions where exposure energy is larger than a certain threshold value. If this value is set higher than the intensity of high-order diffraction features, resolution limits based on diffraction effects will be overcome. This could be performed by formulating resists containing absorbing additives. Structures as small as 100 nm have been fabricated using this approach. Other methods based on nonlinear effects which may enhance feature resolution have also been predicted.[125−128]

Another drawback of TPL is that it is an inherently serial technique. Fabrication is a voxel-by-voxel process, and it may take minutes to hours to scan complex 3D structures. This problem effectively precludes direct mass production of structures using TPL. An interesting way to reduce scanning times is offered by the vector scanning mode.[129] In this approach, only the profile of the 3D structure is scanned and the material inside is further polymerized under UV lamp exposure after development. The laser scanning time is significantly reduced against the raster mode, where the whole volume that needs to be polymerized is scanned by the laser focal spot. Figure 10d,e shows a microbull structure fabricated by these methods.[129] Alternatively, fabrication can be sped up if a preexposure step is combined with subsequent TPA photopolymerization. The preexposure creates short-chain photopolymers in the unsolidified resin which effectively reduce the required dose for TPA photopolymerization or equivalently increase the maximum allowable scanning velocity. This approach has been applied to the fabrication of line patterns with widths ranging from 0.28 to 0.70 μm and aspect ratios ranging from 2.9 to 6.7.[130]

4. Serial Writing with Charged Particles

Serial writing with charged particles (electrons or ions) is a maskless lithographic technique with low throughput and only suited for small area fabrication. It offers a great flexibility in the feature design, and for this reason it is frequently used in academic research.

4.1. Electron Beam Lithography

Electron-beam (e-beam) lithography uses an electron beam (typically 10−100 eV) to expose an electron-sensitive resist. The impinging electrons generate a cascade of secondary electrons with relatively low energy which form free radicals and radical cations. Deactivation of these intermediate species through fragmentation or reaction with the matrix is the basis for the chemical change (chain scissions) in the resist film upon exposure. Although electron wavelengths on the order of 1 Å can be easily achieved, electron scattering in the resist limits the attainable resolutions to >10 nm. The small penetration depth of low-energy electrons restricts the use of this patterning technique to layers with thickness below 100 nm.

Many resist materials developed for optical lithography can also serve as e-beam resists, although the electron-beam radiation chemistry can differ substantially from the photolytic path, and there is poor correlation between photosensitivity and e-beam sensitivity.[131] PMMA was one of the first polymers recognized to exhibit sensitivity to electron-beam radiation and, in fact, the most frequently used system in e-beam lithography. Lines and spaces with dimensions down to 50 nm and aspect ratios up to 5 have been obtained by this technique.[132]

3D nanofabrication using e-beam lithography has been demonstrated in combination with a two-axes-of-rotation drive system.[133] In this approach, the substrate with the spin-coated resist film is built on a sample holder which has a positional accuracy of a few milliradians and rotates the sample while e-beam writing. A special height-measurement system helps to focus the e-beam on the surface of a rotating or nonplanar sample, enabling high patterning resolution. Pillars with 100 nm diameter and various shapes and aspect ratios below 3 were written on a micrometer-sized sphere by this method (Figure 11a,b).

4.2. Ion Beam Lithography

High-energy ions, such as Ga^+, H^+, or He^+, are able to deeply penetrate the resist material with well-defined paths. The penetration depth depends on the ion energy; e.g., the penetration of a proton beam of energy 1.0 MeV in PMMA is 20 μm, whereas a 3.5 MeV proton will penetrate 160 μm. During its trajectory in the material, the probability that an ion interacts with an electron is several orders of magnitude larger than for nuclear scattering. Because of the high mismatch in mass between the ion and the electron, ion−electron interactions do not result in any significant deviation in the trajectory of the ion from the straight-line path. These features allow ion beam writing to fabricate HAR structures with smooth and vertical side walls and high packing densities.[134] Figure 11c shows an example of a 10 μm thick SU-8 film written with a proton beam with lines with 60 and 120 nm width supported by pillars with 2 μm diameter. This configuration ensures the integrity of the narrow walls with aspect ratio > 160 during development. AFM charac-

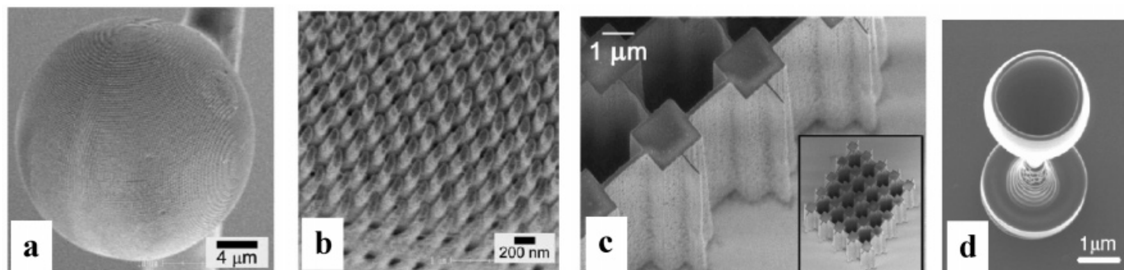

Figure 11. Lithography with high-energy beams: (a) PMMA sphere patterned with 3D arrays of 200 nm pillars, (b) by electron-beam lithography. (Reprinted from ref 133, Copyright 2004, with permission from Elsevier.) (c) Proton-beam fabricated SU-8 pillars of 10 μm height and 2 μm width. Pillars are supported by lines with 60 and 120 nm width (aspect ratio > 160) to ensure stability during development. (Reprinted with permission from ref 135. Copyright 2003 American Institute of Physics.) (d) FIB milling: wine glass made by 3D carbon deposition using a FIB and phenantrene gas. Diameter 2.75 μm, height 12 μm, fabrication time 600 s. (Reprinted with permission from ref 142. Copyright 2005 IOP Publishing Limited.)

terization of the roughness of these structures gave a sidewall roughness of 2.5 nm.[135]

Similar to e-beam writing, the low-energy secondary electrons trigger the chemical reactions that lead to lithographic imaging. Due to the efficient nature of the interaction, ion beam writing does not require specially developed amplified resists. In fact, in ion beam lithography a high-sensitivity resist exposed at the correct dose might require so few ions that statistical fluctuations in the number of ions per pixel can lead to poor dimensional control. HAR voids of 100 nm width and 2 μm depth have been obtained by proton beam lithography in positive resists, such as PMMA, and negative resists, such as SU-8.[136] Tilted structures with submicrometer resolution have been obtained by varying the incidence angle of the ions.[137,138]

4.3. Scanning Probe Resist Lithography

Scanning probe microscopes (SPM) are capable of controlling the movement of an atomically sharp tip in close proximity to or in contact with a surface with subnanometer accuracy by using piezoelectric positioners. The electrons emitted from the SPM tip can be used to expose a resist the same way e-beam lithography does. The exposure is done by moving the SPM tip over the surface while applying a bias voltage that is high enough to produce emission of electrons from the tip (a few tens of volts). Writing speed is very slow, but precision is very high. The emitted electrons induce chemical changes locally at the resist film, and development affords patterns with nanometer resolution. In particular, lines of 20 nm thickness and an aspect ratio of 10 have been reported.[139]

5. Micro- and Nanomachining

Machining involves milling material from surfaces in a controlled way. It can be combined with deposition of materials at certain surface locations to form complex patterns. Machining is a resistless patterning method and can be applied to many different materials.

5.1. Focused Ion Beam

An ion beam can be used as a nanomachining tool.[140] Gallium ions emitted from the ion source are focused by an electric field and impinge on the polymer surface placed in vacuum. Rotation of the specimen allows milling of 3D shapes with the focused ion beam (FIB). To make an accurate shape, redeposition of the material is avoided by reaction with a reactive gas. The gaseous compound is then evacuated from the specimen chamber by a vacuum pump. While gallium ions collide with the specimen surface, secondary electrons are detected, enabling simultaneous imaging of the milled structure.

By tilting or rotating the sample stage during milling, FIB milling can be used to generate tilted patterns.[141,142] Additionally, when phenanthrene gas is used as a source gas, diamond-like carbon films can be deposited on the surface of the specimen in three dimensions. The minimum dimension of this 3D shape is decided by the material gas concentration and the flight distance of a secondary electron. Figure 11d shows an example of a microwine glass made by this method.[142]

FIB milling has a high spatial resolution, but it is a relatively slow, serial patterning process. Conventional FIB has a material removal rate of 1−10 atoms per incident ion, which is approximately one million times less efficient than the removal rate per incident proton for proton beam writing.

5.2. Scanning Probe Nanomachining

A substrate can be mechanically nanomachined using SPM tips acting as engraving tools and displacing resist material from certain regions of the substrate. The process requires direct contact between the surface and the tip. Writing is facilitated by heating the tip above the glass-transition temperature, T_g, of the polymer resist. The resolution of this method is limited by the tip size and the resist thickness and typically varies from 0.1 nm to micrometer size. Contamination and wear of the tips, and thus the degradation of the edge resolution with time, are issues to be considered because high loading forces may be involved. For thick films, nanomachining with scanning probes results in formation of holes or trenches surrounded by walls consisting of displaced material. Fabrication of real HAR structures is therefore limited.

This approach has been applied to SPM-based high-density data storage in polycarbonate (PC) films.[143] The tip is brought in contact with the PC surface and heated above its T_g. By exerting a small force on the sample, local melt pits are formed in the PC film. The throughput of the process can be increased by using arrays of tips.[144−147] With the development of larger arrays with individual control of force, vertical position, and current advances, we might see these techniques becoming standard fabrication processes in the future.

6. Direct Writing and Material Deposition

The term direct writing describes fabrication methods that employ a computer-controlled translation stage which moves

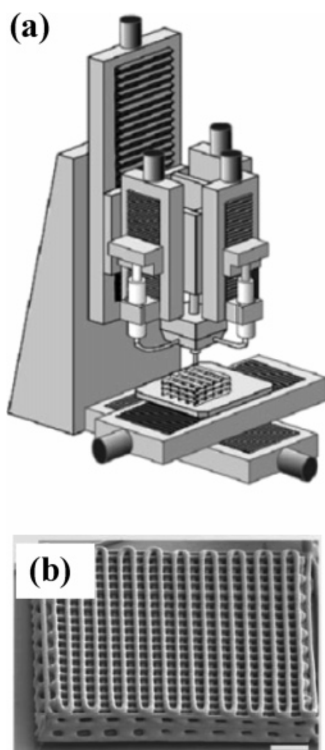

Figure 12. Direct writing. (a) Apparatus for robotic deposition apparatus. Inks are housed in individual syringes mounted on the *z*-axis motion stage and deposited through a nozzle onto a moving *x*−*y* stage. (Reprinted with permission from ref 149. Copyright 2002 Wiley-VCH.) (b) 3D periodic structure (10 layers) fabricated by deposition of a polyelectrolyte solution with a filament diameter of 1 μm. Scale bar corresponds to 100 μm. (Reprinted by permission from Macmillan Publishers Ltd: Nature (ref 148). Copyright 2004.)

a material delivery tool across a substrate. 3D patterns with controlled architecture and composition are created by sequential, layer-by-layer deposition of a fluid which solidifies in a posterior step (Figure 12a). The delivery tools can be ink-jet print heads or filament microextruders. Appropriate rheological behavior of the ink (viscosity, viscoelastic properties) is the main restriction of this method. This implies that a wide range of materials can be used. The technique enables writing patterns with lines in any arbitrary design by programming the movement of the writing head. Submicrometer structures made from polyelectrolyte solutions (Figure 12b) and colloidal suspensions have been reported.[148−150] Feature sizes range from hundreds of micrometers down to the submicrometer scale.

7. Moulding

Photolithography cannot easily be performed on polymeric substrates (e.g., those used in microfluidics or plastic electronics) or curved substrates. It cannot pattern large areas (e.g., 1 m^2) with high resolution in a single step. In addition, the chemicals involved (resist etchants and developers, solvents, etc.) are incompatible with many interesting organic electronic materials. It also has the disadvantage of high capital and operational cost. As a consequence, new patterning techniques enabling micro- and nanoprocessing of plastics have been explored during the last 10 years. Some of the oldest and conceptually simplest forms of plastics macroscale processing (embossing, moulding, stamping, or printing) are now being re-examined for their potential adaptation to nanofabrication.

Moulding has been known for centuries as a process for replicating service tools. Here the surface relief of a well-engineered hard master tool (also named mould or stamp) is transferred into a soft material. Several methods have been developed in the past decade to obtain micro- and nanostructured polymer surfaces using moulding strategies. These can be classified according to the softening/hardening principle involved: (i) temperature-based processing (hot embossing or nanoimprint lithography (NIL) and thermal injection moulding thermoplastic polymers), (ii) light-initiated polymerization (UV-NIL and step and flash NIL), (iii) thermal activated polymerization ("soft lithography"), and (iv) solvent-based processing. An overview of the processing steps involved in these technologies is given in Figure 13.

The great advantage of moulding is that it does not use energetic beams, and therefore, its resolution is not limited by the effects of wave diffraction, scattering and interference in a resist, or backscattering from the substrate. The same mould can be used repeatedly to fabricate a large number of nanostructures, and therefore, this method can be scaled up and has the capability of large-area, low-cost patterning. Resolution is mainly determined by the fabrication method used to prepare the mould and the mechanical strength of the embossed polymeric material. Prerequisites for moulding are the availability of a suitable mould and the possibility of removing the moulded material from it without damage to either the replica or the mould. The latter requirement especially holds for micro- and nanomoulding of HAR structures since high mechanical friction is generated due to the large effective contact area. For the same reasons, moulding in its simplest version is not suitable for fabrication of tilted or re-entrant structures. However, if combined with transfer processes, additional possibilities are opened. These will be reviewed in the next sections.

7.1. Mould Fabrication

Mould fabrication is the most time- and cost-consuming step and usually constitutes the biggest limitation in the industrial application of moulding to patterning surfaces.[23] For this reason, a master is usually fabricated and copies of the master in other hard materials are preferentially used as moulds for imprinting. In this way, the risk of mould damage and loss is reduced.[151] Masters are typically fabricated from silicon or silicon dioxide by reactive ion etching technologies (RIE) or deposition of nickel or other metals on patterned resist substrates (LIGA process).[152] Masters for UV moulding, which need to be transparent to UV light, are usually made from etched quartz, etched chrome on quartz substrates, or patterned HSQ films on quartz substrates.

Fabrication of HAR silicon masters by RIE usually starts with patterning the desired relief structure at low aspect ratio by e-beam lithography using an organosilicon resist film. After development, the wafer surface is dry etched in oxygen plasma. Under these conditions, the organosilicon polymer is converted into a thin layer of refractory silica which acts as an etch barrier and allows site-selective etching. Alternatively, a bilayer system can be used. In this case, the wafer is coated first with a thick, planarizing layer of hard baked organic resist followed by application of a thin organosilicon resist. The silicon layer is irradiated and selectively removed from either the exposed or the unexposed areas in a wet developing process, providing a protective stencil for transfer of the resist image to the planarizing layer by RIE. Modern dry etching processing allows precise control over the

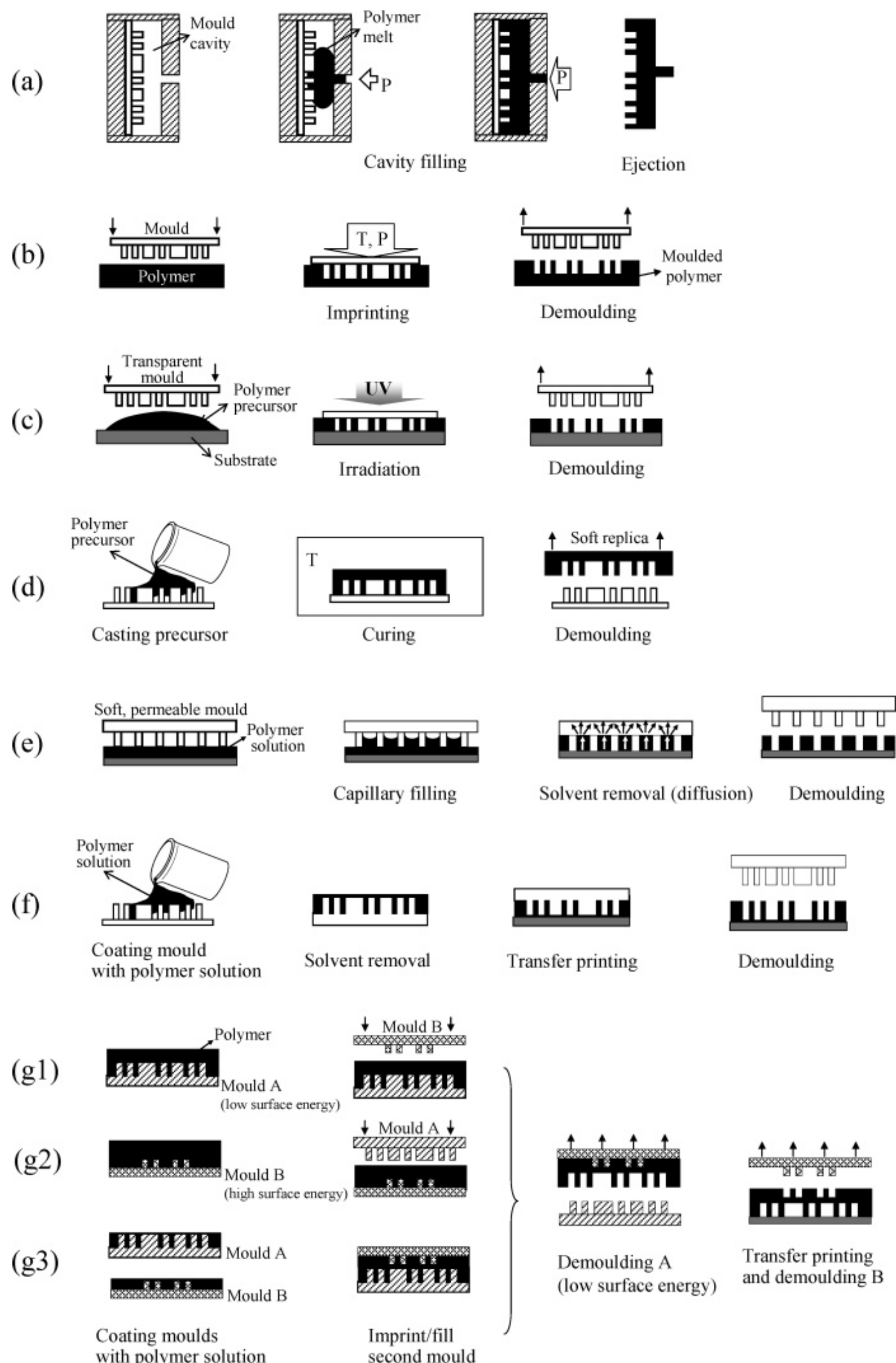

Figure 13. Comparison of different moulding processes. (a) Injection moulding (NIL) (b) hot embossing or nanoimprint lithography. (c) UV NIL. (d) Soft lithography. (e) Solvent-assisted moulding. (f) Reversal imprinting or transfer moulding. (g) Multilayer printing: "duo-mould" approach. The schematic g1, g2, and g3 represents three variants of this process.

dimensions, shape, and aspect ratio of the etched channels. As an example, aspect ratios exceeding 15 have been reported in single lines with 800 nm height and 40 nm width and close-packed lines with 155 nm height and 25 nm width using the bilayer process.[153] The use of dry development schemes avoids collapse of the HAR structures that occurs in wet development due to capillary effects (section 2.1.2.4).

Alternatively, HAR X-ray lithography can be performed on thick PMMA layers, and the resist-patterned surface can be electroplated in a nickel galvanic bath. After resist stripping, a nickel master is obtained.[154,155] This method is known as "Lithographie-Galvanoformung-Abformung" (LIGA) technology and has been established as a useful method for production of HAR masters but so far lacks the commercial viability due to the high cost related to the exposure procedure.[156] Typically, the sidewalls of the HAR structures of a LIGA-fabricated mould are vertical, planar, and very smooth. However, tapered moulds with tilted walls that favor demoulding can also be fabricated by tilted or rotating X-ray exposure.[73]

Rapid 3D microfabrication of masters has also been achieved by etching poly(tetrafluorethylene) (PTFE) using synchrotron radiation.[157] Due to its thermostability, resistance to chemicals, and very low adhesion, PTFE may be one of the most suitable materials for moulding soft polymer melts. The etching rate is on the order of 100 μm min^{-1}. This means that processing for a 1000 μm height microstructure takes about 10 min, much shorter than the deep X-ray lithography

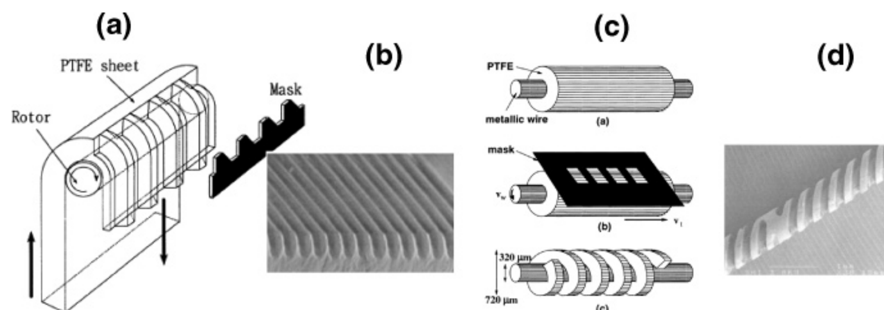

Figure 14. Experimental configuration for the production of PTFE masters by etching using synchrotron radiation: fabrication of patterned PTFE sheets (a, b) and fabrication of rods patterned with helical structures (c, d). (Reprinted from ref 157, Copyright 2004, with permission from Elsevier.)

involved in the LIGA process. Due to the directional emission of synchrotron radiation, HAR structures are also created easily. Moreover, dry etching avoids the problem of structure collapse, since no solvent development is required. Some experimental setups are represented in Figure 14. The PTFE sheet is attached to a cylindrical rotor behind a mask. Using a saw-tooth mask and rotation during irradiation creates long line and space patterns of trapezoidal shapes parallel to the synchrotron light (Figure 14a). In addition, helical structures can be fabricated by rotating the wire and simultaneously moving it parallel to the wire axis (Figure 14b).

7.2. Demoulding: Mould Treatment

During demoulding, pattern damage due to adhesion, friction (because of surface roughness), trapping of the polymer (because of negative slopes of cavity sidewalls), or mechanical stress (shrinkage during cooling) can occur.[158] As a result, the polymer structures or parts of the wall profile are either ripped away or deformed during demoulding. For HAR structures, the shear usually results in a stretching of the total structure when the stamp is pulled away.[159] This may be avoided using moulds with low sidewall roughness and tapered geometries.[73]

Antisticking surface coatings can also be used to facilitate mould release. These surface layers lower the surface tension of the mould surface and reduce adhesion. Different strategies can be employed.[73] (i) Use of fluoropolymer films deposited (noncovalent bonded) on the stamps with the help of a CF_4/H_2 or CHF_3 plasma treatment. These films are only weakly bonded to the substrate and need to be renewed after a few moulding processes. (ii) Treatment of silicon masters with perfluorosilanes, e.g., 1*H*,1*H*,2*H*,2*H*-perfluorodecyl-trichlorosilane.[160] (iii) Treatment of Ni or alumina stamps with fluorinated alkyl phosphoric acid derivatives.[161] The wearing and stability of the nonsticky coating layer strongly influence the mould durability. Alternatively, moulds made of fluoropolymers, such as Teflon (T_g = 240 °C), can be used. These moulds are fabricated by casting a fluoropolymer solution on the master and drying off the solvent or imprinting the fluoropolymer melt.

Other interesting strategies to facilitate demoulding include slow directional demoulding, introduction of pressed air into the cavities, or use of multilayer polymer films with antiadhesive properties.

7.3. Embossing Thermoplastic Materials: Nanoimprint Lithography (NIL)

The basis of hot embossing (or NIL) and thermal injection moulding is the shaping of thermoplastic polymers by conformal contact of a nanostructured mould using heat and pressure.[162] The viscosity of the material is significantly reduced by increasing the temperature of the polymer and/or mould, so that pressure application causes the polymer melt to flow into the cavities of the mould. The melt is hardened by cooling, and the mould can then be separated from the polymer leaving a stable reproduction of the relief.

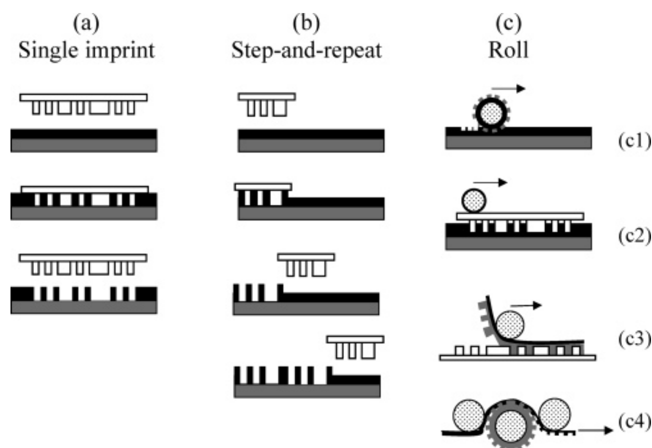

Figure 15. Available processes for large area NIL: (a) single imprint, (b) step-and-repeat, (c) different ways of roll NIL: (c1) imprints using a cylinder mould; (c2) a flat mould is used in conjunction with a roller to press it against the polymer film; (c3) like c2 but using a flexible backing; (c4) roll-to-roll NIL.

Injection moulding and hot embossing differ in their applications and process conditions (Figure 13a,b). In injection moulding, a polymer melt with relatively low viscosity is injected with high pressure through a nozzle into a closed cavity containing a structured mould insert. In NIL, whole polymer sheets are compressed between the plates of an embossing press against the mould.[163,164] In theory, the resolution limit of these techniques is met when the cavity size approaches the radius of gyration of the polymer chain. In fact, polymer surfaces patterned with 25 nm features were already reported in the first stages of the development of these technologies.[163,165]

Moulding nanosized patterns over large areas by NIL requires homogeneous temperatures and pressures during heating and cooling (to avoid differences in penetration of the stamp in the polymer layer) and severe accuracy in the alignment of the master and the film over the whole imprinting area. Different configurations (Figure 15) have been developed for imprinting large areas: single-imprint, steppers,[166,167] and rollers.[168] For any of these techniques the process conditions (temperature, time, pressure) vary depending on the pattern geometry, e.g., distribution of large and small structures over the wafer area, the area of the processed

wafer, and the geometry of the structures (radius of curvature, free-standing structures, or connected structures).

In single-imprint processing (Figure 15a), the embossing master and planar polymer substrate are mounted between heating plates that also contain cooling channels where high heat capacity oil is circulated in the cooling phase. This configuration allows heating and cooling of master and substrate independently. At the beginning of the embossing cycle, both are heated separately in a vacuum chamber to a temperature above the T_g or the melting temperature, T_m, of the polymer material. The master is brought into contact with the substrate and then embossed with a sensor feedback-controlled force. Still applying the embossing force, the master−substrate sandwich is cooled to temperatures slightly below T_g or T_m before the embossing tool is mechanically removed from the substrate. This process has been used to imprint 2 in. wafers with 100 nm features in less than 2 min ("wafer-scale NIL").[169,170]

A high-throughput variant of the embossing equipment has been developed that uses semitransparent moulds and flash heating by an infrared lamp. Heating occurs only in the polymer film. As a result, the subsequent cooling involves less energy transfer and proceeds faster. Patterns with 80 nm wide lines and aspect ratios exceeding 5 were obtained on poly(vinyl alcohol) (PVA) films.[171]

In step-and-repeat NIL, large areas are imprinted using a small mould and a multistep procedure. First the mould imprints, then moves to a new area of the wafer and imprints again (Figure 15b).[167] The process is repeated until the entire wafer is imprinted. This technology offers two main advantages: alignment accuracy is higher in small area imprinting, and the expensive fabrication of large moulds is avoided.

In roll NIL, a cylinder mould is used for embossing. There are several variants of roll NIL, as shown in Figure 15c.

(i) A cylindrical mould (made by bending a thin metal film mould around a smooth roller) is pressed into a thin film of resist, and the rotation of the roller pushes the sample forward (Figure 15c1). Arrays of PC nanopillars with diameters between 30 and 100 nm and aspect ratios > 2 produced by this method have been reported.[172]

(ii) A flat mould is placed directly on the substrate, and a smooth roller is rotated over the mould (Figure 15c2). The slight deformation of the flat mould under the pressure of the roller imprints patterns in the resist.

(iii) The polymer is supported by a flexible backing and pressed into the flat mould using a roller (Figure 15c3). The roller also assists demoulding.

(iv) A polymer foil is continuously embossed while being squeezed through heated rolls, one of them being covered with a surface-structured metal shim (roll-to-roll patterning, Figure 15c4). The foils are normally several tens of micrometers thick. The bending of the shim helps to reduce the contact area and processing times and might even ease demoulding. Roller imprint machines have the advantage of better uniformity, less imprint force, simple machine construction, and the ability to continuously use a mask on a large substrate.

For each method, the roller temperature is set well above the T_g of the polymer, while the temperature of the film and support are set below T_g; therefore, only the area in contact with the roller is heated and imprinted.

7.3.1. HAR Structures Produced by NIL

Imprinting HAR structures with NIL is complicated since the polymer needs to flow over long distances to fill up the cavities. In addition, due to stresses produced by shear and tensile forces at the mould−polymer surface during master release, HAR structures can easily break during demoulding.[173] This means that HAR imprinting requires a careful balance between good resist−mould wetting properties for accurate replication and good mould release properties for demoulding. Typically PMMA, PC, and polystyrene (PS) are used for NIL, although these materials hardly satisfy the seemingly contradictory requirements. A great opportunity exists for developing new polymer formulations more suitable for HAR NIL applications.[174] Block copolymers possessing dual surface properties through microphase segregation will certainly be exploited to solve this problem.[175]

The demoulding temperature must be selected carefully. High temperatures favor faster demoulding and increase throughput but compromise the mechanical integrity of the features and may result in elongated and collapsed structures. Temperatures slightly below T_g are recommended and have permitted demoulding PMMA pillars with a 200 nm diameter and an aspect ratio of 2 (demoulding temperature 90 °C). Pillars with an aspect ratio of 4 were also fabricated but could not be demoulded without severe damage.[176] Other authors succeeded in forming 1 μm height PMMA nanopillars with diameters ranging between 250 nm and 1 μm by imprinting a 500 nm PMMA film at 10 MPa and 200 °C and demoulding at room temperature.[177]

Low mechanical stability of the moulded features is another concern. This can be improved using semicrystalline or liquid crystalline (LC) polymers as resists. The hard crystalline domains enhance the mechanical stability of the material and allow fabrication of features with higher aspect ratio. In addition, material flow during the cavity filling process may favor the alignment of the macromolecular chains along the feature long axis. This will result in enhanced crystallization and consequently improved axial mechanical properties.[178]

7.3.2. Secondary Structures by NIL

Figure 16 shows the forces acting on the polymer film in NIL and the resulting flow profile during cavity filling. Initially, the melt flows into the cavity from the borders and wets the cavity walls. The material located at the central region of the cavity is under compressive stress, and this causes buckling of the film (formation of a central region with a convex profile). Periodic capillary waves at the surface of the melt are developed as a consequence of electrohydrodynamic instabilities resulting from charges in the polymer and the image charges on the mould, with boundaries at the cavity walls (see section 10). Capillary wave peaks grow sequentially from the boundary, eventually touching the cavity top. Figure 16 shows the formation of one central peak, but if the cavity is large enough, the process may continue until an array of pillars is formed next to the boundary. At the end of the embossing process, complete filling is achieved when the surface properties and processing parameters (pressure and temperature) have been properly selected.[159,179]

The flow profile is a result of the balance of electrostatic interactions, capillary action, and surface energy minimization effects under the external pressure. This balance can be controlled by the processing parameters and the mould geometry and may be exploited to generate a second structurization level of the cavity space.[179,180] In this context,

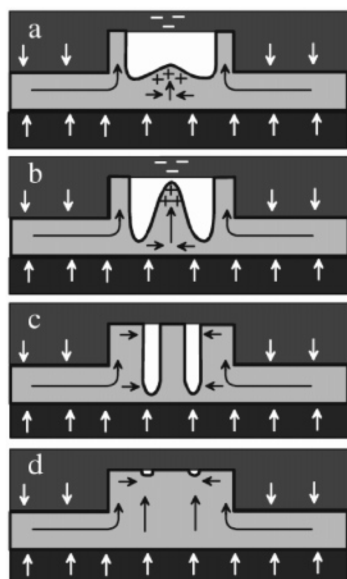

Figure 16. Dynamics of polymer flow into a cavity during NIL: (a) polymer melt flows up the cavity walls; (b, c) electrohydrodynamic instabilities result in a capillary wave peak growing in the center of the cavity until it touches the cavity top; (d) polymer melt continues filling the cavity to completion. (Reprinted with permission from ref 179. Copyright 2005 IOP Publishing Limited.)

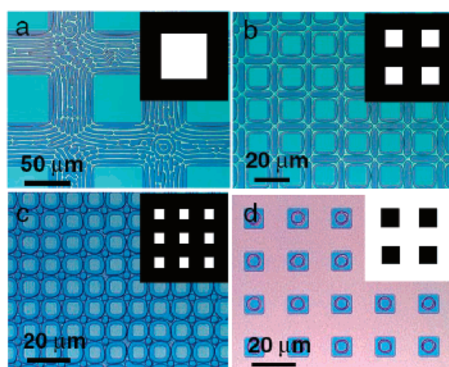

Figure 17. Mound structures obtained for different mould geometries during incomplete cavity filling in NIL. All structures are 75 nm high. The insets show original mould designs where black corresponds to cavities. (Reprinted with permission from ref 179. Copyright 2005 IOP Publishing Limited.)

arrays of periodic pillars within the mould cavities have been generated by hot embossing PMMA.[179] The shape and size of the pillars depends on the embossing stamp geometry and tend to align along structure boundaries. Figure 17 depicts these results.

7.3.3. 3D Patterns with NIL

A large variety of vertical profiles can be imprinted into polymers by NIL, but fabrication of structures oriented in any direction differing from normal to the substrate or structures with re-entrant corners is difficult since they would be damaged during demoulding.[181] The combination, however, of NIL and other patterning techniques has allowed the fabrication of the 3D structures. Patterns of 2 μm wide and ~10 μm deep concentric rings fabricated by X-ray lithography were superposed onto imprinted PMMA hemispheres (Figure 18).[129,182] Undoubtedly, such combinations hold great fabrication potential and should be thoroughly exploited in the future.

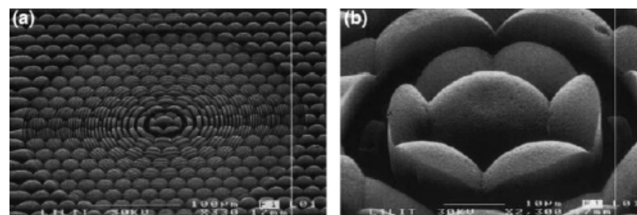

Figure 18. 3D patterns obtained by superposition of imprinting and X-ray lithographic steps on a PMMA resist layer. (Reprinted from ref 129, Copyright 2004, with permission from Elsevier.)

7.4. Moulding UV-Sensitive Materials: UV NIL

UV NIL makes use of UV-curable polymeric precursors for imprinting. The material is coated onto a substrate and pressed against a UV-transparent mould (made of quartz, indium−tin oxide (ITO),[183,184] or HSQ[185,186]). UV irradiation causes hardening of the patterned film which can be subsequently demoulded (Figure 13c).

Some advantages of UV NIL vs thermal NIL can be pointed out. (i) UV curing is rapid (its time scale can be as short as tenths of a second). Therefore, high throughput can be achieved. (ii) UV NIL can be performed at room temperature and low pressure (<1 bar). This is critical for moulding polymer films onto delicate substrates (e.g., fragile indium tin oxide-coated substrates). The mechanical properties of the mould are less stringent, and such moulds can be obtained economically by replicating a master. Poly(dimethylsiloxane) (PDMS) elastomers, being transparent within the 340−600 nm region, have already been used as mould materials for UV NIL.[187] (iii) The final properties of the imprinted polymer can be fine tuned by the mix ratio of the components or the irradiation time. (iv) The low viscosity of the polymeric precursors facilitates filling of HAR cavities.

Acrylates are most often used for UV NIL formulations, mainly because of their commercial availability, low viscosity, and capability for rapid photopolymerization via radical propagation. However, oxygen is a strong radical inhibitor in this process, and this limits the application of acrylates in UV NIL. Vinyl ethers have been suggested as prime candidates to replace acrylates.[188] Their polymerization proceeds via a cationic mechanism which is insensitive to oxygen and very rapid. In addition, the vinyl ether monomers have significantly lower viscosities than acrylates, and cavity filling proceeds more rapidly. Vinyl ether formulations adhere more strongly to moulds and double the required force for mould release. This limitation is overcome by the higher tensile strength of vinyl formulations (up to five times stronger than acrylates).

During UV curing, the materials volume shrinks between 3% and 15%, and this facilitates demoulding. In fact, UV NIL deliberately uses monomers with high shrinkage upon cross-linking (e.g., trimethylolpropane triacrylate). An optimum level of shrinkage has been demonstrated to exist at which the stress experienced by the polymer during demoulding is minimized.[189] This means that irradiation times and doses have to be optimized for each material and pattern type in order to achieve appropriate mechanical properties and shrinkage of the UV-cured structures. Long UV curing times may cause excessive shrinkage and brittleness of the resin. This increases the likelihood of cracking or breaking during demoulding. Insufficient UV curing leads to low cohesive strength of the polymer. This increases the probability of pattern distortion during demoulding and collapse of structures.[190] Several articles provide a profound analysis

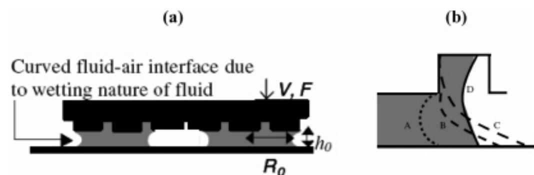

Figure 19. (a) Representation of the forces acting in SFIL: as the mould moves toward the substrate at a velocity V, the curvature of the fluid−air interface exerts a capillary force that pulls the mould to the wafer. R_0 is the initial drop radius, and h_0 is the initial gap height between the mould and the wafer. Applied forces, F, and viscous forces exerted by the fluid balance the capillary force. (b) Simulation of flow profile during cavity filling in SFIL: (A) fluid−air interface as it reaches the lower corner of a feature. (B) The upper contact line pins to the corner, while the bottom contact line moves along the wafer surface. (C) The upper contact line moves vertically to the top corner of the feature. At this point, the interface is able to reconfigure into a stable low surface energy conformation (D). The flow front arrest at the edges depends on the drop volume, aspect ratio, and edge geometry of the cavity and the velocity, force, and time of the imprinting step. (Reprinted from ref 197. Copyright 2005, with permission from Elsevier.)

of the factors for successful replication and demoulding of HAR structures with UV NIL. The influence of surface roughness, vertical walls and surface energy of the mould, peeling angle, UV polymerization time, resin transparency, and addition of high shrinkage monomers has been analyzed and reported.[189,191,192]

The combination of UV NIL with the step-and-repeat processing technique has given rise to "step and flash imprint lithography" (SFIL) as a high-throughput, low-cost approach to generate relief patterns over large areas.[193,194] In SFIL, the photopolymerizable precursor is not spin coated but delivered in the form of small drops on the substrate. The multidroplet geometry seems to favor filling of the mould cavities.[195] When the mould approaches the coated substrate, the fluid droplets spread out and fill the cavities under capillary action. Next, the mould is pressed against the substrate to close the gap. The assembly is irradiated with UV light which cures the photopolymer to make it a solidified replica. Because of its ability to pattern at room temperature and low pressure, the mould can be stepped to pattern the whole wafer area as in a stepper lithography tool. Already in the early publications of SFIL, 60 nm PMMA with an aspect ratio of 6 and 80 nm lines with aspect ratio 14 were reported.[196]

Fluid dynamics is an important issue in SFIL (Figure 19).[197] Attractive capillary forces between the mould and the wafer balance the repellant viscous forces generated during imprinting. Issues governing fluid flow of the liquid monomer between the substrate and the mould include the following: number of initial monomer drops and relative volume of drops dispensed, flow front arrest at edges of high aspect ratio features and mould edges, air entrapment during feature filling, mould velocity and force used for imprint, and imprint time. Recent studies explore the imprint time results for increasing numbers of monomer drops and for various patterns of drop dispense for a perfectly rigid mould.[197]

7.5. Soft Lithography

The term soft lithography is applied to a collection of pattern−replication methods which rely on an elastomeric mould.[198] This is a replica of a micro- or nanostructured hard master and prepared by casting and thermal curing a liquid prepolymer (usually PDMS) on the master (Figure 13d). The PDMS mould can be considered the final moulded structure, or it can also be used as a mould (stamp) in a subsequent moulding process. Its elastomeric character allows it to be released easily from the master (or moulded polymer), even in the presence of complex and fragile structures. Moreover, its low interfacial free energy and chemical inertness reduce irreversible adhesion.

Structures with 3 μm lateral dimensions and aspect ratios up to 7 have been obtained by moulding PDMS onto SU-8 lithographic patterned surfaces;[199] posts with diameter 30 μm and aspect ratios up to 19 were obtained by moulding PDMS onto laser-machined wax films;[200] and walls with thickness 20 μm and aspect ratio 15 were obtained from X-ray LIGA moulds.[201] The accuracy of soft lithographic replication with PDMS precursors is, in principle, only limited by the size of the precursor molecules and the atomic-scale separation of the master and mould (a lower limit of 0.1−0.2 nm for van der Waals contacts has been estimated).

Soft lithography can be applied to large area fabrication and plastics-based manufacturing. It is relatively cheap and flexible in terms of geometry and curvature of the surfaces and master material and has a controlled surface chemistry which can be modified by plasma treatment and reaction with organosilanes. This is especially important when complex organic functional groups as needed in chemistry, biochemistry, and biology are involved. For these reasons, soft lithography constitutes an interesting alternative to photolithography and overcomes some of its limitations.

The low Young's modulus of PDMS limits its use in HAR patterning of submicrometer structures.[198] Gravity, adhesion, and capillary forces exert stress on the soft elastomeric features and may cause them to collapse, generating defects in the pattern that is formed (Figure 20). The geometrical conditions for pattern stability have been predicted with different theoretical models.[83,202−208] A number of alternative materials have been proposed to improve the mechanical stability of the elastomeric stamp in applications involving HAR submicrometer features: composite PDMS,[206,207,209] bilayer PDMS,[204,207,210] photocurable PDMS,[209,211] polyolefins,[212] PDMS with polymer-reinforced sidewalls,[213] fluoropolymers,[214−216] photocurable perfluoropolyethers,[217] photocurable fluorinated organic−inorganic hybrids,[214,218−222] and photocurable polyurethane acrylates.[223,224]

Patterning techniques based on flexible PDMS stamps for moulding fall under the term "soft moulding" and present the following advantages over moulding with hard masters.[3] (i) The elasticity and low surface energy of the PDMS mould facilitate the demoulding step. (ii) The use of an elastomeric mould offers the possibility to manipulate the size and shape of features present on the mould by mechanical deformation. (iii) A range of materials and topographies can be moulded. (iv) Soft and low-cost masters enable large-area and high-throughput processing. (v) Multiple PDMS moulds can be inexpensively generated from a single master, and therefore, this technique is highly appropriate for applications where low costs are required. The resolution of soft moulding is limited by the 1 nm surface roughness of the PDMS mould.

Different soft moulding processes have been reported in the literature depending on the material to be moulded by the PDMS stamp and the hardening mechanism, mainly UV moulding of photocurable precursors, solvent-assisted moulding of polymer films, and moulding in capillaries.[2,3] Given the low mechanical stability of the elastomeric stamp, soft

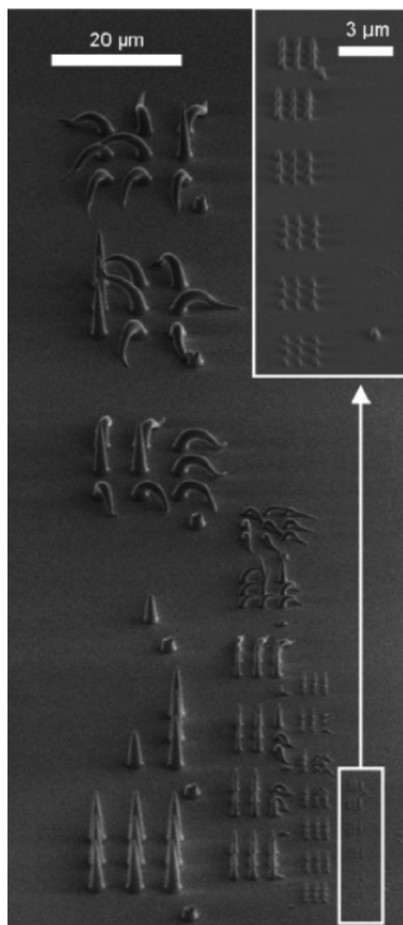

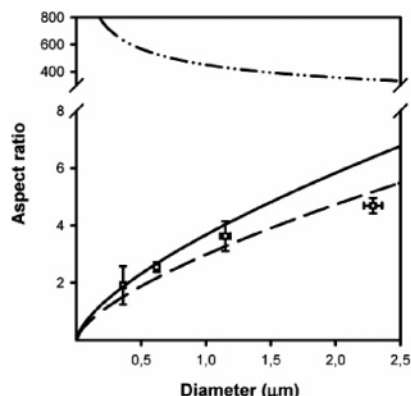

Figure 20. Arrays of PDMS pillars with different dimensions show the limited mechanical stability of HAR structures with this material. Pillar diameter increases from right to left (360 nm, 620 nm, 1.15 μm, 2.3 μm), while post height increases from the bottom to the top of the image. The inset shows a magnified image of the posts with the smallest diameter. The diagram below shows the experimental (squares) and theoretical (lines) critical aspect ratio of PDMS posts of different diameters. The different lines correspond to different theories. (Reprinted with permission from ref 208. Copyright 2005 American Chemical Society.)

relief structures may not be able to withstand the compressive forces necessary for HAR soft moulding, and therefore, most of these techniques can only be applied to low aspect ratio patterning; however, the softness of PDMS is highly advantageous when the master to be replicated possesses 3D re-entrant structures.[109] Replication of such structures is possible because the elasticity of PDMS allows it to pull away from cavities or overhangs during mould release. Two-

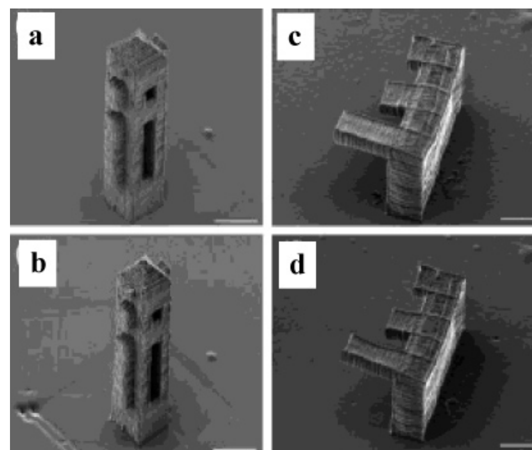

Figure 21. Replication of structures with re-entrant features, protrusions, high aspect ratio, and long overhangs by soft lithography. (a, c) Original structures made by two-photon lithography using SU-8 resist. (b, d) Replicas in acrylic resin obtained after soft moulding with PDMS. The scale bars are 10 μm. (Reprinted with permission from ref 109. Copyright 2004 American Chemical Society.)

photon lithographic masters containing 300 μm high and 10 μm wide towers (Figure 21a) have been first replicated accurately with PDMS and then with an acrylic resin (Figure 21b) despite having an aspect ratio of 30. Similarly, structures with undercuts at 90° could be replicated: Figure 21c shows a photoresist wall with 2.5 μm thick cantilevers protruding at 90° with lengths of 5, 10, and 20 μm and a width of 10 μm that could be replicated in PDMS and subsequently in the acrylic resin (Figure 21d).[109]

7.6. Solvent-Assisted Moulding

This terminology has been applied to moulding processes which rely on the use of solvents for softening polymer films.[225−229] It has the advantage over NIL that it does not require high temperatures or high pressures. Typically, soft PDMS moulds are used. The solvent can be either briefly applied to the surface of the mould or retained in the polymer film after spin coating. By placing the two surfaces in contact, the polymer solution is drawn into the cavities of the mould by capillary forces (Figure 13e). The solvent is slowly removed from the mould−polymer interface by diffusion into and evaporation through the soft, permeable mould. After completion of the evaporation, the mould is removed, leaving a hardened and accurate replica.[227,230] Swelling of the elastomer by the solvent is a potential restriction of the technique as it may cause distortion of the topographic features.[231] In general, solvents with relatively high vapor pressure and moderately high surface tension (e.g., methanol, ethanol, and acetone) are used with PDMS moulds to ensure rapid evaporation and minimal swelling. When solvents with high surface tension are required, surface modification of the PDMS mould may be necessary to increase its wettability by the polymer solution. This can be performed via plasma activation and subsequent treatment with poly(urethaneacrylate).[232]

Mould permeability is an important characteristic in this process as it prevents trapping of air pockets between polymer and mould and allows accurate replication. In fact, interesting results have been reported using moulds with different permeabilities. Whereas accurate replicas were obtained with permeable moulds (e.g., PDMS), imperfect

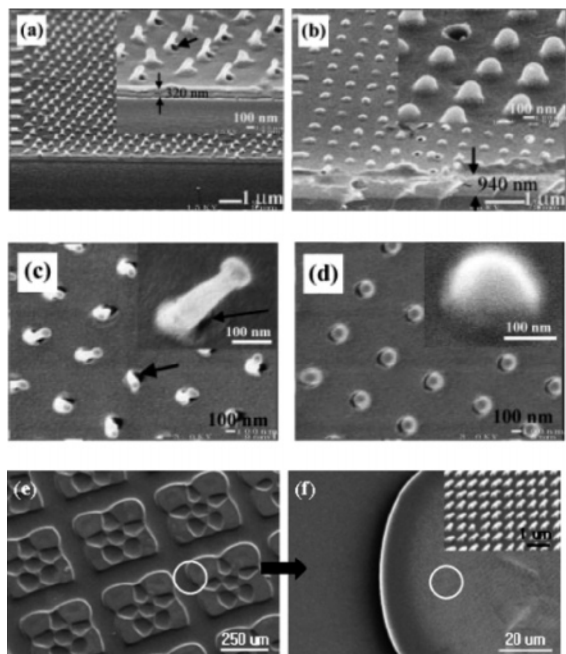

Figure 22. Nanostructures formed by solvent-assisted moulding using a poly(urethaneacrylate) semipermeable mould with different cavity heights and different polymer layer thicknesses. Insets show magnified views of the structures. (a) Nanopillars of poly(3-trimethoxysilylpropyl methacrylate polyethylene glycol methyl ether) with reduced diameter obtained from moulds with height 300 nm and polymer layers with thickness >800 nm. (b) Hemispheres obtained with mould height 300 nm and polymer thickness <500 nm. (c) Mushroom-like pillars with reduced diameter obtained with mould height 500 nm and polymer thickness >800 nm. (d) Nanospheres obtained with mould height 500 nm and polymer thickness <500 nm. (Reprinted with permission from ref 225. Copyright 2005 Wiley-VCH.) (e, f) Hierarchical structures obtained by two-step moulding of PS and PMMA films. (Reprinted with permission from ref 234. Copyright 2006 American Chemical Society.)

filling was obtained using impermeable moulds. The final geometry of the features is a function of the thickness of the initial polymer layer and the height of the features in the mould.[225] Depending on the initial polymer film thickness, nanohemispheres and nanopillars were obtained from a single polyacrylate mould possessing 300 nm deep and 150 nm wide holes and a poly(ethylene glycol)-acrylate moulded material (Figure 22a,b). If a stamp with 500 nm deep voids was used, mushroom-like nanopillars and nanospheres were obtained in thick and thin polymer films, respectively (Figure 22c and d). Although a detailed explanation of how these features are formed is still lacking, structure formation is explained as a consequence of the interplay between hydrodynamic and Laplace pressures in the cavities and the wetting behavior of the polymer solution and the stamp. Exploitation of this process could be interesting as a method to provide different 3D structures from a single mould.[233]

In a similar approach, multiscale hierarchical structures have been obtained from PS and PMMA films by two-step capillary imprinting process using toluene as a solvent.[234] Micrometer structures were obtained using a PDMS mould and heating at 150 °C for 1 h (low aspect ratio). Nanometer pillars with 100 nm diameter and aspect ratios < 4 were obtained on top of the micrometer structures using a hard polyurethane mould and slight pressure at 120 °C for 5 min (Figure 22 e,f).

The throughput of this technique depends on the rates of solvent adsorption in the mould and evaporation from the polymer surface. In practice, the process typically takes 10 min. These long cycle times represent a throughput limitation of the method. The low stability of the PDMS stamp under these conditions is another drawback of the technique. For this reason, pressure-assisted processes have been reported, where the patterning process is accelerated by applying an external pressure.[226] This process is not compatible with a soft stamp because the microstructures may collapse under pressure, and therefore, a stiff but permeable and solvent-resistant fluoropolymer mould is used.[226]

8. Transfer Printing

Transfer printing (also called “reversal imprinting” or “polymer bonding”) is a method to transfer negative replicas from a soft mould to a different substrate. A polymer layer is spin coated onto the mould instead of onto the substrate. After the solvent evaporates, a thin polymer film remains on the surface and can be transferred to a bare substrate by “bonding” them under suitable temperature and pressure (Figure 13f).[235−240] This method is advantageous over NIL for substrates which cannot be easily spin coated with a polymer film, such as flexible polymer substrates. In addition, successful and reliable pattern transfer can be achieved at low printing temperatures and pressures (30 °C below T_g and 1 MPa).[235] Because pattern formation does not involve polymer flow, this process is more tolerant with regard to mould geometry and yields better pattern uniformity than NIL. This is especially important in replicating HAR structures or particular stamp topologies with cavities separated over large distances, such as polymer flow in long cavities or over large areas for which NIL would be very complicated.[236]

Transfer printing requires prior surface treatment of the mould and substrate to which the patterned polymer film will be transferred in order to reduce (or improve) the mould−polymer (or polymer-substrate) affinity. Pattern transfer can be facilitated using adhesive layers, like polyelectrolytes.[241,242] In this way, PS-patterned films have been transferred from a PDMS master to a substrate coated with a polycation layer. Previous exposure of the PS to oxygen plasma is necessary to generate the complementary negative charge on the PS film to interact with the polycation layer and form a highly adhesive junction. Slightly increasing the mould temperature also helps in the transfer process. Arrays of HAR structures (>4) from different polymers (poly(4-vinylpyridine), PS, and PMMA) onto a number of different substrates (flexible or rigid) were generated by this technique, demonstrating its flexibility and versatility.[241,242]

In principle, use of hard moulds in transfer printing allows patterning dense nanostructures; however, difficulties in demoulding may arise because of strong adhesion to the mould. Improved results have been achieved using hard PDMS mixtures to build a two-component stamp consisting of a soft, thin PDMS layer and a thicker, harder, more highly cross-linked polysiloxane as a support.[206] Alternatively, moulds made from UV-curable polyurethane acrylates[241,242] or PVA[243] have also given good results. PVA is especially interesting as mould material because of its water solubility.

8.1. 3D Patterns by Multistep Transfer Printing

The imprinting and transfer printing technologies can be combined to obtain complex patterns. The "duo-mould imprinting" process using two silicon moulds and one or two different resist materials is an example of this combination (Figure 13g).[244] The key factor is, again, a differential treatment of the mould surfaces to enable transfer. This can be achieved by treating the mould surfaces with coupling agents that provide coatings with different surface energies.

Three variants of the duo-mould process have been reported (Figure 13g1, g2, g3). They use two types of moulds: a mould A with low surface energy and a second mould B with medium surface energy. In Figure 13g1, a polymer solution is spin coated onto mould A such that it fills up the trenches and forms a thin film. Mould B is then imprinted at a suitable pressure onto the polymer-coated mould A at a temperature above T_g of the polymer. Mould A is separated below T_g of the polymer, thus forming and transferring the 3D structure to mould B. This transfer occurs because of the difference in surface energies of the two moulds. An additional printing step on a high surface energy substrate at a temperature below T_g of the polymer transfers the final 3D structure.

Another process (Figure 13g2) begins with spin coating a polymer film onto mould B with the higher surface energy. Imprinting mould A onto the polymer film on mould B follows. The final step is as in Figure 13g1.

The third process (Figure 13g3) begins with spin coating a polymer film onto both moulds A and B. The coatings can be of similar or dissimilar materials. Then the moulds are pressed together at a temperature above T_g of either polymer. This process is advantageous for high aspect ratio patterning because filling of the moulds during imprinting is not required. The moulds are separated after pressing, and the patterned film is transferred to mould B. The final step is shown in Figure 13g1.

The large difference in surface energy between the two moulds reduces the difference in surface energy between the mould and the substrate required at the final transfer step, especially if it needs to be performed at low transfer temperatures for preserving pattern stability.[245] An alternative is the use of mould and substrate with similar surface energy and a thermosetting polymer that allows higher transfer temperatures.

Transfer printing does not require planar substrates but can also be performed directly over topographies. Interesting 3D structures have been reported by transferring PMMA films over NIL patterned substrates.[246] The geometry of the final structure depends on the transfer temperature, the ratio between the thickness of the transfer film and the distance between features on the NIL patterned substrate, and the mechanical properties of the polymers used.[235,246,247] Figure 23 shows two examples of PMMA gratings transferred at two different temperatures onto a prepatterned silica substrate.[246] At 90 °C (15 °C below T_g) PMMA lines connected by a thin residual PMMA layer were transferred (Figure 23a). At 175 °C only the lines were transferred and the residual film disappeared completely (Figure 23b). This is a consequence of dewetting of the ultrathin film from the mould at a temperature well above T_g.

Figure 23 also shows the effect of the pattern geometry and polymer film thickness on the transferred pattern. When the feature spacing on the underlying substrate is smaller than or comparable to the thickness of the transferred film,

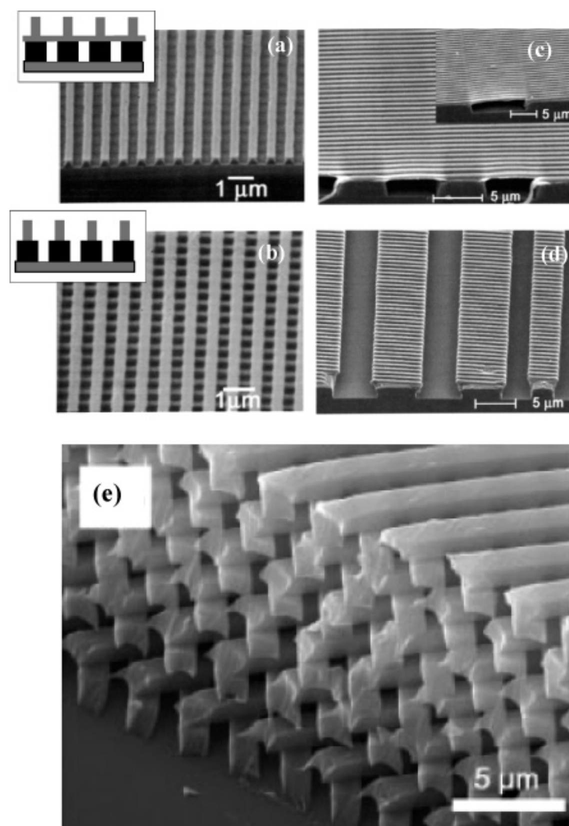

Figure 23. (a−d) PMMA patterns obtained by transfer printing over topographies. (Reprinted with permission from ref 246. Copyright 2002 American Institute of Physics.) (e) 3D layered structures obtained by multistep transfer printing several poly(urethane) structured films. (Reprinted with permission from ref 248. Copyright 2005 Wiley-VCH.)

the polymer film can be imprinted across the raised features (Figure 23c). In this situation, the pattern is transferred over the entire imprint area and suspended polymer structures are formed. On the other hand, when the feature spacing is larger than the polymer film thickness, the suspended part of the film will break during mould separation, leaving the polymer pattern only on the protruding surfaces (Figure 23d).

More complex structures can be fabricated by performing several consecutive transfer printing processes. Figure 23e provides an example where 12 layers of line patterns were stacked to form a 3D structure by multistep transfer printing.[248]

9. Filling Mesoporous Matrices

Synthetic membranes and porous matrices can be used as moulds to confine polymerizable monomers, polymer solutions, or polymer melts. If the membranes are supported on a nonporous substrate, arrays of polymeric structures are obtained after polymerization, evaporation, or cooling and release from the membrane by selectively dissolving it or demoulding. Until recently, this method has only been used to obtain patterns with cylinders with almost any width and height, but the method could be extended to obtain patterns with other geometries if a porous matrix with more complex geometries is used (e.g., mesoporous silicon with interconnected porous structure).

Typically, track-etched PC membranes, anodic alumina (AA) membranes, macroporous silicon, or mesoporous zeolites are used as porous matrices.[249] PC track-etched

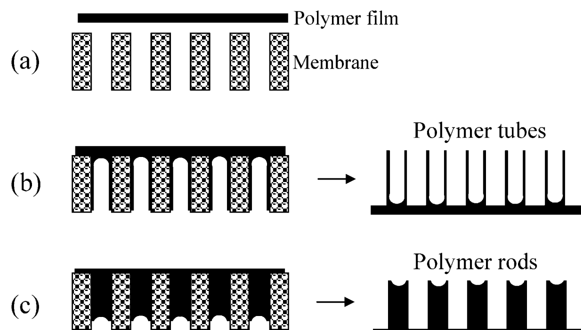

Figure 24. Patterning by filling porous matrices. The structured polymer film obtained after selective removal of the membrane possesses cylinders with dimensions matching that of the pores. The polymeric cylinders may be solid (rods) or hollow (tubes) as a consequence of the filling mechanism driven by the wetting properties of the polymer/membrane system.

membranes contain cylindrical pores of uniform diameter randomly distributed across the membrane surface.[250] Track-etched fabrication is based on the passage of high-energy decay fragments from a radioactive source through a dielectric material.[250] The particles leave behind chemically active damaged tracks that subsequently can be etched to create pores throughout the thickness of the membrane. The pore density is independent of the pore size and only determined by the irradiation process. PC membranes with a wide range of pore diameters (down to 10 nm) and pore densities approaching 10^9 pores cm^{-2} are commercially available.

AA membranes are fabricated through electrochemical anodization of aluminum at temperatures of 0−10 °C in aqueous acidic electrolytes. Different pore diameters (25−400 nm) and interpore distances can be obtained depending on the applied anodization voltage and electrolyte. The pores are arranged in a regular hexagonal lattice, and pore densities as high as 10^{11} cm^{-2} can be achieved. The pores are straight, and their diameters are constant over their entire depth ranging from a few nanometers to hundreds of micrometers (aspect ratios up to 10 000 are feasible). The self-ordered domains possess lateral extensions in the micrometer range, and the dispersity of the pore size distribution is about 8%. The high fragility of through-hole AA membranes limits their use.

Electrochemically etched macroporous silicon membranes with porous diameters between 4 nm and 4 μm and interpore distances between 500 nm and 20 mm are also available. The pores are nearly perfectly aligned and can attain aspect ratios over 250. This process also results in membranes with sizes reaching the square centimeter range.[251−256]

Depending on the polymeric material used for filling, the parameters of the filling process, and the chemistry of the pore wall, the polymeric cylinders may be solid (rods) or hollow (tubes). This is a consequence of the filling mechanism driven by the wetting properties of the polymer/membrane system (Figure 24). The spreading process starts with a "precursor film" which emanates from the macroscopic liquid droplet and covers the substrate and pore walls.[257] As spreading proceeds, more and more of the liquid is transferred into the precursor film until it covers a finite area and has an equilibrium thickness in the nanometer range or fills the pore completely.

Interesting crystallization and orientation effects occur in the pores as a consequence of confinement and controlled surface interactions. These can be exploited for gaining an additional structuration level and will be described in the following sections.

9.1. With Polymer Precursors

Ordered arrays of polyaniline (PANI) nanotubes have been fabricated by in situ polymerization on AA membranes.[258] The crystal structure of the PANI nanotubes presented higher symmetry than crystalline PANI in the bulk. This was attributed to the confinement effects of the AA membrane which makes the macromolecular chains arrange in a more ordered conformation. Arrays of glassy carbon nanorods with diameters around 50 nm and aspect ratios above 10 have also been reported by filling AA membranes with furfuryl alcohol-based resins and subsequent pyrolysis.[259] AA membranes with pore diameters between 18 and 80 nm have also been filled with a sol−gel mixture of tetraethoxysilane and the block copolymer Pluronic.[260] This organic−inorganic hybrid forms mesophases of cylindrical morphology when polymerization occurs in bulk; however, when confined in the AA nanopores, the morphology of the mesophase changed and arrays of nanocylinders with different mesostructures were achieved depending on the pore diameter (Figure 25).

9.2. With Polymeric Melts

Polymer melts and polymer solutions can also fill porous matrices when heated to appropriate temperatures or diluted to certain concentrations.[261,262] The filling process is usually slow due to the high viscosity of the filling material, but it can be accelerated by application of vacuum or pressure. Once the pores are completely filled, solidification of the polymer melt is achieved by cooling below T_c in semicrystalline polymers, cooling below T_g in amorphous polymers, or evaporation of the solvent in a polymer solution. Solidification can be performed after spreading or complete filling, resulting in tubes or rods, respectively (Figure 26). The polymeric layer always remains attached to the pore walls upon cooling, even in the case of polymers exhibiting pronounced shrinkage.

The morphology of the polymer typically depends on the method used for filling: melt wetting[261,263] results in more crystalline morphologies than solution wetting.[262,264] This has been demonstrated with poly(vinylidene fluoride), which resulted in amorphous tubes from solution and highly crystalline tubes from the melt.[265] Additional orientation effects have also been reported when filling with liquid crystalline polymers.[266] These effects have not yet been exploited, but they may be interesting in applications because the structure of the crystalline domains has a strong influence on the mechanical, chemical, electrical, and optical properties of the nanotubes.

Wetting of porous matrices has also been performed with block copolymers[267] and multicomponent mixtures.[268] This has enabled the fabrication of arrays of composite nanorods with an aspect ratio of 15 consisting of polystyrene-polybutadiene (PS-PB) with cylindrical morphology.[267] The PS cylinders in the PB matrix have a parallel orientation to the pore axis due to the preferential wetting of the pore walls by the PB block. The period and packing of the microdomains differs from the bulk values due to incommensurability between the pore geometry and the natural period of the copolymer microdomains. PS-PB diblock copolymers exhibiting bulk lamellar morphology produced

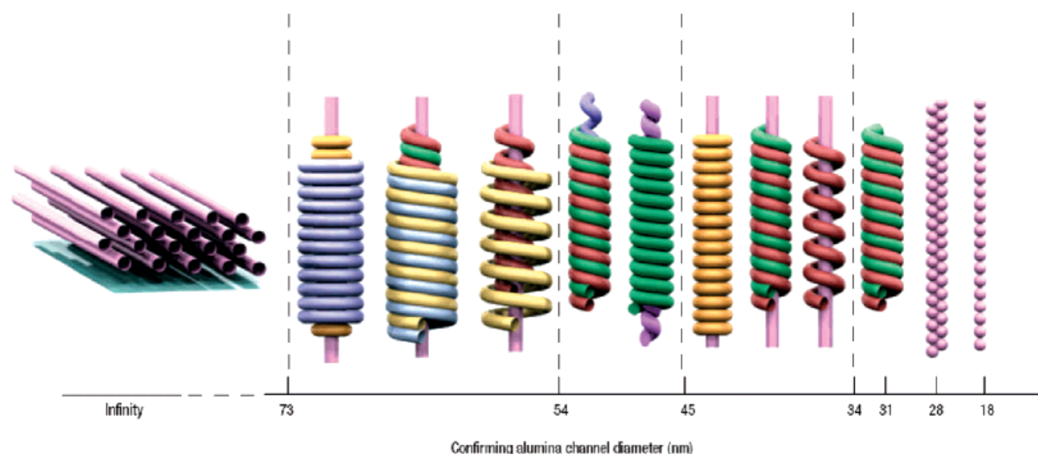

Figure 25. Experimentally observed confined mesostructural evolution of the copolymer Pluronic and tetraethoxysilane mixture with varying alumina nanochannel diameters. (Reprinted by permission from Macmillan Publishers Ltd: Nature Materials (ref 260), copyright 2004.)

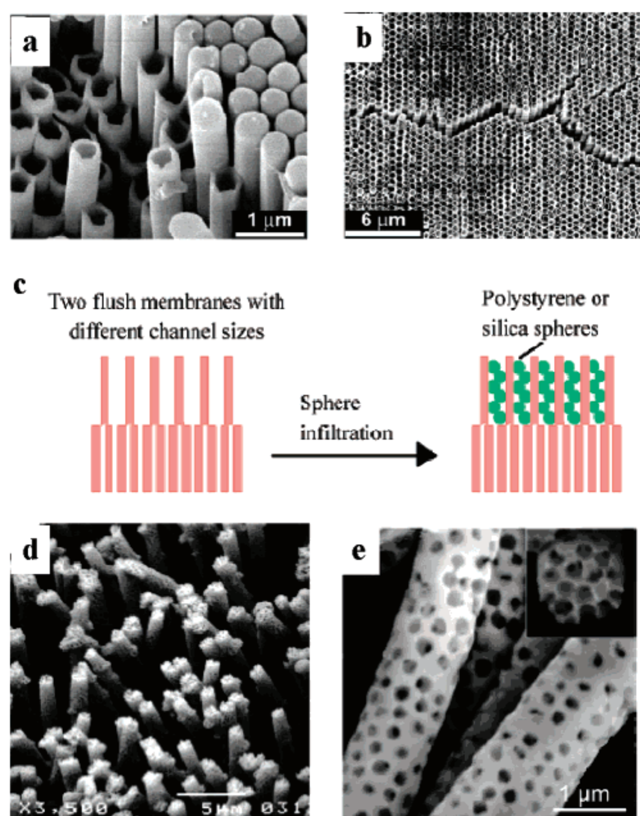

Figure 26. Nanorods and nanotubes obtained by filling porous matrices with polymer melts. (a) Array of tubes and rods of PS obtained from a porous AA membrane. (Reprinted with permission from ref 263 (http://www.sciencemag.org). Copyright 2002 AAAS.) (b) PMMA tubes with long-range hexagonal order obtained by filling macroporous silicon membranes. (Reprinted with permission from ref 263 (http://www.sciencemag.org). Copyright 2002 AAAS.) (c) Mechanism for fabrication of arrays of porous tubes. (Reprinted with permission from ref 269. Copyright 2003 American Chemical Society.) (d, e) Result of filling the pores with a suspension of 300 nm silica beads followed by deposition of gold. (Reprinted with permission from ref 269. Copyright 2003 American Chemical Society.)

concentric cylinders oriented along the nanorod axis in the confined geometry.

Arrays of porous nanotubes have been fabricated by filling a sandwich structure of AA and PC membranes with PS and silica colloidal suspensions (Figure 26c–e).[269] The pore size differences between both membranes locks the particles within the pores of the PC membrane. Electrodeposition and removal of the membrane has produced porous metallic wires with porous size and distribution dictated by the size and arrangement of the colloidal particles within the pores. Most recently, AA with a hierarchical pore structure has been used to grow hierarchical and branched structures with controlled geometry (Figure 27).[270]

As demonstrated from these studies, arrays of HAR rods or tubes with different geometric and material characteristics can be produced by filling porous matrices. However, it must be considered that demoulding HAR structures from the membrane is a difficult, if not impossible, process. Matrix removal is usually performed by dissolving it in acidic or basic solutions, which may also cause swelling of the polymer. The porous matrix is therefore not reusable. Collapse of the rods or tubes during solvent drying is another potential problem.

10. Surface Instabilities

Topography may spontaneously appear at the surface of soft matter as a consequence of inherent polymer relaxation processes[271−273] or by phase separation of incompatible mixtures.[274] When allowed to relax, soft matter will form surface undulations, known as capillary waves, as a result of the inherent entropy of the system balancing the increased energy of the greater surface area. These phenomena occur at temperatures above the glass transition and only if the field gradients are strong enough to overcome the surface tension in the thin liquid film. The relatively low surface energy combined with their compliance makes such an effect important in soft polymer materials. Application of surface destabilizing forces induced by electric fields, temperature gradients, or mechanical stress amplify these effects and have led to interesting pattern morphologies.[275] External control of these effects has generated regular patterns with interesting geometries containing two or more symmetry levels made of one or two different materials. These result as a consequence of the interplay of external fields and material composition and properties.

10.1. Electric Field-Induced Instabilities

Polymer films confined within a plate capacitor and heated above T_g build liquid cylindrical bridges spanning the two

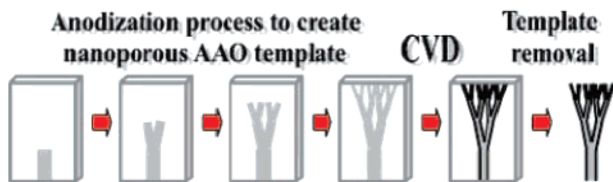

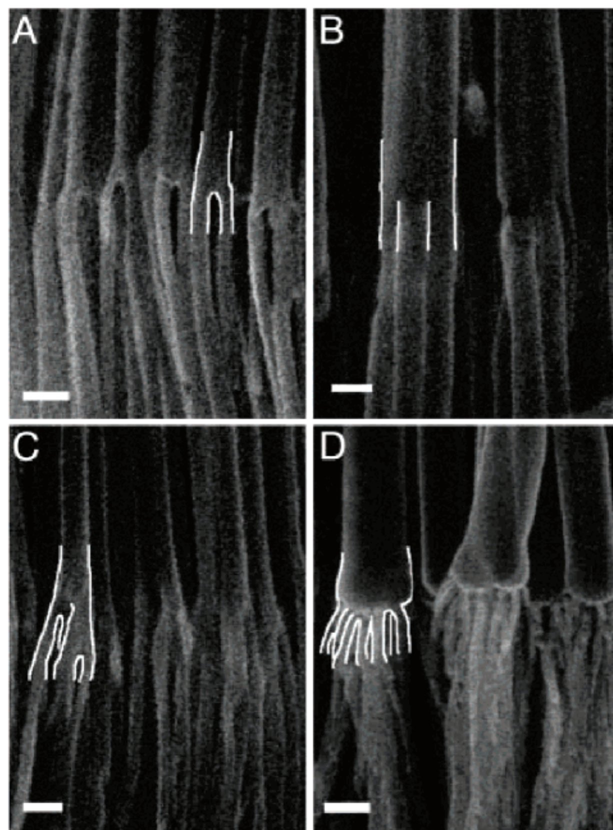

Figure 27. Fabrication of branched nanowire structures by filling porous matrices. Pores with controlled architectures are first obtained by consecutive anodization steps and then used as moulds to cast nanotubes and nanowires of complex geometries. The pictures show examples of carbon nanotubes with multiple branches obtained after selective removal of the membrane and carbonization: (a) 2, (b) 3, (c) 4, and (d) 16 branches. The junctions are highlighted with white line contours. (Reprinted with permission from ref 270. Copyright 2005 National Academy of Sciences, U.S.A.)

capacitor plates upon application of an external electric field (Figure 28a). By cooling the system below T_g while keeping the electric field on, the dynamics of the polymer chains is frozen and the thin film retains the surface pattern.

The origin of the film instability has been explained by considering the balance of forces that act at the polymer−air interface. The surface tension minimizes the surface area and stabilizes the homogeneous polymer film. The electric field, on the other hand, polarizes the dielectric. This results in an effective displacement charge density at the liquid−air interface, which destabilizes the film. A local perturbation in the film thickness results in a pressure gradient which drives a flow of the dielectric liquid in the plane of the film, and this constitutes the onset for the nanostructure formation. The force balance at the liquid surface between the destabilizing electrostatic pressure gradient and the restoring surface tension, γ, determines the lateral wavelength of the pattern given by[276−278]

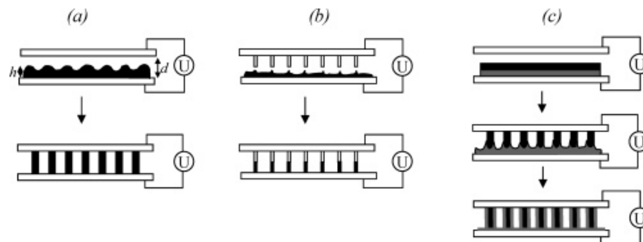

Figure 28. Patterning through electric field-induced instabilities. (a) Representation of the capacitor device. The electrostatic pressure acting at the polymer−air interface causes a surface instability with well-defined wavelength. After a certain time, polymer columns span the gap between the two electrodes. (b) If the top electrode is topographically patterned, replication of the electrode pattern occurs. (c) Hierarchical patterns can be obtained from polymer bilayers.

$$\lambda_i = 2\pi\sqrt{\frac{\gamma U}{\epsilon_0\epsilon_p(\epsilon_p - 1)^2}}E_p^{-3/2}$$

where $E_p = U/(\epsilon_p d - (\epsilon_p - 1)h)$ is the electrostatic pressure for a given electric field in the polymer film, U is the voltage, h is the film thickness, d is the electrode gap, and ϵ_p and ϵ_0 are the dielectric constants of the polymer and air, respectively.

Structured films were obtained from 100 to 200 nm thick PS films spin coated onto silicon wafers that served as electrodes.[279] The opposing electrode was mounted leaving an air gap of 100−1000 nm. The assembly was then heated above T_g, and a voltage (20−50 V) was applied. Depending on the electric field strength, film thickness, gap, and annealing time, surface undulations or columnar structures of $\sim$5 μm in diameter and different lateral distributions were observed (Figure 29a,b). The aspect ratio of the structures was in all cases <1, but higher values should be achievable.

The pattern periodicity and symmetry can be influenced using a structured upper electrode. This causes a laterally varying electric field which focuses the formation of instabilities (Figure 28 b). The pattern period is determined by the interplay of two lateral length scales intrinsic to the experiment: the destabilization wavelength, λ_i, and the periodicity of the upper electrode, λ_m, and can be switched discretely by changing the applied voltage. The aspect ratio of the structures is given by the electrode spacing, the lateral density of topographic features on the master wafer, and the initial film thickness of the polymer layer. Because the polymer is redistributed from a film into lateral structures spanning the electrodes, the width of these structures is determined by a volume conservation regulation.

Electrostatic field-induced instabilities have been recently analyzed on the basis of nonlinear 3D simulations. In accordance with the experimental results, hexagonal packing of columns is produced in spatially homogeneous electric fields.[279−281] By tuning the film thickness, topography of the top electrode, and applied voltage and using a topographically patterned electrode, patterns with more complex geometries have been predicted (Figure 31 c).

Electrical fields have been also used to generate hierarchical patterns from bilayers of PMMA and PS (Figure 28c).[282] The authors take advantage of the differences in the characteristic time constants at which electric field-induced instabilities develop at each interface of the polymer−

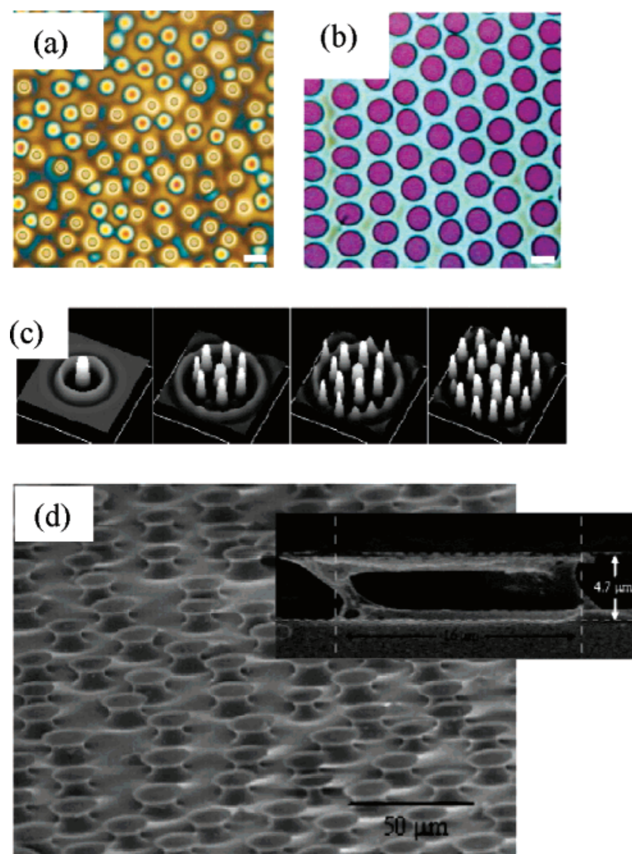

Figure 29. Patterns obtained under an electric field. (a) A 93 nm PS film was annealed for 18 h at 170 °C under an applied voltage of 50 V. (b) The thickness of the PS film was doubled (h = 193 nm); this leads to a denser packing of columns. The scale bars correspond to 10 μm in a and 5 μm in b. (Reprinted by permission from Macmillan Publishers Ltd: Nature (ref 279), copyright 2000.) (c) The simulated spatiotemporal evolution of a 25 nm thick film between two electrodes, where the top electrode pattern consists of a central circular patch and the electrode spacing is 80 nm, is represented. (Reprinted with permission from ref 280. Copyright 2005 American Chemical Society.) The SEM image in d shows the 3D micropattern obtained from a bilayer of PS-PMMA. The mushroom-like structures are composed of PS pillars surrounded by PMMA. The inset shows the SEM image of a single "cage" after washing with cyclohexane to remove the PS component. (Reprinted with permission from ref 283. Copyright 2006 American Chemical Society.)

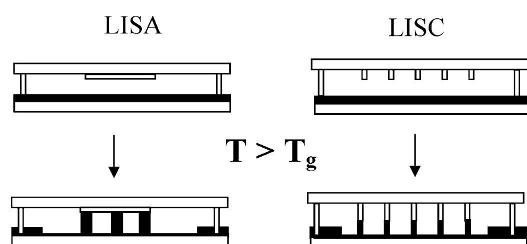

Figure 30. Patterning through temperature-induced instabilities (LISA and LISC approaches).

polymer−air trilayer system. These differences lead to a lateral redistribution of both materials under the electric field and therefore to a lateral structure exhibiting two independent characteristic dimensions: 3 μm thick PS columns surrounded by a 200 nm thick PMMA rim. When combining this process with preferential wetting of the top electrode by one of the polymers, unique 3D structures as shown in Figure 29d, where one polymer is encased by the other, have also been obtained.[283]

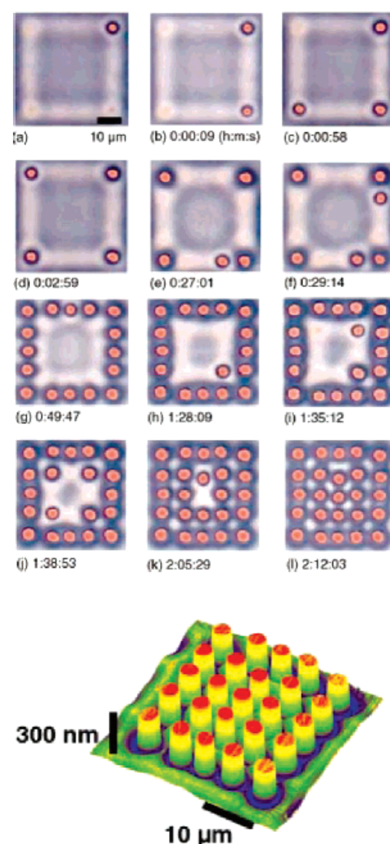

Figure 31. Time evolution of the growth of a LISA array formed under a square mask pattern. (Reprinted with permission from ref 292. Copyright 2001 American Institute of Physics.)

This approach has also been applied to pattern films of block copolymers. Block copolymers possess two different dielectric interfaces (the interface between the two chemically different blocks and the polymer−air interface) that may respond in an independent, different way upon application of an electrical field. This feature has been exploited to fabricate surfaces patterned in two different length scales simultaneously, one resulting from the polymer−air surface instabilities and the other from the microdomain alignment.[284] Hexagonally packed columns composed of oriented microdomains were obtained.

A less commonly used strategy to liquefy a glassy polymer film is absorption of vapor from a solvent atmosphere.[285] Vapor absorption has a number of advantages. As opposed to evaporating solutions, the amount of solvent in the material can be controlled by adjusting the surrounding solvent vapor pressure and thereby the viscosity of the liquefied polymer. It can be modified easily, even in situ. Diffusion of the solvent molecules into the polymer matrix results in an increase of the free volume and a lowering of the glass-transition temperature. For example, for PS a toluene uptake of 14% is sufficient to lower the glass-transition temperature to room temperature. By combining solvent absorption with thin film destabilization via electrical fields, hierarchical patterns have been obtained.[285] Solidification of the patterned film by drying in solvent-free air leads to large volume contraction (40%) and therefore lateral contraction of the replicated pattern, giving rise to a secondary pattern formation process.

10.2. Temperature-Induced Instabilities

Surface instabilities in polymeric thin films confined between two close surfaces and a small air gap have also been found in the absence of external electric fields. Heating the polymer above its glass-transition temperature leads to a significant increase of polymer charge density and charge mobility. In the absence of an upper substrate on the top of the melt, the charges in polymer film are uniformly distributed across the flat surface. However, if a substrate with finite conductivity is placed near the polymer film, the image charge will be induced in the substrate (Figure 30). The interplay of the charges and image charges can cause instability and formation of patterns. This process has been named "lithographically induced self-assembly", LISA.[286]

These effects have been demonstrated in PMMA films placed between a lower substrate and an upper surface separated from the film by a gap using a spacer.[286] The gap between the polymer film and the mask was set to be 2−7 times the initial film thickness. The mask, polymer film, and substrate were heated uniformly above T_g and subsequently cooled down to room temperature. During the heating−cooling cycle, the initially flat polymer film self-assembled into periodic pillar arrays.

The temperature gradient across the polymer−air double layer seems to play a role in the development of the pillars.[287−289] Pillars with 1−3 μm diameter were observed in 100 nm PS films with gaps between 120 and 600 nm when a temperature difference between the lower and upper substrate between 10 and 55 °C was applied.

If the surface of the mask has a protruding pattern, the pillar array is found only under the protruding pattern with the edge of the array aligned to the boundary of the mask pattern (Figure 30). The lattice structure is determined by the shape and size of the mask pattern, gap, polymer film thickness, and surface energy difference between the polymer and the upper substrate. In fact, using a low surface energy material as the upper substrate, the pillars spread and form mesas with lateral dimensions identical to those of the surface protrusions.[290] This process has been called "lithographically induced self-construction", LISC. The influence of the interface energies has also been reported in PMMA films by comparing the patterns obtained using an air-filled gap against those obtained from a perfluoropolyether oil-filled gap.[291] Arrays of ordered pillars were obtained in both systems, but the temperatures at which they formed were different (135 and 160 °C, respectively).

A real-time analysis of the evolution of PMMA patterns in the presence of a protrusion has provided evidence for the kinetics of pillar generation and reveals that the pillar arrays form in an orderly manner: one pillar forms at a time, starting under the corners of a mask pattern, then the edges, and later propagating to the center of the mask pattern (Figure 31).[292] The total time for a complete LISA process in a 135 nm thick PMMA film with a 175 nm air gap at 120 °C is more than 2 h. This time was measured after the appearance of the first pillar, which itself took about 1 h to form. It was found that the rate of pillar formation decreases with increased gap and PMMA film thickness.

The interplay of electrodynamics, fluid hydrodynamics, and polymer and surface chemistry in the LISA process is generally accepted, but a clear picture of how much these parameters influence the growth and periodicity of the pillars is still missing.[293] The limits of the technique are also unclear: aspect ratios above 0.5 have not been reported so far, and the question of large area patterning is still open. Attempts to theoretically describe these experiments and those using external electrical fields have been published.[294] A possible influence that these effects may have in imprinting processes, with protrusions appearing when the master approaches the polymer film, has been suggested.[295]

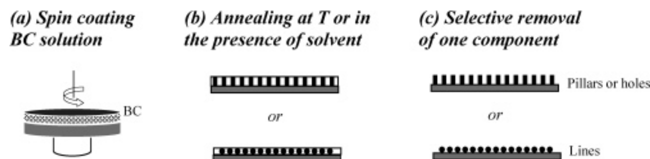

Figure 32. BC-based patterning strategy.

11. Patterning Through Self-Assembly of Block Copolymers

Block copolymers (BCs) consist of two or more chemically different polymer chains (or blocks) joined by a covalent bond to form a larger, more complex macromolecule. Because of connectivity constraints and the incompatibility between the blocks, BCs spontaneously self-assemble into nanometer-sized, phase-separated domains that exhibit ordered morphologies at temperatures below a characteristic order−disorder transition temperature, T_{OD}. The equilibrium morphology in each BC system is determined by the relative chain lengths of the blocks and the Flory−Huggins interaction parameter, χ. For example, diBCs having two blocks of comparable volume exhibit a lamellar motif. Increasing the degree of compositional asymmetry between the two blocks leads to gyroid, cylindrical, and finally spherical phases. TriBCs show richer phase behavior than diBCs because of their two independent compositional order parameters and three Flory−Huggins interaction parameters, the subtle interplay of which gives a varied morphospace.

Thin films of BCs with homogeneous long-range morphology can be regarded as periodic nanopatterned surfaces. The size of the pattern is determined by the chain dimensions and ranges between 10 and 100 nm.[296−298] This length scale is particularly interesting for patterning technologies because it is hard to achieve via top-down approaches. Generating BC patterns avoids the use of complicated and expensive masters or projection optics.[296] However, it requires appropriate chemical designs, control of the BC morphology over large areas, and the possibility of selective removal of one block to obtain an ordered nanopattern of a second or third block on the surface. See Figure 32 for a representation of a BC-based patterning strategy.

11.1. BC Morphology in Thin Film Geometry

A confined geometry, as in thin films, may spatially constrain the BC bulk morphology, and therefore, thin films of BCs may exhibit different morphologies than those present in bulk. The deviation from bulk behavior is commonly referred to as "surface reconstruction" in the literature, in analogy to the lateral rearrangements of the topmost atomic layers of a crystal surface in classical surface science.

The film thickness and affinity of the surface for each block mostly determine the final morphology of a BC thin film. Blocks that have a preferential affinity for a particular interface (e.g., polymers with polar functional groups and metal oxide surfaces) will segregate and enrich it.[299] A weakly interacting interface attracts neither component block

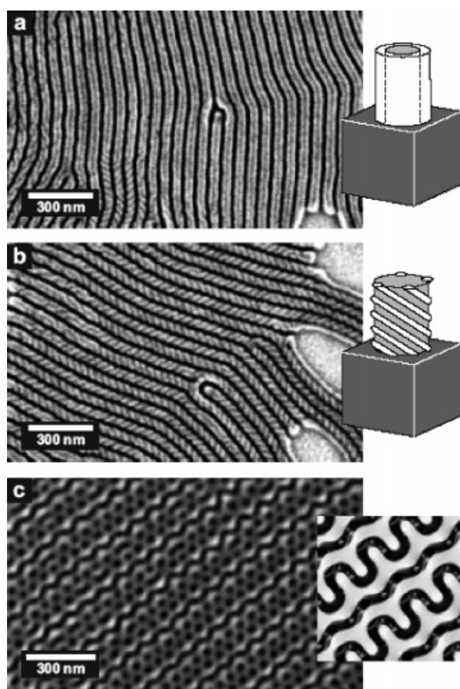

Figure 33. SEM pictures of 60 nm thick films of a triBC along with the expected morphology of the thin film structure.[323,330] (a) Core−shell cylinders, (b) helices wound around a cylindrical core, (c) (112) plane of an ideal double-gyroid structure. Bright areas are poly(2-vinylpyridine) blocks, gray areas are PS blocks, and the darkest areas are poly(*tert*-butyl methacrylate) blocks after staining with OsO_4. (Reprinted with permission from ref 323. Copyright 2002 Wiley-VCH.)

to a significant extent. A noninteracting interface such as air, an inert gas, or vacuum does not bond with either component but does introduce surface tension. According to these basic rules, cylindrical diBCs have been shown to arrange in parallel, perpendicular, or random orientation depending on the substrate surface energy[300−308] and film thickness.[309−312] Hybrid morphologies that combine surface-parallel and surface-perpendicular components across the polymer film thickness have also been found in thicker films. This is a consequence of the different surface reconstruction effects induced by the two distinct surfaces (substrate and air). Moreover, special morphologies differing from those found in bulk samples, like “perforated lamellae with spheres”[313] or “cylinders with necks”,[314] have been reported. All these effects have been extensively studied (both theoretically and experimentally) and can be exploited to generate lines, grooves, or arrays of pillars or holes across the substrate after selective removal of one block.[315−323] More complex patterns can be obtained from triblock thin films (Figure 33 shows some examples),[323−329] but studies in this field are still preliminary.[298]

In the praxis, “neutral surfaces” are most frequently used to induce perpendicular orientation of BC morphologies. These are surfaces with low surface energy and negligible interaction with either component block. Experimentally, this condition is typically achieved by end grafting a layer of the random copolymer onto the substrate surface.[303−308]

While the self-assembled structure in BCs is locally very precise, its orientation across the whole BC film is hard to control. Domains having sizes of several tens of nanometers typically nucleate randomly and grow a polygranular texture across the BC thin film. The development of long-range lateral order is a kinetically slow process and requires long annealing times. This can be accelerated by increasing the chain mobility by heating to temperatures between the highest T_g of the components and T_{OD}, or using solvents as plasticizers (spin casting, solvent casting),[330−337] or inducing chain reorientation under application of electrical fields.[338−341] Quenching of the annealed structures is performed by reducing the temperature or quickly removing the solvent from the thin film.[330,331,342]

A systematic study of the effect of the substrate material, surface treatment, annealing conditions, copolymer molecular weight, and film thickness on the orientation of cylindrical domains has been published for PS-PMMA copolymers.[338,343] Thin films on bare oxide surfaces rendered parallel alignment of PMMA cylinders due to the higher affinity of this polymer for hydrophilic oxide surfaces, whereas films on neutral surfaces showed perpendicular orientation. Long-range hexagonal ordered arrays were obtained after long thermal annealing times from films with thickness close to the BC repeating length (∼40 nm) (Figure 34). After selectively removing the PMMA component, a PS matrix with a regular pattern of hexagonal close-packed holes with a diameter of 18 nm and an aspect ratio of 2 was obtained. Cylinder-forming polystyrene-polybutadiene-polystyrene (PS-PB-PS) triblock copolymers have also shown a rich variety of structures depending on the film thickness (Figure 35).[344,345] Such a behavior has been theoretically modeled, and complex phase diagrams predicting the phase morphology for various surface field strength, film thickness, and interaction parameters of the blocks have been reported.[346,347]

11.2. Hierarchical Patterns

BC designs are limited to periodic structures with symmetries mainly determined by the composition of the blocks. However, when combining the BCs microphase separation behavior with additional patterning and self-organization strategies, surface patterns with more complex lateral hyperstructures can be obtained. These strategies include (i) annealing of BC films over topographically[309,348] or chemically[349] patterned substrates, (ii) imprinting BC films with a master, (iii) combining BC self-ordering with liquid crystalline and semicrystalline order,[350−352] and (iv) adding homopolymer to the BC composition to form blends.[296,323] Hierarchical patterns including structures at different length scales have been achieved.

Spin coating and annealing a BC film over topographically structured surfaces produces BC films with nonhomogeneous thickness. As a consequence, BC films with different morphologies will develop in the thicker and thinner regions.[353,354] This has been demonstrated with PS-PMMA cylinder phases annealed over silicon nitride substrates patterned with micrometer wide gratings.[355] Similar results were obtained from cylinders forming polystyrene-polyisoprene (PS-PI) films on silicon gratings.[348] Thicker regions (valleys) exhibited in-plane cylinder orientation, and thinner regions (hills) displayed vertically aligned cylindrical domains.

BC films can also be imprinted with topographically patterned masters. Depending on the dimensions of the master features and the film thickness, hierarchical arrangement of parallel and perpendicular domains may be achieved. In this context, PS-PMMA perpendicular and parallel cylinder morphologies have been obtained.[356] After oxygen plasma etching of the PMMA component, PS membranes

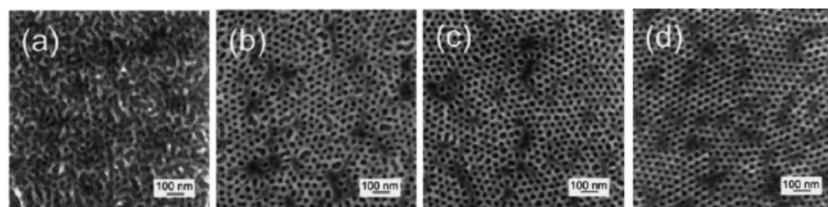

Figure 34. SEM micrographs of a PS matrix obtained from thin films of PS-PMMA on a neutral surface. The hexagonal ordered PMMA cylinders perpendicularly oriented with respect to the neutral surface were etched by UV radiation exposure to yield a PS matrix with cylindrical holes. The series shows how the orientation of the cylinders improves with increasing annealing time: (a) 3.5, (b) 6, (c) 15, and (d) 34 h. (Reprinted with permission from ref 344. Copyright 2001 American Institute of Physics.)

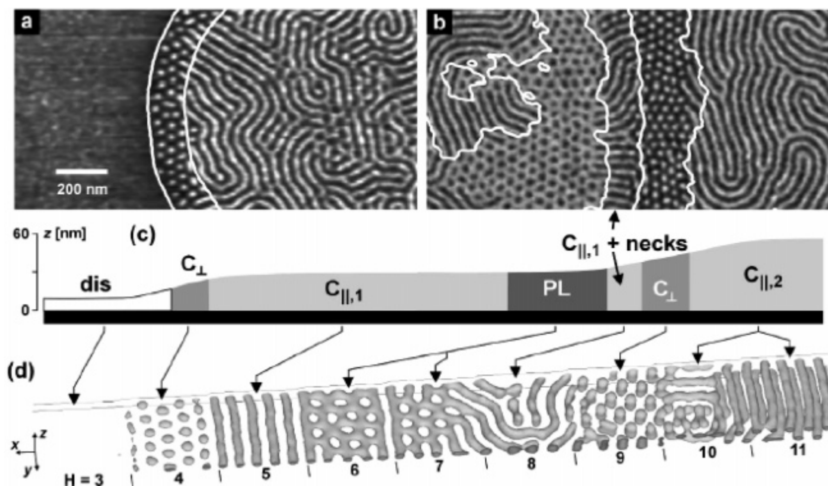

Figure 35. BC morphologies obtained from a PS-PB-PS film with varying thickness. A featureless film surface was obtained in very thin films. Isolated PS domains, parallel oriented PS cylinders, perforated PS lamella, parallel-oriented PS cylinders of ellipsoidal cross section, perpendicularly oriented PS cylinders, and finally two layers of parallel-oriented PS cylinders were observed with increasing film thickness. (a, b) Tapping-mode scanning force microsropy phase images of the film. Bright (dark) domains correspond to PS (PB) microdomains. Contour lines calculated from the corresponding height images (in c) are superimposed. (c) Height profile of the phase images shown in a and b. (d) Simulated morphologies with increasing thickness from left to right. (Reprinted with permission from ref 345 (http://link.aps.org/abstract/PRL/v89/p035501). Copyright 2002 by the American Physical Society.)

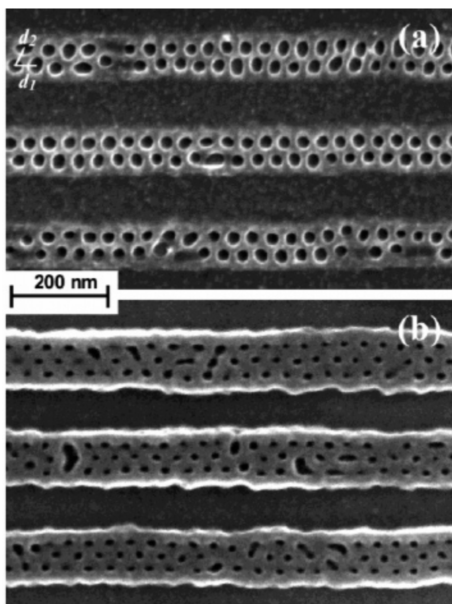

Figure 36. SEM images of a PS-patterned film obtained from a PS-PMMA thin film that was imprinted with a mould patterned with gratings of (a) 20 nm periodicity and 100 nm gap and (b) 210 nm periodicity and 120 nm gap. (Reprinted with permission from ref 357. Copyright 2004 American Chemical Society.)

with 100 nm deep holes were obtained (Figure 36). PS-PI-PS triblock copolymers were moulded with soft PDMS masters in the presence of a toluene solvent. Stripes with a controlled morphology of the BC were obtained.[357] By embossing stretched elastomeric triBCs, patterns with reduced dimensions may be obtained after stress release.[175]

Studies of BC patterns on chemically patterned substrates usually concentrate on the effect of the substrate pattern periodicity on film morphology. In particular, when the period of the substrate pattern approaches molecular dimensions, these studies predict (almost universally) a surface-perpendicular orientation of the block domains.[358−361] Some experimental results on this topic have also been published.[362−364]

BCs with a liquid crystalline or semicrystalline component offer an additional length scale of competing order, i.e., the periodicity of the crystalline (or liquid crystalline) phase. The final microstructure depends upon whether microphase separation or crystallization occurs first. In general, systems with $T_{OD} > T_m$ have been employed. This implicates that crystallization of the semicrystalline block occurs after microphase separation of the BC. Consequently, the BC morphology dictates the growth direction of the crystal.[350−352] The crystallization behavior of polybutadiene-poly(ethylene oxide) (PB-PEO) films has been reported for these systems.[350] Directed crystal growth results in a vertical orientation of the crystalline lamellae, giving patterned surfaces with molecular periodicity, well aligned on macroscopic distances. This provides regular nanophases of soft−hard, hydrophobic−hydrophilic units. Polystyrene-polyethylene (PS-PE) thin films also form surface-perpendicular crystalline PE cylinders.[351]

Table 2. Capabilities of HAR and 3D Patterning Techniques for Industrial and Large-Area Manufacture (++ High; + Medium; − Low)

technique	HAR capability	3D capability	wet processing	mask or mould	flexible design	cost	large area	throughput
UV	++	+	yes	yes	−	+	+	++
X-ray	++	+	yes	yes	−	++	+	+
modulated	+	++	yes	yes	−	++	+	+
interference lithography	+	++	yes	no	+	+	++	+
laser prototyping	++	++	yes	no	++	+	++	+
serial writing	+	+	yes	no	−	++	−	−
machining	+	+	no	no	+	++	−	−
material deposition	++	++	no	no	++	+	+	+
moulding	++	+	no	yes	+	−	++	++
filling membranes	++	−	yes	yes	−	+	−	−
surface instabilities	+	−	no	optional	−	−	+	+
block copolymers	+	+	yes	no	+	−	++	+

Blending BCs with homopolymers offers interesting combinations of micro- and nanostructured films.[296] The final morphology strongly depends on the molecular weight of the homopolymer and the composition of the blend. These films are usually fabricated by diffusing homopolymer molecules from a selective solvent into the BC film. In this way, homopolymer molecules are incorporated into a microphase ordered block copolymer by either swelling the host microdomains or inducing new morphological transformations.[365−367] An interesting study shows an increase in the aspect ratio of perpendicularly oriented cylindrical microdomains of PS-PMMA thin films upon addition of PMMA homopolymer.[367]

12. Comparison of Patterning Methods

Table 2 compares the different patterning methods described in the previous sections in terms of structuring capability and application feasibility in an industrial context. Cost, flexibility, and throughput are the most relevant issues when it comes to manufacturing. It is evident that none of the available methods satisfies all criteria.

Photolithography is now a well-established method capable of patterning small features across wafer-size areas at high throughput with current state-of-the-art irradiation sources and steppers. However, the high cost of the masks, equipment, and photoresist materials limits its application to high added value products (e.g., electronics, photonics). In addition, available resist materials require a wet development step that may be incompatible with stringent pattern geometries (structure collapse of HAR features during drying, structure damage during development of patterns with coexisting features with different sizes). Novel SC−CO_2 processable resists may help at this point, but the high cost of SC drying equipment will be hard to overcome.

Photolithographic patterning of complex structures is possible using multiexposure methods and specialized resists. The complexity of the achievable designs correlates with the number of coating/exposure steps, and this limits the industrial implementation of these strategies. Interference lithography provides increased throughput in 3D patterning at the cost of reduced flexibility of pattern geometry (only symmetric structures). Two-photon laser scanning overcomes the flexibility issue and allows serial writing of arbitrary geometries and patterning over surface topographies that deviate significantly from planarity. However, writing speeds are slow, and the irradiation sources require high-intensity laser beams. Development of novel materials with better TPA cross section will certainly enable application of this strategy.

Serial methods based on writing or machining with charged particles (electrons or ions) accomplish similar tasks using a scanned beam of high-energy particles rather than photons but also share the slow-speed inconvenience. In addition, such irradiation sources are not available in every lab and involve very expensive equipment.

Lithography does not offer any flexibility in the choice of the patterned material and strictly requires photosensitive formulations. Writing patterns by direct deposition of small quantities of material with micro- to nanometer accuracy may attract more interest in the future in terms of material versatility. Almost any material and any pattern can be written by this method provided that the material solution (or dispersion) has the appropriate rheological properties. These can be easily tuned by changing the solvent and concentration. The capability of this technique for high-throughput patterning relies on the development of rapid delivery tools with nanometer accuracy positional control.

Moulding methods constitute at this moment the only reasonable alternative for low-cost, high-throughput patterning which also offers considerable flexibility in the choice of material. However, moulding in its simplest conception is not applicable to obtaining patterns possessing re-entrant features, and therefore, it is very limited in the geometrical design. When combined with transfer steps, moulding can indeed create complex geometries by stacking layers with different pattern designs. An interesting issue for the future will be the exploitation of matter self-ordering phenomena (phase separation, crystallization, etc.) in confined dimensions to create moulded nanostructures with interesting material designs (anisotropy, orientation, etc.).

Surface capillary waves and nanoscale phase separation effects exploit soft-matter ordering phenomena to build periodic patterns and do not require the use of any mask or mould. Particularly interesting is the fact that these methods may generate complex topographical patterns where different materials are combined in different structuration levels. The length scale at which microphase separation occurs in BCs, 10−100 nm, is particularly interesting for patterning at the submicrometer scale.[296] Indeed, by tuning molecular parameters (block number and length, composition, species), microphase domains with a variety of motifs, chemistries, and tailored size and periodicity might be created. Furthermore, recent developments in block copolymer synthesis, such as atom transfer radical polymerization, have greatly widened the spectrum of available copolymer materials or decreased their cost of manufacture. Moreover, being a self-assembly driven process, the BC morphologies obtained are

thermodynamically stable, and therefore BC patterns are self-healing.

Application of BCs in nanopatterning a surface requires a different sensitivity of the blocks against an etching method in order to permit the selective removal of one block.[311,312,368−375] Wet etching is not recommendable because of possible swelling of the second block or debonding from the substrate surface. Dry etching with plasmas seems to be a better possibility. BCs containing an organometallic polymer (e.g., poly(isoprene-*b*-ferrocenyldimethylsilane)) are good candidates for this purposs since they are much more resistant against O_2 plasma etching than their organic counterparts. Additionally, BCs containing PS and PI or PB as the other component do also show selective etching. Ozone cleaves the double bonds in the unsaturated polymers, so that they can be etched away in experimental conditions under which PS remains fairly stable. Additional systems and strategies must be developed to solve these problems.

13. Applications

13.1. Biosensors with Increased Sensitivity, Miniaturization, and Throughput

HAR patterns possess an increased active surface area per unit substrate surface area. In on-chip sensor technology, increased surface area leads to increased sensitivities and improved detection limits. This is due to the fact that the ability to detect any target depends on the density of complementary capture probes immobilized on the chip. High-sensitivity immunoassay chips have been fabricated from HAR patterns of pillars with diameters of 80−1000 nm and heights of 1−3 μm using imprinting technology.[177] The sensitivity of these chips has been reported to be 2−3 times higher than on flat surfaces.

Similarly, HAR patterns can be used in continuous flow microreactors. Heterogeneous reactions conducted in microreactors, whereby the catalyst or one reactant is grafted onto the surface of the microchannels, proceed at higher reaction rates and therefore higher throughput if the surface area is increased. In microfluidics, larger cross-sectional area leads also to increased fluid flow and better analysis performance. The higher sensitivity and throughput achieved through HAR patterns permit a reduction in the lateral size of microdevices and further miniaturization of such systems. These are important issues for chemical and biochemical applications such as microreactors, micromixers, chromatographic columns, or DNA concentrators to allow larger fluid flow volume for good sensitivity, performance, and multitasking within a small area.[376−379] In integrated microfluidics, 3D patterning offers the possibility of building buried channels and closed reservoirs. Examples of flyover channels connecting vertical microtank structures based on X-ray and e-beam lithography have been reported.[70]

13.2. Drug Delivery

Major efforts are currently spent on new methods for precise and minimally invasive drug delivery. Transdermal delivery is widely recognized as one of the most promising techniques. Delivery occurs through the skin via an array of microneedles with typical lengths between 150 and 200 μm. The microneedles penetrate the skin and deliver the drug under the skin surface. This method allows a wide range of delivery rates with minimum invasiveness and high patient comfort.

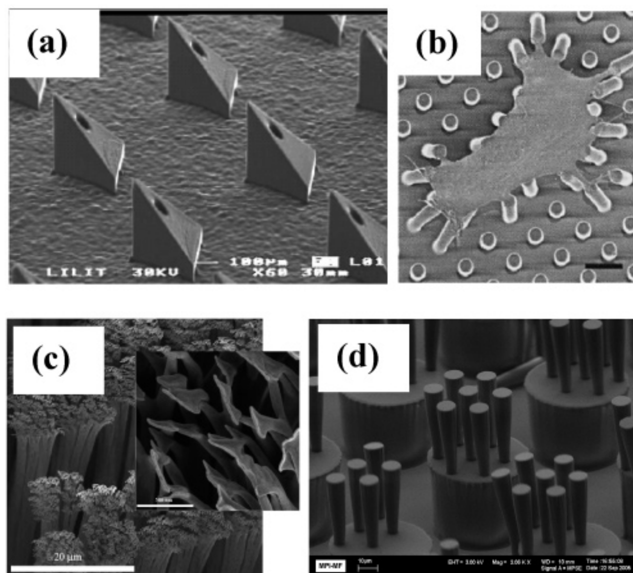

Figure 37. Examples of applications of HAR and 3D patternerd surfaces. (a) Replicated array of PMMA microneedles with height 400 μm. (Reprinted with permission from ref 381. Copyright 2005 IOP Publishing Limited.) (b) SEM picture of a smooth muscle cell attached to an array of PDMS posts printed with fibronectin which act as force sensors. Scale bar indicates 10 μm. (Reprinted with permission from ref 382. Copyright 2003 National Academy of Sciences, U.S.A.) (c) SEM micrographs of gecko's arrays of setae and (inset) details of the spatulae at the tip of the setae.[415] (d) Microfabricated bioinspired adhesives by lithography (layer-by-layer exposure) using SU-8.

To this end, arrays of 400 μm long microneedles have been fabricated by a combination of double-exposure X-ray lithography, LIGA technology, soft moulding using water-soluble PVA, and replication with PMMA[380] (Figure 37a). In addition to the advantages mentioned above, microneedle arrays made of polymeric materials allow disposable delivery by enabling low-cost mass fabrication schemes.

13.3. Force Sensors

Patterned surfaces have become important tools for the study of cell behavior and attachment to surfaces. Arrays of HAR pillars have been used as sensors for mechanical forces in studies in cell biology. Cells are plated on the patterned substrates and cause the pillars to bend while attaching to the substrate. The bending angle reflects the traction force exerted by the cell. In this way, the pillars work as spatially resolved mechanical sensors (Figure 37b).[381−384]

13.4. Tissue Engineering and Implant Fabrication

Tissue engineering relies on the ability of cultured cells to construct new tissue around an artificial scaffold. This depends on the cell chemotactic response to the scaffold surface that controls processes such as adhesion, growth, mobility, differentiation, or apoptosis. Cell−scaffold interaction is dominated by the type and length scale of the surface topography. As an example, microchannels and ridges in the scaffold promote contact guidance to orient cells, providing organization and mechanical strength required by healthy tissue.[385−392] The chemical composition and mechanical properties of the scaffold also influence the chemotactic response of the cell. Therefore, extension of the described patterning techniques to biocompatible materials will certainly impact tissue engineering in the future.

Cell attachment and growth onto surfaces is not always beneficial. Specific surfaces need to be engineered to cause cell repellence or selective repellence of a group of cells and specific adherence of others. Intravascular stents for treatment of coronary blockage constitute an instructive example.[393−395] Once inserted in the blood vessel, the stent needs to be endotelized quickly in order to avoid activation of the immune system. Patterns of parallel grooves in the direction of flow on the inner surface of stents have been demonstrated to increase endothelial cell migration rates, resulting in decreased time to total coverage of the prosthetic surface.[395] On the other hand, the long-term performance of stents is strongly related to the control of platelet activation and adherence of inflammatory cells to their surface, which leads to a negative dogging effect. One way to improve this consists of coating the stent with drug diluting polymers that release antiproliferative and antiinflammatory substances. Another method would be to exploit the selective response of cells to patterned surfaces with different length scales. Studies in this area are currently being performed, and patterning methods for a real application will be required.

13.5. Biofouling

Biofouling is a big concern in the marine world. The surfaces of ships and under-sea pipelines need to be treated to avoid attachment of marine microorganisms, algae, or crustacei which weaken their durability and reduce their performance. Surface patterning with structures at length scales that are too small for these species to attach to would be highly beneficial for improving durability and long-term stability. Some examples of micropatterned coatings with increased stability against biofouling have already been reported.[396−398]

13.6. Biomimetic Surfaces

Microstructured surfaces are responsible for several unique effects occurring in nature. The wax microrelief of the Lotus leaves causes water repellence and leads to an efficient self-cleaning mechanism. The subwavelength structured surface of the cornea of the moth eye acts as an effective antireflecting medium, suiting the purpose of night camouflage. The streamlined 3D rib pattern of the sharkskin reduces turbulent wall shear stress in fluid media and allows higher flow velocities (improvements in aircraft technology and swimwear based on these features have already been accomplished). The development of bioinspired artificial surfaces possessing these properties depends on the availability of patterning techniques to reproduce these complicated structures.[261,399]

Surface microstructure also plays an important role in many biological attachment systems. The attachment pads of many insects and the feet of geckos are structured with micro- to nanometer sized hairs with particular dimensions and geometries (Figure 37c,d).[400−403] This HAR pattern seems to be the key to their ability to walk across vertical walls and ceilings. Some attempts to fabricate adhesive surfaces with similar characteristics have been reported during the last 5 years, but none of them has been able to approach the complexity of the natural structures (not to mention their performance).[404−407] Future improvements in HAR patterning will certainly impact this area as well.

13.7. Photonic Structures

Photonic crystals are microstructured materials in which the dielectric constant is periodically modulated on a length scale comparable to the desired wavelength of operation. A simple example consists of a periodic array of voids within a dielectric matrix. Multiple interference between waves scattered from each unit cell of the structure may open a "photonic band gap": a range of frequencies, analogous to the electronic band gap of a semiconductor, within which no propagating electromagnetic modes exist. These systems have attracted great interest in recent years owing to their capabilities in controlling emission and propagation of light waves as well as their potential applications in optoelectronics and information processing. Some progress in creating such periodic 3D patterns has been achieved by IL[75,90,408−411] and more recently BCs.[412]

14. Conclusions

With the increasing interest in the properties associated to complex structured surfaces made of low-cost polymeric materials, different patterning strategies have arisen and some in particular have become well established. This has required parallel development of novel technologies and materials which are specific for each methodology. Although each patterning method is championed by different groups to be the best procedure, in reality there is no "best" method (nor material) for their fabrication. All methods have their own specificity and potentials that in many cases do not cover the entire spectrum of the fabrication needs. In addition, most of the reported methods still remain at the proof-of-principle stage, and the way to real and large-scale manufacture of surfaces with aleatoric designs still represents a big challenge. At the moment, the suitable strategy strictly depends on the surface geometry required for a particular application, and future development will probably exploit smart combinations of various strategies. This will extend the fabrication potential to a wider class of micro- and nano-objects that pave the road to novel device categories and performances.

15. References

(1) Wallraff, G. M.; Hinsberg, W. D. *Chem. Rev.* **1999**, *99*, 1801.
(2) Gates, B. D.; Xu, Q. B.; Stewart, M.; Ryan, D.; Willson, C. G.; Whitesides, G. M. *Chem. Rev.* **2005**, *105*, 1171.
(3) Gates, B. D.; Xu, Q. B.; Love, J. C.; Wolfe, D. B.; Whitesides, G. M. *Ann. Rev. Mater. Res.* **2004**, *34*, 339.
(4) Geissler, M.; Xia, Y. N. *Adv. Mater.* **2004**, *16*, 1249.
(5) Rothschild, M. *Mater. Today* **2005**, 18.
(6) Brunner, T. A. *J. Vac. Sci. Technol. B* **2003**, *21*, 2632.
(7) Ito, T.; Okazaki, S. *Nature* **2000**, *406*, 1027.
(8) Willson, C. G.; Trinque, B. C. *J. Photopolym. Sci. Technol.* **2003**, *16*, 621.
(9) Rothschild, M.; Bloomstein, T. M.; Kunz, R. R.; Liberman, V.; Switkes, M.; Palmacci, S. T.; Sedlacek, J. H. C.; Hardy, D.; Grenville, A. *J. Vac. Sci. Technol. B* **2004**, *22*, 2877.
(10) Gil, D.; Brunner, T. A.; Fonseca, C.; Seong, N.; Streefkerk, B.; Wagner, C.; Stavenga, M. *J. Vac. Sci. Technol. B* **2004**, *22*, 3431.
(11) Ito, H. *Adv. Polym. Sci.* **2005**, *172*, 37.
(12) http://www.Dupont.com/pcm.
(13) http://www.tok.co.jp/products/products-e2.htm.
(14) http://www.insulectro.com/dryfilm.htm.
(15) http://www.thinktink.com/stack/volumes/voli/store/specs/4615spec.htm.
(16) http://www.jsits.com/kpr/facility.htm.
(17) Koukharenko, E.; Kraft, M.; Ensell, G. J.; Hollinshead, N. *J. Mater. Sci.: Mater. Electron.* **2005**, *16*, 741−747.
(18) Ito, H.; Willson, C. G. In *Polymers in Electronics*; Davidson, T., Ed.; ACS Symposium Series 242; American Chemical Society: Washington, DC, 1984; pp 11−23.
(19) Teh, W. H.; Duerig, U.; Drechsler, U.; Smith, C. G.; Guentherodt, H. J. *J. Appl. Phys.* **2005**, *97*, 054907/054901.
(20) Lorenz, H.; Despont, M.; Fahrni, N.; Brugger, J.; Vettiger, P.; Renaud, P. *Sens. Actuators, A: Phys.* **1998**, *64*, 33.

(21) Houbertz, R.; Frohlich, L.; Popall, M.; Streppel, U.; Dannberg, P.; Brauer, A.; Serbin, J.; Chichkov, B. N. *Adv. Eng. Mater.* **2003**, *5*, 551.
(22) Haas, K. H.; Wolter, H. *Curr. Opin. Solid State Mater. Sci.* **1999**, *4*, 571.
(23) Junarsa, I.; Nealeya, P. F. *J. Vac. Sci. Technol. B* **2004**, *22*, 2685.
(24) Yang, R.; Wang, W. *Sens. Actuators, B: Chem.* **2005**, *110*, 279.
(25) Chuang, Y. J.; Tseng, F. G.; Lin, W. K. *Microsyst. Technol.* **2002**, *8*, 308.
(26) Malek, C. K.; Yajamanyam, S. *J. Vac. Sci. Technol. B* **2000**, *18*, 3354.
(27) Chan-Park, M. B.; Zhang, J.; Yan, Y.; Yue, C. Y. *Sens. Actuators, B: Chem.* **2004**, *B101*, 175.
(28) Cheng, C.-M.; Chen, R.-H. *Microelectron. Eng.* **2004**, *71*, 335.
(29) Cheng, C.-M.; Chen, R.-H. *J. Micromech. Microeng.* **2001**, *11*, 692.
(30) Meyer, P.; El-Kholi, A.; Schulz, J. *Microelectron. Eng.* **2002**, *63*, 319.
(31) Williams, J. D.; Wang, W. *Microsyst. Technol.* **2004**, *10*, 694.
(32) Tanaka, T.; Morigami, M.; Atoda, N. *J. Electrochem. Soc.* **1993**, *140*, L115.
(33) Namatsu, H.; Kurihara, K.; Nagase, M.; Iwadate, K.; Murase, K. *Appl. Phys. Lett.* **1995**, *66*, 2655.
(34) Cao, H. B.; Nealey, P. F.; Domke, W. D. *J. Vac. Sci. Technol. B* **2000**, *18*, 3303.
(35) Shibata, T.; Ishii, T.; Nozawa, H.; Tamamura, T. *Jpn. J. Appl. Phys. 1* **1997**, *36*, 7642.
(36) Tanaka, T.; Morigami, M.; Oizumi, H.; Ogawa, T.; Uchino, S. *Jpn. J. Appl. Phys. 2* **1994**, *33*, L1803.
(37) Tanaka, T.; Morigami, M.; Oizumi, H.; Soga, T.; Ogawa, T.; Murai, F. *J. Electrochem. Soc.* **1994**, *141*, L169.
(38) Kondo, T.; Juodkazis, S.; Misawa, H. *Appl. Phys. A* **2006**, *81*, 1583.
(39) Tanaka, T.; Morigami, M.; Atoda, N. *Jpn. J. Appl. Phys. 1* **1993**, *32*, 6059.
(40) Yamashita, Y. *Jpn. J. Appl. Phys. 1* **1996**, *35*, 2385.
(41) Namatsu, H.; Yamazaki, K.; Kurihara, K. *J. Vac. Sci. Technol. B* **2000**, *18*, 780.
(42) DeSimone, J. M. *Science* **2002**, *297*, 799.
(43) Namatsu, H. *J. Photopolym. Sci. Technol.* **2002**, *15*, 381.
(44) Namatsu, H. *Jpn. J. Appl. Phys., Part 2* **2004**, *43*, L456.
(45) Namatsu, H.; Sato, M. *Jpn. J. Appl. Phys., Part 2* **2005**, *44*, L227.
(46) King, J. W.; Williams, L. L. *Curr. Opin. Solid State Mater. Sci.* **2003**, *7*, 413.
(47) Namatsu, H. *J. Vac. Sci. Technol. B* **2000**, *18*, 3308.
(48) Goldfarb, D. L.; de Pablo, J. J.; Nealey, P. F.; Simons, J. P.; Moreau, W. M.; Angelopoulos, M. *J. Vac. Sci. Technol. B* **2000**, *18*, 3313.
(49) Jones, C.; Zweber, A.; DeYoung, J.; McClain, J.; Carbonell, R.; DeSimone, J. *Crit. Rev. Solid State Mater. Sci.* **2004**, *29*, 97.
(50) Zhang, X.; Pham, J. Q.; Ryza, N.; Green, P. F.; Johnston, K. P. *J. Vac. Sci. Technol. B:* **2004**, *22*, 818.
(51) Sundararajan, N.; Yang, S.; Ogino, K.; Valiyaveettil, S.; Wang, J.; Zhou, X.; Ober, C. K.; Obendorf, S. K.; Allen, R. D. *Chem. Mater.* **2000**, *12*, 41.
(52) Weibel, G. L.; Ober, C. K. *Microelectron. Eng.* **2002**, *65*, 145.
(53) Ober, C. K.; Gabor, A. H.; Gallagher Wetmore, P.; Allen, R. D. *Adv. Mater.* **1997**, *9*, 1039.
(54) Flowers, D.; Hoggan, E. N.; Carbonell, R. G.; DeSimone, J. M. *Abstr. Pap. Am. Chem. S* **2002**, *224*, U502, ACS Fall Meeting, Boston (MA), August 18−22 (2002).
(55) Hoggan, E. N.; Flowers, D.; Wang, K.; DeSimone, J. M.; Carbonell, R. G. *Ind. Eng. Chem. Res.* **2004**, *43*, 2113.
(56) Peele, A. G.; Shew, B. Y.; Vora, K. D.; Li, H. C. *Microsyst. Technol.* **2005**, *11*, 221.
(57) Dentinger, P. M.; Krafcik, K. L.; Simison, K. L.; Janek, R. P.; Hachman, J. *Microelectron. Eng.* **2002**, *61−2*, 1001.
(58) Loechel, B. *J. Micromech. Microeng.* **2000**, *10*, 108.
(59) O'Brien, J.; Hughes, P. J.; Brunet, M.; O'Neill, B.; Alderman, J.; Lane, B.; O'Riordan, A.; O'Driscoll, C. *J. Micromech. Microeng.* **2001**, *11*, 353.
(60) Lin, C. H.; Lee, G. B.; Chang, B. W.; Chang, G. L. *J. Micromech. Microeng.* **2002**, *12*, 590.
(61) Williams, J. D.; Wang, W. J. *J. Microlith. Microfab.* **2004**, *3*, 563.
(62) Malek, C. K.; Jackson, K. H.; Bonivert, W. D.; Hruby, J. *J. Micromech. Microeng.* **1996**, *6*, 228.
(63) Achenbach, S. *Microsyst. Technol.* **2004**, *10*, 493.
(64) Achenbach, S.; Mappes, T.; Mohr, J. *J. Vac. Sci. Technol. B* **2004**, *22*, 3196.
(65) Bogdanov, A. L.; Peredkov, S. S. *Microelectron. Eng.* **2000**, *53*, 493.
(66) Mata, A.; Fleischman, A. J.; Roy, S. *J. Micromech. Microeng.* **2006**, *16*, 276.
(67) Han, M.; Lee, W.; Lee, S.-K.; Lee, S. S. *Sens. Actuators, A: Phys.* **2004**, *A111*, 14.
(68) Romanato, F.; Cojoc, D.; Di Fabrizio, E.; Galli, M.; Bajoni, D. *J. Vac. Sci. Technol. B* **2003**, *21*, 2912.
(69) Sato, H.; Houshi, Y.; Shoji, S. *Microsyst. Technol.* **2004**, *10*, 440.
(70) Romanato, F.; Tormen, M.; Businaro, L.; Vaccari, L.; Stomeo, T.; Passaseo, A.; Di Fabrizio, E. *Microelectron. Eng.* **2004**, *73−74*, 870.
(71) Mekaru, H.; Utsumi, Y.; Hattori, T. *Microsyst. Technol.* **2002**, *9*, 36.
(72) Park, J.-Y.; Kim, K.-T.; Shin, H.-J.; Moon, S.; Pak, J. J. *Microsyst. Technol.* **2005**, *11*, 168.
(73) Turner, R.; Desta, Y.; Kelly, K.; Zhang, J.; Geiger, E.; Cortez, S.; Mancini, D. C. *J. Micromech. Microeng.* **2003**, *13*, 367.
(74) Awazu, K.; Wang, X.; Fujimaki, M.; Kuriyama, T.; Sai, A.; Ohki, Y.; Imai, H. *J. Vac. Sci. Technol. B* **2005**, *23*, 934.
(75) Cuisin, C.; Chelnokov, A.; Lourtioz, J. M.; Decanini, D.; Chen, Y. *J. Vac. Sci. Technol. B* **2000**, *18*, 3505.
(76) Cuisin, C.; Chen, Y.; Decanini, D.; Chelnokov, A.; Carcenac, F.; Madouri, A.; Lourtioz, J. M.; Launois, H. *J. Vac. Sci. Technol. B* **1999**, *17*, 3444.
(77) Galas, J. C.; Belier, B.; Aassime, A.; Palomo, J.; Bouville, D.; Aubert, J. *J. Vac. Sci. Technol. B* **2004**, *22*, 1160.
(78) Kudryashov, V.; Yuan, X. C.; Cheong, W. C.; Radhakrishnan, K. *Microelectron. Eng.* **2003**, *67−68*, 306.
(79) Waits, C. M.; Modafe, A.; Ghodssi, R. *J. Micromech. Microeng.* **2003**, *13*, 170.
(80) Wu, H. K.; Odom, T. W.; Whitesides, G. M. *Anal. Chem.* **2002**, *74*, 3267.
(81) Chen, C. C.; Hirdes, D.; Folch, A. *Proc. Natl. Acad. Sci. U.S.A.* **2003**, *100*, 1499.
(82) Totsu, K.; Esashi, M. *J. Vac. Sci. Technol. B* **2005**, *23*, 1487.
(83) Lee, T. W.; Jeon, S.; Maria, J.; Zaumseil, J.; Hsu, J. W. P.; Rogers, J. A. *Adv. Funct. Mater.* **2005**, *15*, 1435.
(84) Jeon, S.; Menard, E.; Park, J.-U.; Maria, J.; Meitl, M.; Zaumseil, J.; Rogers, J. A. *Adv. Mater.* **2004**, *16*, 1369.
(85) Jeon, S.; Menard, E.; Park, J. U.; Maria, J.; Meitl, M.; Zaumseil, J.; Rogers, J. A. *Adv. Mater.* **2004**, *16*, 1369.
(86) Jeon, S.; Park, J. U.; Cirelli, R.; Yang, S.; Heitzman, C. E.; Braun, P. V.; Kenis, P. J. A.; Rogers, J. A. *Proc. Natl. Acad. Sci. U.S.A.* **2004**, *101*, 12428.
(87) Dang, H.; Tan, J. L.-P.; Horn, M. W. *J. Vac. Sci. Technol. B* **2003**, *21*, 1143.
(88) Chen, X. L.; Zaidi, S. H.; Brueck, S. R. J.; Devine, D. J. *J. Vac. Sci. Technol. B* **1996**, *14*, 3339.
(89) Fernandez, A.; Decker, J. Y.; Herman, S. M.; Phillion, D. W.; Sweeney, D. W.; Perry, M. D. *J. Vac. Sci. Technol. B* **1997**, *15*, 2439.
(90) Campbell, M.; Sharp, D. N.; Harrison, M. T.; Denning, R. G.; Turberfield, A. J. *Nature* **2000**, *404*, 53.
(91) Meisel, D. C.; Wegener, M.; Busch, K. *Phys. Rev. B* **2004**, *70*, 165104/165101.
(92) Sharp, D. N.; Campbell, M.; Dedman, E. R.; Harrison, M. T.; Denning, R. G.; Turberfield, A. J. *Opt. Quant. Electron.* **2002**, *34*, 3.
(93) Chan, T. Y. M.; Toader, O.; John, S. *Phys. Rev. E* **2005**, *71*, 046605/046601.
(94) Li, E.; Xi, J.; Chicharo, J. *Smart Mater. Struct.* **2006**, *15*, S158.
(95) Wang, X.; Xu, J. F.; Su, H. M.; Zeng, Z. H.; Chen, Y. L.; Wang, H. Z.; Pang, Y. K.; Tam, W. Y. *Appl. Phys. Lett.* **2003**, *82*, 2212.
(96) Wu, L.; Zhong, Y.; Chan, C. T.; Wong, K. S.; Wang, G. P. *Appl. Phys. Lett.* **2005**, *86*, 241102/241101.
(97) Ullal, C. K.; Maldovan, M.; Thomas, E. L.; Chen, G.; Han, Y.-J.; Yang, S. *Appl. Phys. Lett.* **2004**, *84*, 5434.
(98) Zhong, Y. C.; Zhu, S. A.; Su, H. M.; Wang, H. Z.; Chen, J. M.; Zeng, Z. H.; Chen, Y. L. *Appl. Phys. Lett.* **2005**, *87*, 061103/061101.
(99) Sharp, D. N.; Turberfield, A. J.; Denning, R. G. *Phys. Rev. B* **2003**, *68*, 205102/205101.
(100) Pang, Y. K.; Lee, J. C. W.; Lee, H. F.; Tam, W. Y.; Chan, C. T.; Sheng, P. *Opt. Express* **2005**, *13*, 7615.
(101) Wang, X.; Xu, J.; Lee, J. C. W.; Pang, Y. K.; Tam, W. Y.; Chan, C. T.; Sheng, P. *Appl. Phys. Lett.* **2006**, *88*, 051901/051901.
(102) Saravanamuttu, K.; Blanford, C. F.; Sharp, D. N.; Dedman, E. R.; Turberfield, A. J.; Denning, R. G. *Chem. Mater.* **2003**, *15*, 2301.
(103) Gombert, A.; Blasi, B.; Buhler, C.; Nitz, P.; Mick, J.; Hossfeld, W.; Niggemann, M. *Opt. Eng.* **2004**, *43*, 2525.
(104) Bertsch, A.; Lorenz, H.; Renaud, P. *Sens. Actuators, A: Phys.* **1999**, *A73*, 14.
(105) Sun, H.-B.; Kawata, S. *Adv. Polym. Sci.* **2004**, *170*, 169.
(106) Teh, W. H.; Durig, U.; Salis, G.; Harbers, R.; Drechsler, U.; Mahrt, R. F.; Smith, C. G.; Guntherodt, H. J. *Appl. Phys. Lett.* **2004**, *84*, 4095.
(107) Juodkazis, S.; Mizeikis, V.; Seet, K. K.; Miwa, M.; Misawa, H. *Nanotechnology* **2005**, *16*, 846.
(108) Houbertz, R.; Schulz, J.; Froehlich, L.; Domann, G.; Popall, M.; Serbin, J.; Chichkov, B. *Mater. Res. Soc. Symp. Proc.* **2003**, *780*, 175.

(109) LaFratta, C. N.; Baldacchini, T.; Farrer, R. A.; Fourkas, J. T.; Teich, M. C.; Saleh, B. E. A.; Naughton, M. J. *J. Phys. Chem. B* **2004**, *108*, 11256.
(110) Saita, S.; Yamaguchi, T.; Kawai, T.; Irie, M. *ChemPhysChem* **2005**, *6*, 2300.
(111) Albota, M.; Beljonne, D.; Bredas, J. L.; Ehrlich, J. E.; Fu, J. Y.; Heikal, A. A.; Hess, S. E.; Kogej, T.; Levin, M. D.; Marder, S. R.; McCord-Maughon, D.; Perry, J. W.; Rockel, H.; Rumi, M.; Subramaniam, C.; Webb, W. W.; Wu, X. L.; Xu, C. *Science* **1998**, *281*, 1653.
(112) Rumi, M.; Ehrlich, J. E.; Heikal, A. A.; Perry, J. W.; Barlow, S.; Hu, Z. Y.; McCord-Maughon, D.; Parker, T. C.; Rockel, H.; Thayumanavan, S.; Marder, S. R.; Beljonne, D.; Bredas, J. L. *J. Am. Chem. Soc.* **2000**, *122*, 9500.
(113) Yu, T.; Ober, C. K.; Kuebler, S. M.; Zhou, W.; Marder, S. R.; Perry, J. W. *Adv. Mater.* **2003**, *15*, 517.
(114) Cumpston, B. H.; Ananthavel, S. P.; Barlow, S.; Dyer, D. L.; Ehrlich, J. E.; Erskine, L. L.; Heikal, A. A.; Kuebler, S. M.; Lee, I. Y. S.; McCord-Maughon, D.; Qin, J.; Rockel, H.; Rumi, M.; Wu, X.-L.; Marder, S. R.; Perry, J. W. *Nature* **1999**, *398*, 51.
(115) Zhou, W.; Kuebler, S. M.; Braun, K. L.; Yu, T.; Cammack, J. K.; Ober, C. K.; Perry, J. W.; Marder, S. R. *Science* **2002**, *296*, 1106.
(116) Nguyen, L. H.; Straub, M.; Gu, M. *Adv. Funct. Mater.* **2005**, *15*, 209.
(117) Kuebler, S. M.; Braun, K. L.; Zhou, W. H.; Cammack, J. K.; Yu, T. Y.; Ober, C. K.; Marder, S. R.; Perry, J. W. *J. Photochem. Photobiol. A* **2003**, *158*, 163.
(118) Cumpston, B. H.; Ananthavel, S. P.; Barlow, S.; Dyer, D. L.; Ehrlich, J. E.; Erskine, L. L.; Heikal, A. A.; Kuebler, S. M.; Lee, I. Y. S.; McCord-Maughon, D.; Qin, J. Q.; Rockel, H.; Rumi, M.; Wu, X. L.; Marder, S. R.; Perry, J. W. *Nature* **1999**, *398*, 51.
(119) Belfield, K. D.; Ren, X. B.; Van Stryland, E. W.; Hagan, D. J.; Dubikovsky, V.; Miesak, E. J. *J. Am. Chem. Soc.* **2000**, *122*, 1217.
(120) Lu, Y.; Hasegawa, F.; Goto, T.; Ohkuma, S.; Fukuhara, S.; Kawazu, Y.; Totani, K.; Yamashita, T.; Watanabe, T. *J. Mater. Chem.* **2004**, *14*, 75.
(121) Strehmel, V.; Sarker, A. M.; Lahti, P. M.; Karasz, F. E.; Heydenreich, M.; Wetzel, H.; Haebel, S.; Strehmel, B. *ChemPhysChem* **2005**, *6*, 267.
(122) Strehmel, B.; Amthor, S.; Schelter, J.; Lambert, C. *ChemPhysChem* **2005**, *6*, 893.
(123) Wang, Y.; He, G. S.; Prasad, P. N.; Goodson, T. *J. Am. Chem. Soc.* **2005**, *127*, 10128.
(124) Strehmel, B.; Sarker, A. M.; Detert, H. *ChemPhysChem* **2003**, *4*, 249.
(125) Schwarz, C. J.; Nampoothiri, A. V. V.; Jasapara, J. C.; Rudolph, W.; Brueck, S. R. J. *J. Vac. Sci. Technol. B* **2001**, *19*, 2362.
(126) Yin, X.; Fang, N.; Zhang, X.; Martini, I. B.; Schwartz, B. J. *Appl. Phys. Lett.* **2002**, *81*, 3663.
(127) Gerry, C. C. *Phys. Rev. A* **2003**, *67*, 043801/043801.
(128) Gerry, C. C.; Benmoussa, A. *Phys. Rev. A* **2002**, *65*, 033822/033821.
(129) Tormen, M.; Businaro, L.; Altissimo, M.; Romanato, F.; Cabrini, S.; Perennes, F.; Proietti, R.; Sun, H.-B.; Kawata, S.; Di Fabrizio, E. *Microelectron. Eng.* **2004**, *73*−*74*, 535.
(130) Pan, E. Y.; Pu, N. W.; Tong, Y. P.; Yau, H. F. *Appl. Phys. B* **2003**, *77*, 485.
(131) Bilenberg, B.; Scholer, M.; Shi, P.; Schmidt, M. S.; Boggild, P.; Fink, M.; Schuster, C.; Reuther, F.; Gruetzner, C.; Kristensen, A. *J. Vac. Sci. Technol. B* **2006**, *24*, 1776.
(132) Elsner, H.; Meyer, H. G. *Microelectron. Eng.* **2001**, *57*−*58*, 291.
(133) Yamazaki, K.; Namatsu, H. *Microelectron. Eng.* **2004**, *73*−*74*, 85.
(134) van Kan, J. A.; Bettiol, A. A.; Ansari, K.; Teo, E. J.; Sum, T. C.; Watt, F. *Int. J. Nanotechnol.* **2004**, *1*, 464.
(135) van Kan, J. A.; Bettiol, A. A.; Watt, F. *Appl. Phys. Lett.* **2003**, *83*, 1629.
(136) Ansari, K.; van Kan, J. A.; Bettiol, A. A.; Watt, F. *Appl. Phys. Lett.* **2004**, *85*, 476.
(137) Munnik, F.; Benninger, F.; Mikhailov, S.; Bertsch, A.; Renaud, P.; Lorenz, H.; Gmur, M. *Microelectron. Eng.* **2003**, *67*−*68*, 96.
(138) Osipowicz, T.; van Kan, J. A.; Sum, T. C.; Sanchez, J. L.; Watt, F. *Nucl. Instrum. Methods B* **2000**, *161*, 83.
(139) Soh, H. T.; Guarini, K. W.; Quate, C. F. *Scanning Probe Lithography*; Kluwer Academic Publishers: New York, 2001.
(140) Vasile, M. J.; Nassar, R.; Xie, J. S. *J. Vac. Sci. Technol. B* **1998**, *16*, 2499.
(141) Fu, Y.; Bryan, N. K. A. *J. Vac. Sci. Technol. B* **2005**, *23*, 984.
(142) Fujii, T.; Iwasaki, K.; Munekane, M.; Takeuchi, T.; Hasuda, M.; Asahata, T.; Kiyohara, M.; Kogure, T.; Kijima, Y.; Kaito, T. *J. Micromech. Microeng.* **2005**, *15*, S286.
(143) Mamin, H. J.; Terris, B. D.; Fan, L. S.; Hoen, S.; Barrett, R. C.; Rugar, D. *IBM J. Res. Dev.* **1995**, *39*, 681.
(144) Minne, S. C.; Manalis, S. R.; Atalar, A.; Quate, C. F. *J. Vac. Sci. Technol. B* **1996**, *14*, 2456.
(145) Despont, M.; Drechsler, U.; Yu, R.; Pogge, H. B.; Vettiger, P. *J. Microelectromech. Syst.* **2004**, *13*, 895.
(146) Vettiger, P.; Cross, G.; Despont, M.; Drechsler, U.; Durig, U.; Gotsmann, B.; Haberle, W.; Lantz, M. A.; Rothuizen, H. E.; Stutz, R.; Binnig, G. K. *IEEE Nanotechnol.* **2002**, *1*, 39.
(147) Vettiger, P.; Despont, M.; Drechsler, U.; Durig, U.; Haberle, W.; Lutwyche, M. I.; Rothuizen, H. E.; Stutz, R.; Widmer, R.; Binnig, G. K. *IBM J. Res. Dev.* **2000**, *44*, 323−340.
(148) Gratson, G. M.; Xu, M. J.; Lewis, J. A. *Nature* **2004**, *428*, 386.
(149) Smay, J. E.; Gratson, G. M.; Shepherd, R. F.; Cesarano, J.; Lewis, J. A. *Adv. Mater.* **2002**, *14*, 1279.
(150) Therriault, D.; White, S. R.; Lewis, J. A. *Nat. Mater.* **2003**, *2*, 347.
(151) Kim, Y. S.; Lee, N. Y.; Lim, J. R.; Lee, M. J.; Park, S. *Chem. Mater.* **2005**, *17*, 5867.
(152) Kim, S.-H.; Lee, S.-H.; Kim, Y.-K. *J. Micromech. Microeng.* **2002**, *12*, 128.
(153) van Delft, F. C. M. J. M.; Weterings, J. P.; van Langen-Suurling, A. K.; Romijn, H. *J. Vac. Sci. Technol. B* **2000**, *18*, 3419.
(154) Kupka, R. K.; Bouamrane, F.; Cremers, C.; Megtert, S. *Appl. Surf. Sci.* **2000**, *164*, 97.
(155) Singleton, L. *J. Photopolym. Sci. Technol.* **2003**, *16*, 413.
(156) Malek, C. K.; Saile, V. *Microelectron. J.* **2004**, *35*, 131.
(157) Katoh, T.; Nishi, N.; Fukagawa, M.; Ueno, H.; Sugiyama, S. *Sens. Actuators, A: Phys.* **2001**, *A89*, 10.
(158) Guo, L. J. *J. Phys. D: Appl. Phys.* **2004**, *37*, R123.
(159) Heyderman, L. J.; Schift, H.; David, C.; Gobrecht, J.; Schweizer, T. *Microelectron. Eng.* **2000**, *54*, 229.
(160) Jung, G. Y.; Li, Z. Y.; Wu, W.; Chen, Y.; Olynick, D. L.; Wang, S. Y.; Tong, W. M.; Williams, R. S. *Langmuir* **2005**, *21*, 1158.
(161) Keil, M.; Beck, M.; Frennesson, G.; Theander, E.; Bolmsjo, E.; Montelius, L.; Heidari, B. *J. Vac. Sci. Technol. B* **2004**, *22*, 3283.
(162) Schift, H.; Heyderman, L. J.; Gobrecht, J. *Chimia* **2003**, *56*, 543.
(163) Chou, S. Y.; Krauss, P. R.; Renstrom, P. J. *Appl. Phys. Lett.* **1995**, *67*, 3114.
(164) Sotomayor Torres, C. V. *Alternative Lithography*; Kluwer Academic: New York, 2003.
(165) Schift, H.; David, C.; Gabriel, M.; Gobrecht, J.; Heyderman, L. J.; Kaiser, W.; Koppel, S.; Scandella, L. *Microelectron. Eng.* **2000**, *53*, 171.
(166) Makela, T.; Haatainen, T.; Ahopeito, J.; Isotalo, H. *J. Vac. Sci. Technol. B* **2001**, *19*, 487.
(167) Haatainen, T.; Ahopelto, J. *Phys. Scr.* **2003**, *67*, 357.
(168) Tan, H.; Gilbertson, A.; Chou, S. Y. *J. Vac. Sci. Technol. B* **1998**, *16*, 3926.
(169) Heidari, B.; Maximov, I.; Montelius, L. *J. Vac. Sci. Technol. B* **2000**, *18*, 3557.
(170) Heidari, B.; Maximov, I.; Sarwe, E. L.; Montelius, L. *J. Vac. Sci. Technol. B* **1999**, *17*, 2961.
(171) Yoon, H.; Lee, K. M.; Khang, D.-Y.; Lee, H. H.; Choi, S.-J. *Appl. Phys. Lett.* **2004**, *85*, 1793.
(172) Guo, C.; Feng, L.; Zhai, J.; Wang, G.; Song, Y.; Jiang, L.; Zhu, D. *ChemPhysChem* **2004**, *5*, 750.
(173) Becker, H.; Heim, U. *Sens. Actuators, A: Phys.* **2000**, *A83*, 130.
(174) Jung, G. Y.; Ganapathiappan, S.; Ohlberg, D. A. A.; Olynick, D. L.; Chen, Y.; Tong, W. M.; Williams, R. S. *Nano Lett.* **2004**, *4*, 1225.
(175) Fichet, G.; Stutzmann, N.; Muir, B. V. O.; Huck, W. T. S. *Adv. Mater.* **2002**, *14*, 47.
(176) Schift, H.; Park, S.; Jung, B.; Choi, C.-G.; Kee, C.-S.; Han, S.-P.; Yoon, K.-B.; Gobrecht, J. *Nanotechnology* **2005**, *16*, S261.
(177) Kuwabara, K.; Ogino, M.; Motowaki, S.; Miyauchi, A. *Microelectron. Eng.* **2004**, *73*−*74*, 752.
(178) Stutzmann, N.; Tervoort, T. A.; Bastiaansen, C. W. M.; Feldman, K.; Smith, P. *Adv. Mater.* **2000**, *12*, 557.
(179) Schift, H.; Heyderman, L. J.; Maur, M. A. D.; Gobrecht, J. *Nanotechnology* **2001**, *12*, 173.
(180) Hirai, Y.; Konishi, T.; Yoshikawa, T.; Yoshida, S. *J. Vac. Sci. Technol. B* **2004**, *22*, 3288.
(181) Mouroulis, P.; Hartley, F. T.; Wilson, D. W.; White, V. E.; Shori, A.; Nguyen, S.; Zhang, M.; Feldman, M. *Opt. Express* **2003**, *11*, 270.
(182) Tormen, M.; Romanato, F.; Altissimo, M.; Businaro, L.; Candeloro, P.; Di Fabrizio, E. M. *J. Vac. Sci. Technol. B* **2004**, *22*, 766.
(183) Dauksher, W. J.; Nordquist, K. J.; Mancini, D. P.; Resnick, D. J.; Baker, J. H.; Hooper, A. E.; Talin, A. A.; Bailey, T. C.; Lemonds, A. M.; Sreenivasan, S. V.; Ekerdt, J. G.; Willson, C. G. *J. Vac. Sci. Technol. B* **2002**, *20*, 2857.
(184) Bailey, T. C.; Resnick, D. J.; Mancini, D.; Nordquist, K. J.; Dauksher, W. J.; Ainley, E.; Talin, A.; Gehoski, K.; Baker, J. H.; Choi, B. J.; Johnson, S.; Colburn, M.; Meissl, M.; Sreenivasan, S. V.; Ekerdt, J. G.; Willson, C. G. *Microelectron. Eng.* **2002**, *61*−*2*, 461.
(185) Mancini, D. P.; Gehoski, K. A.; Ainley, E.; Nordquist, K. J.; Resnick, D. J.; Bailey, T. C.; Sreenivasan, S. V.; Ekerdt, J. G.; Willson, C. G. *J. Vac. Sci. Technol. B* **2002**, *20*, 2896.

(186) Resnick, D. J.; Mancini, D.; Dauksher, W. J.; Nordquist, K.; Bailey, T. C.; Johnson, S.; Sreenivasan, S. V.; Ekerdt, J. G.; Willson, C. G. *Microelectron. Eng.* **2003**, *69*, 412.
(187) Bender, M.; Plachetka, U.; Ran, J.; Fuchs, A.; Vratzov, B.; Kurz, H.; Glinsner, T.; Lindner, F. *J. Vac. Sci. Technol. B* **2004**, *22*, 3229.
(188) Kim, E. K.; Stacey, N. A.; Smith, B. J.; Dickey, M. D.; Johnson, S. C.; Trinque, B. C.; Willson, C. G. *J. Vac. Sci. Technol. B* **2004**, *22*, 131.
(189) Chan-Park, M. B.; Lam, Y. C.; Laulia, P.; Joshi, S. C. *Langmuir* **2005**, *21*, 2000.
(190) Viallet, B.; Gallo, P.; Daran, E. *J. Vac. Sci. Technol. B* **2005**, *23*, 72.
(191) Chan-Park, M. B.; Yan, Y. H.; Neo, W. K.; Zhou, W. X.; Zhang, J.; Yue, C. Y. *Langmuir* **2003**, *19*, 4371.
(192) Chan-Park, M. B.; Neo, W. K. *Microsyst. Technol.* **2003**, *9*, 501.
(193) Resnick, D. J.; Dauksher, W. J.; Mancini, D.; Nordquist, K. J.; Bailey, T. C.; Johnson, S.; Stacey, N.; Ekerdt, J. G.; Willson, C. G.; Sreenivasan, S. V.; Schumaker, N. *J. Vac. Sci. Technol. B* **2003**, *21*, 2624.
(194) Schuetter, S. D.; Dicks, G. A.; Nellis, G. F.; Engelstad, R. L.; Lovell, E. G. *J. Vac. Sci. Technol. B* **2004**, *22*, 3312.
(195) Colburn, M.; Choi, B. J.; Sreenivasan, S. V.; Bonnecaze, R. T.; Willson, C. G. *Microelectron. Eng.* **2004**, *75*, 321.
(196) Colburn, M.; Grot, A.; Choi, B. J.; Amistoso, M.; Bailey, T.; Sreenivasan, S. V.; Ekerdt, J. G.; Willson, C. G. *J. Vac. Sci. Technol. B* **2001**, *19*, 2162.
(197) Reddy, S.; Bonnecaze, R. T. *Microelectron. Eng.* **2005**, *82*, 60.
(198) Xia, Y. N.; Whitesides, G. M. *Angew. Chem., Int. Ed.* **1998**, *37*, 551.
(199) Denoual, M.; Griscom, L.; Toshiyoshi, H.; Fujita, H. *Jpn. J. Appl. Phys., Part 1* **2003**, *42*, 4598.
(200) Schmitz, G. J.; Brucker, C.; Jacobs, P. *J. Micromech. Microeng.* **2005**, *15*, 1904.
(201) Kim, K.; Park, S.; Lee, J. B.; Manohara, H.; Desta, Y.; Murphy, M.; Ahn, C. H. *Microsyst. Technol.* **2002**, *9*, 5.
(202) Delamarche, E.; Schmid, H.; Michel, B.; Biebuyck, H. *Adv. Mater.* **1997**, *9*, 741.
(203) Hui, C. Y.; Jagota, A.; Lin, Y. Y.; Kramer, E. J. *Langmuir* **2002**, *18*, 1394.
(204) Bietsch, A.; Michel, B. *J. Appl. Phys.* **2000**, *88*, 4310.
(205) Sharp, K. G.; Blackman, G. S.; Glassmaker, N. J.; Jagota, A.; Hui, C. Y. *Langmuir* **2004**, *20*, 6430.
(206) Odom, T. W.; Love, J. C.; Wolfe, D. B.; Paul, K. E.; Whitesides, G. M. *Langmuir* **2002**, *18*, 5314.
(207) Schmid, H.; Michel, B. *Macromolecules* **2000**, *33*, 3042.
(208) Roca-Cusachs, P.; Rico, F.; Martinez, E.; Toset, J.; Farre, R.; Navajas, D. *Langmuir* **2005**, *21*, 5542.
(209) Choi, K. M.; Rogers, J. A. *J. Am. Chem. Soc.* **2003**, *125*, 4060.
(210) Rogers, J. A.; Paul, K. E.; Whitesides, G. M. *J. Vac. Sci. Technol. B* **1998**, *16*, 88.
(211) Choi, S. J.; Yoo, P. J.; Baek, S. J.; Kim, T. W.; Lee, H. H. *J. Am. Chem. Soc.* **2004**, *126*, 7744.
(212) Csucs, G.; Kunzler, T.; Feldman, K.; Robin, F.; Spencer, N. D. *Langmuir* **2003**, *19*, 6104.
(213) Suh, K. Y.; Langer, R.; Lahann, J. *Appl. Phys. Lett.* **2003**, *83*, 4250.
(214) Choi, D. G.; Jeong, J. H.; Sim, Y. S.; Lee, E. S.; Kim, W. S.; Bae, B. S. *Langmuir* **2005**, *21*, 9390.
(215) Khang, D. Y.; Kang, H.; Kim, T.; Lee, H. H. *Nano Lett.* **2004**, *4*, 633.
(216) Khang, D. Y.; Lee, H. H. *Langmuir* **2004**, *20*, 2445.
(217) Rolland, J. P.; Hagberg, E. C.; Denison, G. M.; Carter, K. R.; De Simone, J. M. *Angew. Chem., Int. Ed.* **2004**, *43*, 5796.
(218) Eo, Y. J.; Kim, J. H.; Ko, J. H.; Bae, B. S. *J. Mater. Res.* **2005**, *20*, 401.
(219) Kim, S. Y.; Augustine, S.; Eo, Y. J.; Bae, B. S.; Woo, S. I.; Kang, J. K. *J. Phys. Chem. B* **2005**, *109*, 9397.
(220) Eo, Y. J.; Lee, T. H.; Kim, S. Y.; Kang, J. K.; Han, Y. S.; Bae, B. S. *J. Polym. Sci. Polym. Phys.* **2005**, *43*, 827.
(221) Kim, W. S.; Kim, K. S.; Eo, Y. J.; Yoon, Y.; Bae, B. S. *J. Mater. Chem.* **2005**, *15*, 465.
(222) Jeong, J. H.; Sim, Y. S.; Sohn, H.; Lee, E. S. *Microelectron. Eng.* **2004**, *75*, 165.
(223) Yoo, P. J.; Choi, S. J.; Kim, J. H.; Suh, D.; Baek, S. J.; Kim, T. W.; Lee, H. H. *Chem. Mater.* **2004**, *16*, 5000.
(224) Ge, H. X.; Wu, W.; Li, Z. Y.; Jung, G. Y.; Olynick, D.; Chen, Y. F.; Liddle, J. A.; Wang, S. Y.; Williams, R. S. *Nano Lett.* **2005**, *5*, 179.
(225) Suh, K. Y.; Choi, S. J.; Baek, S. J.; Kim, T. W.; Langer, R. *Adv. Mater.* **2005**, *17*, 560.
(226) Khang, D. Y.; Lee, H. H. *Adv. Mater.* **2004**, *16*, 176.
(227) Kim, Y. S.; Suh, K. Y.; Lee, H. H. *Appl. Phys. Lett.* **2001**, *79*, 2285.
(228) Suh, K. Y.; Lee, H. H. *Adv. Funct. Mater.* **2002**, *12*, 405.
(229) Suh, K. Y.; Kim, Y. S.; Lee, H. H. *Adv. Mater.* **2001**, *13*, 1386.
(230) Suh, K. Y.; Lee, H. H. *J. Micromech. Microeng.* **2005**, *15*, 400.
(231) Lee, J. N.; Park, C.; Whitesides, G. M. *Anal. Chem.* **2003**, *75*, 6544.
(232) Lee, J.; Kim, M. J.; Lee, H. H. *Langmuir* **2006**, *22*, 2090.
(233) del Campo, A.; Greiner, C.; Álvarez, I.; Arzt, E. *Adv. Mater.,* in press.
(234) Jeong, H. E.; Lee, S. H.; Kim, J. K.; Suh, K. Y. *Langmuir* **2006**, *22*, 1640.
(235) Huang, X. D.; Bao, L. R.; Cheng, X.; Guo, L. J.; Pang, S. W.; Yee, A. F. *J. Vac. Sci. Technol. B* **2002**, *20*, 2872.
(236) Borzenko, T.; Tormen, M.; Schmidt, G.; Molenkamp, L. W.; Janssen, H. *Appl. Phys. Lett.* **2001**, *79*, 2246.
(237) Zhao, X. M.; Xia, Y. N.; Whitesides, G. M. *Adv. Mater.* **1996**, *8*, 837.
(238) Zhao, X. M.; Xia, Y. N.; Whitesides, G. M. *J. Mater. Chem.* **1997**, *7*, 1069.
(239) Childs, W. R.; Nuzzo, R. G. *Adv. Mater.* **2004**, *16*, 1323.
(240) Childs, W. R.; Nuzzo, R. G. *J. Am. Chem. Soc.* **2002**, *124*, 13583.
(241) Kim, Y. S.; Hammond, P. T. *Polym. Mater. Sci. Eng.* **2004**, *90*, 599.
(242) Kim, Y. S.; Lee, H. H.; Hammond, P. T. *Nanotechnology* **2003**, *14*, 1140.
(243) Schaper, C. D. *J. Vac. Sci. Technol. B* **2003**, *21*, 2961.
(244) Kong, Y. P.; Low, H. Y.; Pang, S. W.; Yee, A. F. *J. Vac. Sci. Technol. B* **2004**, *22*, 3251.
(245) Zhao, W.; Low, H. Y. *J. Vac. Sci. Technol. B* **2006**, *24*, 255.
(246) Bao, L. R.; Cheng, X.; Huang, X. D.; Guo, L. J.; Pang, S. W.; Yee, A. F. *J. Vac. Sci. Technol. B* **2002**, *20*, 2881.
(247) Ooe, H.; Morimatsu, M.; Yoshikawa, T.; Kawata, H.; Hirai, Y. *J. Vac. Sci. Technol. B* **2005**, *23*, 375.
(248) Lee, J. H.; Kim, C. H.; Ho, K. M.; Constant, K. *Adv. Mater.* **2005**, *17*, 2481.
(249) Liu, T. B.; Burger, C.; Chu, B. *Prog. Polym. Sci.* **2003**, *28*, 5.
(250) Packard, R. E.; Pekola, J. P.; Price, P. B.; Spohr, R. N. R.; Westmacott, K. H.; Zhu, Y. Q. *Rev. Sci. Instrum.* **1986**, *57*, 1654.
(251) Steinhart, M.; Wehrspohn, R. B.; Gosele, U.; Wendorff, J. H. *Angew. Chem., Int. Ed.* **2004**, *43*, 1334.
(252) Wehrspohn, R. B.; Schilling, J. *MRS Bull.* **2001**, *26*, 623.
(253) Chazalviel, J. N.; Ozanam, F.; Gabouze, N.; Fellah, S.; Wehrspohn, R. B. *J. Electrochem. Soc.* **2002**, *149*, C511.
(254) Lehmann, V. *J. Electrochem. Soc.* **1993**, *140*, 2836.
(255) Lehmann, V.; Foll, H. *J. Electrochem. Soc.* **1990**, *137*, 653.
(256) Birner, A.; Gruning, U.; Ottow, S.; Schneider, A.; Muller, F.; Lehmann, V.; Foll, H.; Gosele, U. *Phys. Status Solidi A* **1998**, *165*, 111.
(257) Steinhart, M.; Wendorff, J. H.; Wehrspohne, R. B. *ChemPhysChem* **2003**, *4*, 1171.
(258) Xiong, S.; Wang, Q.; Xia, H. *MRS Bull.* **2004**, *39*, 1569.
(259) Rahman, S.; Yang, H. *Nano Lett.* **2003**, *3*, 439.
(260) Wu, Y. Y.; Cheng, G. S.; Katsov, K.; Sides, S. W.; Wang, J. F.; Tang, J.; Fredrickson, G. H.; Moskovits, M.; Stucky, G. D. *Nat. Mater.* **2004**, *3*, 816.
(261) Lee, W.; Jin, M.-K.; Yoo, W.-C.; Lee, J.-K. *Langmuir* **2004**, *20*, 7665.
(262) Song, G. J.; She, X. L.; Fu, Z. F.; Li, J. J. *J. Mater. Res.* **2004**, *19*, 3324.
(263) Steinhart, M.; Wendorff, J. H.; Greiner, A.; Wehrspohn, R. B.; Nielsch, K.; Schilling, J.; Choi, J.; Gosele, U. *Science* **2002**, *296*, 1997.
(264) Cepak, V. M.; Martin, C. R. *Chem. Mater.* **1999**, *11*, 1363.
(265) Steinhart, M.; Senz, S.; Wehrspohn, R. B.; Gosele, U.; Wendorff, J. H. *Macromolecules* **2003**, *36*, 3646.
(266) Steinhart, M.; Murano, S.; Schaper, A. K.; Ogawa, T.; Tsuji, M.; Gosele, U.; Weder, C.; Wendorff, J. H. *Adv. Funct. Mater.* **2005**, *15*, 1656.
(267) Xiang, H.; Shin, K.; Kim, T.; Moon, S. I.; McCarthy, T. J.; Russell, T. P. *Macromolecules* **2004**, *37*, 5660.
(268) Steinhart, M.; Jia, Z. H.; Schaper, A. K.; Wehrspohn, R. B.; Gosele, U.; Wendorff, J. H. *Adv. Mater.* **2003**, *15*, 706.
(269) Li, F.; He, J. B.; Zhou, W. L. L.; Wiley, J. B. *J. Am. Chem. Soc.* **2003**, *125*, 16166.
(270) Meng, G. W.; Jung, Y. J.; Cao, A. Y.; Vajtai, R.; Ajayan, P. M. *Proc. Natl. Acad. Sci. U.S.A.* **2005**, *102*, 7074.
(271) Sferrazza, M.; Xiao, C.; Jones, R. A. L.; Bucknall, D. G.; Webster, J.; Penfold, J. *Phys. Rev. Lett.* **1997**, *78*, 3693.
(272) Sferrazza, M.; Xiao, C.; Bucknall, D. G.; Jones, R. A. L. *J. Phys.: Condens. Matter* **2001**, *13*, 10269.
(273) Sferrazza, M.; Xiao, C.; Jones, R. A. L.; Penfold, J. *Philos. Mag. Lett.* **2000**, *80*, 561.
(274) Sprenger, M.; Walheim, S.; Schafle, C.; Steiner, U. *Adv. Mater.* **2003**, *15*, 703.
(275) Assender, H.; Bliznyuk, V.; Porfyrakis, K. *Science* **2002**, *297*, 973.
(276) Lin, Z. Q.; Kerle, T.; Baker, S. M.; Hoagland, D. A.; Schaffer, E.; Steiner, U.; Russell, T. P. *J. Chem. Phys.* **2001**, *114*, 2377.
(277) Lin, Z. Q.; Kerle, T.; Russell, T. P.; Schaffer, E.; Steiner, U. *Macromolecules* **2002**, *35*, 3971.
(278) Schafer, E.; Thurn-Albrecht, T.; Russell, T. P.; Steiner, U. *Europhys. Lett.* **2001**, *53*, 518.

(279) Schaffer, E.; Thurn-Albrecht, T.; Russell, T. P.; Steiner, U. *Nature* **2000**, *403*, 874.
(280) Verma, R.; Ashutosh, S.; Kargupta, K.; Bhaumik, J. *Langmuir* **2005**, *21*, 3710.
(281) Wu, N.; Pease, L. F.; Russel, W. B. *Langmuir* **2005**, *21*, 12290.
(282) Morariu, M. D.; Voicu, N. E.; Schaffer, E.; Lin, Z. Q.; Russell, T. P.; Steiner, U. *Nat. Mater.* **2003**, *2*, 48.
(283) Dickey, M. D.; Gupta, S.; Amanda, Leach, K.; Collister, E.; Grant, Willson, C.; Russell, T. P. *Langmuir* **2006**, *22*, 4315−4318.
(284) Xiang, H.; Lin, Y.; Russell, T. P. *Macromolecules* **2004**, *37*, 5358−5363.
(285) Harkema, S.; Steiner, U. *Adv. Funct. Mater.* **2005**, *15*, 2016.
(286) Chou, S. Y.; Zhuang, L. *J. Vac. Sci. Technol. B* **1999**, *17*, 3197.
(287) Schaffer, E.; Harkema, S.; Blossey, R.; Steiner, U. *Europhys. Lett.* **2002**, *60*, 255.
(288) Schaffer, E.; Harkema, S.; Roerdink, M.; Blossey, R.; Steiner, U. *Macromolecules* **2003**, *36*, 1645.
(289) Nedelcu, M.; Morariu, M. D.; Harkema, S.; Voicu, N. E.; Steiner, U. *Soft Matter* **2005**, *1*, 62.
(290) Chou, S. Y.; Zhuang, L.; Guo, L. J. *Appl. Phys. Lett.* **1999**, *75*, 1004.
(291) Deshpande, P.; Chou, S. Y. *J. Vac. Sci. Technol. B* **2001**, *19*, 2741.
(292) Deshpande, P.; Sun, X. Y.; Chou, S. Y. *Appl. Phys. Lett.* **2001**, *79*, 1688−1690.
(293) Chen, L.; Zhuang, L.; Deshpande, P.; Chou, S. *Langmuir* **2005**, *21*, 818−821.
(294) Pease, L. F.; Russel, W. B. *J. Chem. Phys.* **2003**, *118*, 3790−3803.
(295) Lazzarino, F.; Gourgon, C.; Schiavone, P.; Perret, C. *J. Vac. Sci. Technol. B* **2004**, *22*, 3318.
(296) Fasolka, M. J.; Mayes, A. M. *Ann. Rev. Mater. Res.* **2001**, *31*, 323.
(297) Ruzette, A. V.; Leibler, L. *Nat. Mater.* **2005**, *4*, 19.
(298) Hamley, I. W. *Angew. Chem., Int. Ed.* **2003**, *42*, 1692.
(299) Radzilowski, L. H.; Carvalho, B. L.; Thomas, E. L. *J. Polym. Sci. Polym. Phys.* **1996**, *34*, 3081−3093.
(300) Suh, K. Y.; Kim, Y. S.; Lee, H. H. *J. Chem. Phys.* **1998**, *108*, 1253.
(301) Huinink, H. P.; Brokken-Zijp, J. C. M.; van Dijk, M. A.; Sevink, G. J. A. *J. Chem. Phys.* **2000**, *112*, 2452.
(302) Wang, Q.; Nealey, P. F.; de Pablo, J. J. *Macromolecules* **2001**, *34*, 3458.
(303) Huang, E.; Pruzinsky, S.; Russell, T. P.; Mays, J.; Hawker, C. J. *Macromolecules* **1999**, *32*, 5299.
(304) Mansky, P.; Russell, T. P.; Hawker, C. J.; Pitsikalis, M.; Mays, J. *Macromolecules* **1997**, *30*, 6810.
(305) Mansky, P.; Russell, T. P.; Hawker, C. J.; Mays, J.; Cook, D. C.; Satija, S. K. *Phys. Rev. Lett.* **1997**, *79*, 237.
(306) Peters, R. D.; Yang, X. M.; Kim, T. K.; Nealey, P. F. *Langmuir* **2000**, *16*, 9620.
(307) Mansky, P.; Liu, Y.; Huang, E.; Russell, T. P.; Hawker, C. *Science* **1997**, *275*, 1458.
(308) Huang, E.; Rockford, L.; Russell, T. P.; Hawker, C. J. *Nature* **1998**, *395*, 757.
(309) Fasolka, M. J.; Harris, D. J.; Mayes, A. M.; Yoon, M.; Mochrie, S. G. J. *Phys. Rev. Lett.* **1997**, *79*, 3018.
(310) Kim, H. C.; Russell, T. P. *J. Polym. Sci. Polym. Phys.* **2001**, *39*, 663.
(311) Park, M.; Harrison, C.; Chaikin, P. M.; Register, R. A.; Adamson, D. H. *Science* **1997**, *276*, 1401.
(312) Harrison, C.; Park, M.; Chaikin, P. M.; Register, R. A.; Adamson, D. H. *J. Vac. Sci. Technol. B* **1998**, *16*, 544.
(313) Harrison, C.; Park, M.; Chaikin, P.; Register, R. A.; Adamson, D. H.; Yao, N. *Macromolecules* **1998**, *31*, 2185.
(314) Konrad, M.; Knoll, A.; Krausch, G.; Magerle, R. *Macromolecules* **2000**, *33*, 5518.
(315) Krausch, G. *Mater. Sci. Eng., R* **1995**, *14*, 1.
(316) Satija, S. K.; Majkrzak, C. F.; Anastasiadis, S. H.; Russell, T. P. *Abstr. Pap. Am. Chem. S.* **1990**, *200*, 107.
(317) Anastasiadis, S. H.; Russell, T. P.; Satija, S. K.; Majkrzak, C. F. *J. Chem. Phys.* **1990**, *92*, 5677.
(318) Anastasiadis, S. H.; Russell, T. P.; Satija, S. K.; Majkrzak, C. F. *Abstr. Pap. Am. Chem. S.* **1989**, *197*, 197.
(319) Anastasiadis, S. H.; Russell, T. P.; Satija, S. K.; Majkrzak, C. F. *Phys. Rev. Lett.* **1989**, *62*, 1852.
(320) Menelle, A.; Russell, T. P.; Anastasiadis, S. H.; Satija, S. K.; Majkrzak, C. F. *Phys. Rev. Lett.* **1992**, *68*, 67.
(321) Russell, T. P.; Menelle, A.; Anastasiadis, S. H.; Satija, S. K.; Majkrzak, C. F. *Makromol. Chem., Makromol. Symp.* **1992**, *62*, 157.
(322) Li, Z.; Qu, S.; Rafailovich, M. H.; Sokolov, J.; Tolan, M.; Turner, M. S.; Wang, J.; Schwarz, S. A.; Lorenz, H.; Kotthaus, J. P. *Macromolecules* **1997**, *30*, 8410.
(323) Krausch, G.; Magerle, R. *Adv. Mater.* **2002**, *14*, 1579.
(324) Boker, A.; Muller, A. H. E.; Krausch, G. *Macromolecules* **2001**, *34*, 7477.
(325) Rehse, N.; Knoll, A.; Magerle, R.; Krausch, G. *Macromolecules* **2003**, *36*, 3261.
(326) Balsamo, V.; Collins, S.; Hamley, I. W. *Polymer* **2002**, *43*, 4207.
(327) Rehse, N.; Knoll, A.; Konrad, M.; Magerle, R.; Krausch, G. *Phys. Rev. Lett.* **2001**, *8703*, 035505.
(328) Elbs, H.; Drummer, C.; Abetz, V.; Krausch, G. *Macromolecules* **2002**, *35*, 5570.
(329) Elbs, H.; Abetz, V.; Hadziioannou, G.; Drummer, C.; Krausch, G. *Macromolecules* **2001**, *34*, 7917.
(330) Elbs, H.; Abetz, V.; Hadziioannou, G.; Drummer, C.; Krausch, G. *Macromolecules* **2001**, *34*, 7917.
(331) Kim, G.; Libera, M. *Macromolecules* **1998**, *31*, 2569.
(332) Kim, G.; Libera, M. *Macromolecules* **1998**, *31*, 2670.
(333) Harant, A. W.; Bowman, C. N. *J. Vac. Sci. Technol. B* **2005**, *23*, 1615.
(334) Sidorenko, A.; Tokarev, I.; Minko, S.; Stamm, M. *J. Am. Chem. Soc.* **2003**, *125*, 12211.
(335) Lin, Z. Q.; Kim, D. H.; Wu, X. D.; Boosahda, L.; Stone, D.; LaRose, L.; Russell, T. P. *Adv. Mater.* **2002**, *14*, 1373.
(336) Park, C.; Yoon, J.; Thomas, E. L. *Polymer* **2003**, *44*, 7779.
(337) Tokarev, I.; Krenek, R.; Burkov, Y.; Schmeisser, D.; Sidorenko, A.; Minko, S.; Stamm, M. *Macromolecules* **2005**, *38*, 507.
(338) Peng, J.; Xuan, Y.; Wang, H.; Yang, Y.; Li, B.; Han, Y. *J. Chem. Phys.* **2004**, *120*, 11163.
(339) Thurn-Albrecht, T.; Steiner, R.; DeRouchey, J.; Stafford, C. M.; Huang, E.; Bal, M.; Tuominen, M.; Hawker, C. J.; Russell, T. P. *Adv. Mater.* **2000**, *12*, 787.
(340) Morkved, T. L.; Lu, M.; Urbas, A. M.; Ehrichs, E. E.; Jaeger, H. M.; Mansky, P.; Russell, T. P. *Science* **1996**, *273*, 931.
(341) Thurn-Albrecht, T.; Schotter, J.; Kastle, G. A.; Emley, N.; Shibauchi, T.; Krusin-Elbaum, L.; Guarini, K.; Black, C. T.; Tuominen, M. T.; Russell, T. P. *Science* **2000**, *290*, 2126.
(342) Thurn-Albrecht, T.; DeRouchey, J.; Russell, T. P.; Kolb, R. *Macromolecules* **2002**, *35*, 8106.
(343) Zhang, Q. L.; Tsui, O. K. C.; Du, B. Y.; Zhang, F. J.; Tang, T.; He, T. B. *Macromolecules* **2000**, *33*, 9561.
(344) Guarini, K. W.; Black, C. T.; Milkove, K. R.; Sandstrom, R. L. *J. Vac. Sci. Technol. B* **2001**, *19*, 2784.
(345) Knoll, A.; Horvat, A.; Lyakhova, K. S.; Krausch, G.; Sevink, G. J. A.; Zvelindovsky, A. V.; Magerle, R. *Phys. Rev. Lett.* **2002**, *89*, 035501.
(346) Knoll, A.; Magerle, R.; Krausch, G. *J. Chem. Phys.* **2004**, *120*, 1105.
(347) Lyakhova, K. S.; Sevink, G. J. A.; Zvelindovsky, A. V.; Horvat, A.; Magerle, R. *J. Chem. Phys.* **2004**, *120*, 1127.
(348) Horvat, A.; Lyakhova, K. S.; Sevink, G. J. A.; Zvelindovsky, A. V.; Magerle, R. *J. Chem. Phys.* **2004**, *120*, 1117.
(349) Park, C.; Cheng, J. Y.; Fasolka, M. J.; Mayes, A. M.; Ross, C. A.; Thomas, E. L.; De Rosa, C. *Appl. Phys. Lett.* **2001**, *79*, 848.
(350) Rockford, L.; Liu, Y.; Mansky, P.; Russell, T. P.; Yoon, M.; Mochrie, S. G. J. *Phys. Rev. Lett.* **1999**, *82*, 2602.
(351) Reiter, G.; Castelein, G.; Hoerner, P.; Riess, G.; Blumen, A.; Sommer, J. U. *Phys. Rev. Lett.* **1999**, *83*, 3844.
(352) De Rosa, C.; Park, C.; Thomas, E. L.; Lotz, B. *Nature* **2000**, *405*, 433.
(353) Osuji, C.; Chao, C. Y.; Bita, I.; Ober, C. K.; Thomas, E. L. *Adv. Funct. Mater.* **2002**, *12*, 753.
(354) Cheng, J. Y.; Ross, C. A.; Thomas, E. L.; Smith, H. I.; Vancso, G. J. *Appl. Phys. Lett.* **2002**, *81*, 3657.
(355) Cheng, J. Y.; Ross, C. A.; Thomas, E. L.; Smith, H. I.; Vancso, G. J. *Adv. Mater.* **2003**, *15*, 1599.
(356) Sundrani, D.; Sibener, S. J. *Macromolecules* **2002**, *35*, 8531.
(357) Li, H. W.; Huck, W. T. S. *Nano Lett.* **2004**, *4*, 1633.
(358) Deng, T.; Chen, C. T.; Honeker, C.; Thomas, E. L. *Polymer* **2003**, *44*, 6549.
(359) Wang, Q. *Macromol. Theor. Simul.* **2005**, *14*, 96.
(360) Balazs, A. C.; Gempe, M. C.; Zhou, Z. X. *Macromolecules* **1991**, *24*, 4918.
(361) Balazs, A. C.; Huang, K. L.; Mcelwain, P.; Brady, J. E. *Macromolecules* **1991**, *24*, 714.
(362) Pereira, G. G.; Williams, D. R. M. *Langmuir* **1999**, *15*, 2125.
(363) Peters, R. D.; Yang, X. M.; Wang, Q.; de Pablo, J. J.; Nealey, P. F. *J. Vac. Sci. Technol. B* **2000**, *18*, 3530.
(364) Boltau, M.; Walheim, S.; Mlynek, J.; Krausch, G.; Steiner, U. *Nature* **1998**, *391*, 877.
(365) Heier, J.; Kramer, E. J.; Groenewold, J.; Fredrickson, G. H. *Macromolecules* **2000**, *33*, 6060.
(366) Mykhaylyk, T. A.; Collins, S.; Hamley, I. W.; Evans, S. D.; Henderson, J. R. *J. Mater. Sci.* **2004**, *39*, 2249.
(367) Roberge, R. L.; Patel, N. P.; White, S. A.; Thongruang, W.; Smith, S. D.; Spontak, R. J. *Macromolecules* **2002**, *35*, 2268.
(368) Jeong, U.; Ryu, D. Y.; Kho, D. H.; Kim, J. K.; Goldbach, J. T.; Kim, D. H.; Russell, T. P. *Adv. Mater.* **2004**, *16*, 533.
(369) Liu, G.; Ding, J.; Hashimoto, T.; Kimishima, K.; Winnik, F. M.; Nigam, S. *Chem. Mater.* **1999**, *11*, 2233.

(370) Lammertink, R. G. H.; Hempenius, M. A.; van den Enk, J. E.; Chan, V. Z. H.; Thomas, E. L.; Vancso, G. J. *Adv. Mater.* **2000**, *12*, 98.
(371) Lammertink, R. G. H.; Hempenius, M. A.; Vancso, G. J. *Langmuir* **2000**, *16*, 6245.
(372) Lammertink, R. G. H.; Hempenius, M. A.; Vancso, G. J.; Shin, K.; Rafailovich, M. H.; Sokolov, J. *Macromolecules* **2001**, *34*, 942.
(373) Cheng, J. Y.; Ross, C. A.; Chan, V. Z. H.; Thomas, E. L.; Lammertink, R. G. H.; Vancso, G. J. *Adv. Mater.* **2001**, *13*, 1174.
(374) Su, Y. W.; Wu, C. S.; Chen, C. C.; Chen, C. D. *Adv. Mater.* **2003**, *15*, 49.
(375) Masuda, H.; Kanezawa, K.; Nakao, M.; Yokoo, A.; Tamamura, T.; Sugiura, T.; Minoura, H.; Nishio, K. *Adv. Mater.* **2003**, *15*, 159.
(376) Kuo, C. W.; Shiu, J. Y.; Chen, P. L. *Chem. Mater.* **2003**, *15*, 2917.
(377) Delamarche, E.; Juncker, D.; Schmid, H. *Adv. Mater.* **2005**, *17*, 2911.
(378) Burns, M. A.; Johnson, B. N.; Brahmasandra, S. N.; Handique, K.; Webster, J. R.; Krishnan, M.; Sammarco, T. S.; Man, P. M.; Jones, D.; Heldsinger, D.; Mastrangelo, C. H.; Burke, D. T. *Science* **1998**, *282*, 484.
(379) Wagler, P. F.; Tangen, U.; Maeke, T.; Mathis, H. P.; McCaskill, J. S. *Smart Mater. Struct.* **2003**, *12*, 757.
(380) Thorsen, T.; Maerkl, S. J.; Quake, S. R. *Science* **2002**, *298*, 580.
(381) Pérennès, F.; Marmiroli, B.; Matteucci, M.; Tormen, M.; Vaccari, L.; Di, Fabrizio, E. *J. Micromech. Microeng.* **2006**, *16*, 473.
(382) Tan, J. L.; Tien, J.; Pirone, D. M.; Gray, D. S.; Bhadriraju, K.; Chen, C. S. *Proc. Natl. Acad. Sci. U.S.A.* **2003**, *100*, 1484.
(383) Mata, A.; Boehm, C.; Fleischman, A. J.; Muschler, G.; Roy, S. *J. Biomed. Mater. Res.* **2002**, *62*, 499.
(384) Kemkemer, R.; Csete, M.; Schrank, S.; Kaufmann, D.; Spatz, J. *Mat. Sci. Eng., C* **2003**, *23*, 437.
(385) Brucker, C.; Spatz, J.; Schroder, W. *Exp. Fluids* **2005**, *39*, 464.
(386) Brown, R. A.; Wiseman, M.; Chuo, C. B.; Cheema, U.; Nazhat, S. N. *Adv. Funct. Mater.* **2005**, *15*, 1762.
(387) Popov, V. K.; Evseev, A. V.; Ivanov, A. L.; Roginski, V. V.; Volozhin, A. I.; Howdle, S. M. *J. Mater. Sci.: Mater. Med.* **2004**, *15*, 123.
(388) Liu, Y.; Sun, S.; Singha, S.; Cho, M. R.; Gordon, R. J. *Biomaterials* **2005**, *26*, 4597.
(389) Kusakabe, H.; Sakamaki, T.; Nihei, K.; Oyama, Y.; Yanagimoto, S.; Ichimiya, M.; Kimura, J.; Toyama, Y. *Biomaterials* **2004**, *25*, 2957.
(390) Hoque, M. E.; Hutmacher, D. W.; Feng, W.; Li, S.; Huang, M. H.; Vert, M.; Wong, Y. S. *J. Biomater. Sci., Polym. E* **2005**, *16*, 1595.
(391) Martina, M.; Subramanyam, G.; Weaver, J. C.; Hutmacher, D. W.; Morse, D. E.; Valiyaveettil, S. *Biomaterials* **2005**, *26*, 5609.
(392) Jones, A. C.; Sakellariou, A.; Limaye, A.; Arns, C. H.; Senden, T. J.; Sawkins, T.; Knackstedt, M. A.; Rohner, D.; Hutmacher, D. W.; Brandwood, A.; Milthorpe, B. K. *J. Mater. Sci., Mater. M.* **2004**, *15*, 529.
(393) Hutmacher, D. W. *J. Biomat. Sci., Polym. E* **2001**, *12*, 107.
(394) Dibra, A.; Kastrati, A.; Mehilli, J.; Pache, J.; von Oepen, R.; Dirschinger, J.; Schomig, A. *Catheter Cardio. Int.* **2005**, *65*, 374.
(395) Simon, C.; Palmaz, J. C.; Sprague, E. A. *J. Long-Term Eff. Med. Implants* **2000**, *10*, 143.
(396) Palmaz, J. C.; Benson, A.; Sprague, E. A. *J. Vasc. Interv. Radiol.* **1999**, *10*, 439.
(397) Granhag, L. M.; Finlay, J. A.; Jonsson, P. R.; Callow, J. A.; Callow, M. E. *Biofouling* **2004**, *20*, 117.
(398) Hoipkemeier-Wilson, L.; Schumacher, J.; Carman, M.; Gibson, A.; Feinberg, A.; Callow, M.; Finlay, J.; Callow, J.; Brennan, A. *Biofouling* **2004**, *20*, 53.
(399) Callow, M. E.; Jennings, A. R.; Brennan, A. B.; Seegert, C. E.; Gibson, A.; Wilson, L.; Feinberg, A.; Baney, R.; Callow, J. A. *Biofouling* **2002**, *18*, 237.
(400) Callies, M.; Chen, Y.; Frédéric, M.; Pépin, A.; Quéré, D. *Microelectron. Eng.* **2005**, *78*−*79*, 100.
(401) Autumn, K.; Liang, Y. A.; Hsleh, S. T.; Zesch, W.; Chan, W. P.; Kenny, T. W.; Fearilng, R.; Full, R. J. *Nature* **2000**, *405*, 681.
(402) Arzt, E.; Gorb, S.; Spolenak, R. *Proc. Natl. Acad. Sci. U.S.A.* **2003**, *100*, 10603.
(403) Gorb, S.; Gorb, E.; Kastner, V. *J. Exp. Biol.* **2001**, *204*, 1421.
(404) Gorb, S.; Jiao, Y. K.; Scherge, M. *J. Comput. Physiol. A* **2000**, *186*, 821.
(405) Geim, A. K.; Dubonos, S. V.; Grigorieva, I. V.; Novoselov, K. S.; Zhukov, A. A.; Shapoval, S. Y. *Nat. Mater.* **2003**, *2*, 461.
(406) Jin, M.; Feng, X.; Feng, L.; Sun, T.; Zhai, J.; Li, T.; Jiang, L. *Adv. Mater.* **2005**, *17*, 1977.
(407) Sitti, M.; Fearing, R. S. *J. Adhesion Sci. Technol.* **2003**, *17*, 1055.
(408) Yurdumakan, B.; Raravikar, N. R.; Ajayan, P. M.; Dhinojwala, A. *Chem. Commun.* **2005**, 3799.
(409) Ye, J.-Y.; Mizeikis, V.; Xu, Y.; Matsuo, S.; Misawa, H. *Opt. Commun.* **2002**, *211*, 205.
(410) Lin, S. Y.; Fleming, J. G.; Hetherington, D. L.; Smith, B. K.; Biswas, R.; Ho, K. M.; Sigalas, M. M.; Zubrzycki, W.; Kurtz, S. R.; Bur, J. *Nature* **1998**, *394*, 251.
(411) Heyderman, L. J.; Ketterer, B.; Bachle, D.; Glaus, F.; Haas, B.; Schift, H.; Vogelsang, K.; Gobrecht, J.; Tiefenauer, L.; Dubochet, O.; Surbled, P.; Hessler, T. *Microelectron. Eng.* **2003**, *67*−*8*, 208.
(412) Kee, C. S.; Han, S. P.; Yoon, K. B.; Choi, C. G.; Sung, H. K.; Oh, S. S.; Park, H. Y.; Park, S.; Schift, H. *Appl. Phys. Lett.* **2005**, *86*.
(413) Yoon, J.; Mathers, R. T.; Coates, G. W.; Thomas, E. L. *Macromolecules* **2006**, *39*, 1913.
(414) Shew, B.-Y.; Li, H.-C.; Pan, C.-L.; Ko, C.-H. *J. Phys. D: Appl. Phys.* **2005**, *38*, 1097.
(415) Rizzo, N. W.; Gardner, K. H.; Walls, D. J.; Keiper-Hrynko, N. M.; SGanzke, T. S.; Hallahan, D. L. *J. R. Soc. Interface* **2006**, *3*, 441.

CR050018Y